BESSY

Highlights 2003

Berliner Elektronenspeicherring-Gesellschaft für Synchrotronstrahlung m.b.H.

Member of the Leibniz Association

Published by:
Berliner Elektronenspeicherring-Gesellschaft für Synchrotronstrahlung m.b.H. – BESSY

Albert-Einstein-Straße 15
12489 Berlin, Germany
phone +49 (0)30 / 6392 2999
fax +49 (0)30 / 6392 2990
www.bessy.de
info@bessy.de

Layout:
Annette Weber, Stitz & Betz GmbH, Dortmund

Printing:
Druckerei Rihn GmbH, Blomberg

ISSN Number: 1611-6127

BESSY

Berliner Elektronenspeicherring-Gesellschaft für Synchrotronstrahlung m.b.H.

Member of the Leibniz Association

Contents

BESSY Inside 04

Scientific Highlights 06
- Archeometry 08
- Atomic Physics 10
- Life Sciences 12
- Solar Energy 14
- Solid State Physics 16
- Nanosciences 18
- Magnetism 24
- Imaging 30

News & Events 34

Future Facilities 40
- Technical Design of the FEL 41
- Metrology Light Source 44

Facility Report 46
- Maschine Status 47
- Beamline Developments 49

User Pages 52

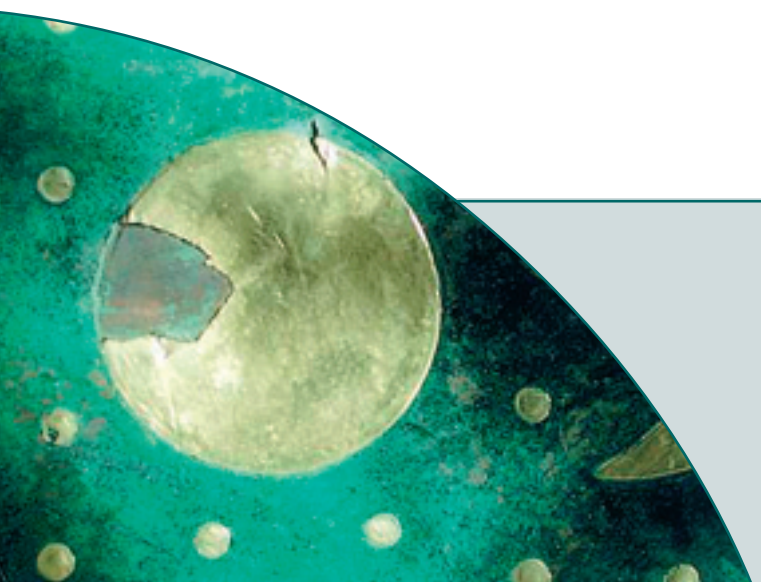

1

Introduction

BESSY Inside

Dear user and friends,

it is mankind's inherent curiosity which urges humans to have a look beyond the horizon. This is still true today as it was several thousand years ago. We know from civilisations in China, Egypt, and the Middle East that they already observed the sky and conducted 'astronomical research' and in Europe places like Stonehenge are well known examples for early Bronze Age observatories. Meanwhile people in Central Europe were apparently still 'sitting-in-the-trees' and drinking met. An unbelievable find near Nebra in Sachsen-Anhalt yet tells us another story. The Nebra Skydisk is a more than 3,500 year old bronze disk with gold inlays showing the moon, stars and several other features. Contemporary and Bronze Age high-tech met when scientists from Halle and Freiberg investigated the composition of the gold inlays using synchrotron radiation. The presentation of the results made BESSY to a one-day 'Centre of Archaeology'. This is only one scientific highlight of 2003. You will find a selection of more highlights on the following pages.

Due to the expanded research opportunities, like providing broadband THz radiation within the beamtime schedule, and a steady growth of the user community which includes industrial users and bio-medical researchers, we look forward to more exciting research in the coming years. We try continually to improve on user service which is by now becoming a real challenge, since for the first time in our history we exceeded the number of 1,000 users a year. More accommodation was urgently needed and we are pleased that the third house of the IBZ was completed by end of 2003. As a regular user you might have noted, that the campus Adlershof is now livelier. This is due to natural sciences faculties of the Humboldt University moving on site and also due to several new shops and cafes which have opened their business. You will find more information at the end of this issue.

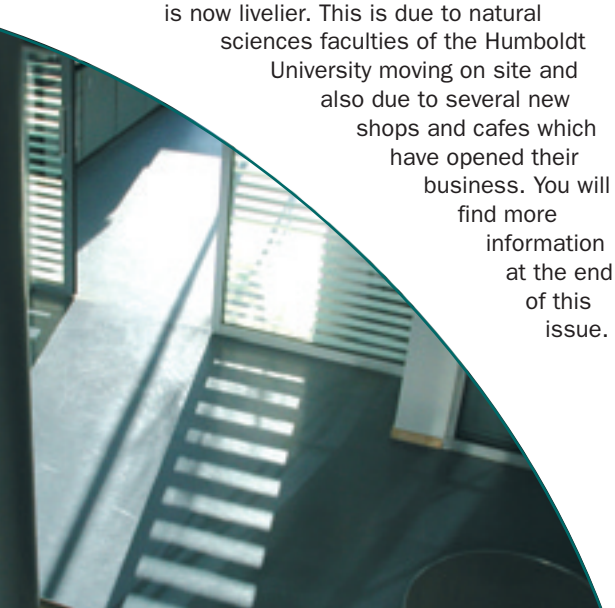

We keep on developing BESSY and pushing hard on our future light source - the FEL - and on cutting edge instrumentation. Two FEL test facilities have been constructed: The Horizontal Bi-Cavitiy Test Facility (HoBiCaT) a test stand for the FEL accelerator section and the femtosecond slicing approach which includes a new beamline design and modifications of the storage ring. The FEL project group has worked out the technical design of the new light source which will be published at the beginning of 2004. But there is even 'more light' at the horizon, since our long term partner PTB received the approval to construct a new Metrology Light Source (MLS) in proximity to BESSY. Ground braking will take place in the summer of 2004.

BESSY also becomes more and more attractive for visitors of all kind and we had more than 9,000 visitors including 'Lange Nacht der Wissenschaften'. This is only the publicly seen part of a successful year, which would not have been possible without the commitment of our staff and the exciting research of our numerous users. We would like to thank them all.

Enjoy reading the Highlights.

Sincerely

Prof. Dr. Dr. h.c. Wolfgang Eberhardt

Prof. Dr. Eberhard Jaeschke

Thomas Frederking

2

Scientific Highlights

Archeometry	*08*
Atomic Physics	*10*
Life Sciences	*12*
Solar Energy	*14*
Solid State Physics	*16*
Nanosciences	*18*
Magnetism	*24*
Imaging	*30*

Scientific Highlights

European Network of Competence at 1600 BC

E. Pernicka[1], M. Radtke[2], H. Riesemeier[2], C.-H. Wunderlich[3]

1 TU Bergakademie Freiberg

2 Bundesanstalt für Materialforschung und -prüfung, Berlin

3 Landesamt für Archäologie in Sachsen-Anhalt, Halle

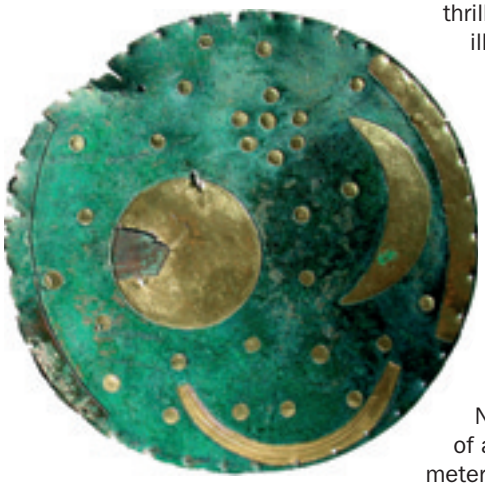

Fig. 1: The Sky Disk of Nebra.

The story has everything of a thriller: treasure hunters, illegal excavations, a sensational find, a secret meeting in a hotel lobby and eventually the lucky rescue of a hoard of several bronze objects featuring the oldest sign of central European astronomy to date: The 'Sky Disc of Nebra', a bronze disk of about 32 cm diameter depicting the night sky with gold inlays (Fig. 1). It was named after identification of the excavation site near the town of Nebra southwest of Halle.

On the disk there are 32 stars, two of originally three curved gold bands along the rim and two complete celestial forms which probably represent the sun and moon or, alternatively, the full and a crescent-shaped moon [1,2]. Two of the curved gold bands on the rim most likely represent horizons while the third is interpreted as a boat. Most of the stars seem to be arranged in an artistic way with aiming to fill the empty spaces between the larger objects more or less regularly. However, a constellation of seven stars can be clearly identified as a representation of the Pleiades whose visibility in the evening sky has been used for calendrical purposes in many cultures.

In addition to the Sky Disk, two swords with gold decorated hilts, two flanged axes, a chisel and two arm spirals, all made of bronze, also belonged to the hoard. These accompanying finds allowed dating securely to the end of the central European Early Bronze Age around 1600 BC. This is truly exceptional, because this makes the 'Sky Disk of Nebra' the earliest astronomically identifiable representation of the night sky, which has considerable implications concerning archaeo-astronomy, the history of religion and archaeology as well as the history of metal technology.

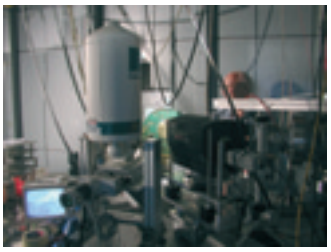

Fig. 2: Experimental set-up at the BAMline.

The technology for producing gold inlays is well known from Mycenae (Greece) and other eastern Mediterranean regions but is unique for central European Bronze Age. Therefore, we were keen to analyse the metal composition of the disk. For the bronze it was possible to take small samples and to analyse them with laboratory equipment. It turned out, that the copper of the bronze originates most likely from a prehistoric copper mine at Mitterberg near Bischofshofen in Austria.

The gold parts had to be analyzed non-destructively by all means. Preliminary analyses have been performed on one star and part of the circular object that had fallen off during the illegal excavation using X-ray fluorescence, scanning electron microscopy, and inductively-coupled plasma mass spectrometry. Due to its physical size it was not possible to apply these techniques directly to the Sky Disk. However, it was important to analyse all gold parts on the Sky Disk, since visual inspection and X-ray radiography had already established that the present appearance of the disk was created in several steps. At least three stars were moved when the horizons were fixed on the disk. In addition, the boat appears not to fit the aesthetic concept of the design since the distance between two of the stars and the boat is much smaller than with any other large gold object on the disk.

We decided to employ synchrotron radiation driven X-ray fluorescence (XRF) to analyse all gold inlays because it offered high spatial resolution, tunability of exciting photon energy, and high element sensitivity. Furthermore, the set-up at the BAMline allowed performing the analysis in air so that the Sky Disk could be positioned free standing in front of the primary beam on a moveable cartridge (Fig. 2).

The results indicate that the gold objects on the disk are generally rich in silver with an average of about 21% Ag and also low amounts of copper which is not uncommon for native gold (Fig. 3a). Only the boat contains considerably less silver and thus must have been applied separately.

References:

[1] H. Meller, Sterne und Weltraum, 12/2003 28-33 (2003).

[2] W. Schlosser, Sterne und Weltraum, 12/2003 34-38 (2003).

[3] E. Pernicka and C.-H. Wunderlich, Archäologie in Sachsen-Anhalt, 1 17-22 (2002).

[4] A. Hartmann, Prähistorische Goldfunde aus Europa. Studien zu den Anfängen der Metallurgie, Band 3, Berlin (1970).

[5] W. Görner et al., Nucl. Instr. Meth. Phys. Res., A 467-468 703-706 (2001).

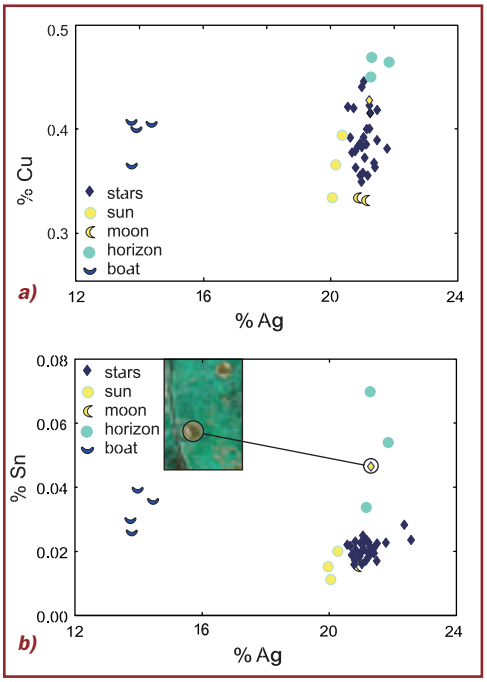

Fig. 3:
a) Ag vs. Cu concentrations in the gold parts of the Sky Disk.

b) Ag vs. Sn concentrations in the gold parts of the Sky Disk.

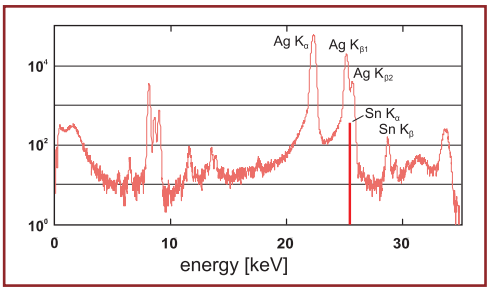

Fig. 4:
XRF spectrum of gold on the Sky Disk with Ag and Sn peaks indicated.

Interestingly, several Bronze Age objects, preferentially found in southeastern Europe [4] show similar silver and copper contents. This gold type is also characterized by low but detectable tin concentrations. So it was important to check for tin concentrations in the gold of the Sky Disk. This was not trivial. The problem is, that small amounts of tin are hidden by massive silver fluorescence in the XRF spectra. In order to obtain tin fluorescence with reasonable peak-to-background ratio it proved to be crucial to adjust the excitation wavelength for the individual elements under investigation (Fig. 4).

At the BAMline, where the wavelength of the primary beam can be adjusted with monochromators [5], it was possible to detect and to quantify tin in all gold objects of the sky disc using optimised settings for tin.
It turned out that indeed the remaining horizon arc and star no. 23 contain significantly more tin than the other stars and the large objects (Fig. 3b). The position of star no. 23 is considered to be moved when the (now missing) horizon was applied. This suggests that the horizons and this single star were made from a third batch of gold that is otherwise indistinguishable from the first one. It is also gratifying that the tin concentrations are consistent with the Bronze Age gold objects from the Carpathian basin (Fig. 5) so that this region seems to be the most likely source of the gold.

However, it has to be noted that so far very little is known about the chemical composition of native gold in central Europe. Therefore, this assignment of the gold origin must be considered as tentative at present. Also, the origin of tin as part of the bronze alloy is still unknown. So for archaeo-metallurgists the thriller goes on.

With the gold from the Carpathian basin, the copper from Austria, and the 'technology transfer' from Mycenae (Greece) the manufacturing of the Nebra Sky Disk can be considered as a very early endeavour based on joint European experience, possibly spiced with symbolism from Egypt or the Levant.

Fig. 5:
An European network.

Contact:
Ernst Pernicka
ernst.pernicka@am.tu-freiberg.de
Martin Radtke
martin.radtke@bam.de

How to excite your neighbour? Try ICD!

S. Marburger[1,2], O. Kugeler[2], U. Hergenhahn[1]

1 MPI für Plasmaphysik, Garching

2 Fritz-Haber-Institut, Berlin

When an atom or molecule is in an excited state, it can lose its excess energy by emitting electromagnetic radiation. This is why a light bulb, a fluorescent tube or even the sun glows. More highly excited states often lose their energy by emitting an electron instead. This energy loss mechanism cannot be perceived sensually. It is nevertheless very important for our fundamental understanding of matter and for technical applications. The best-known way of losing energy by electron ejection is called Auger decay. In this process ejection of one electron due to the rearrangement of the electronic structure occurs only at the atom which was initially excited. Therefore, energy distributions of Auger electrons even from bulk matter are element specific, and can be used e.g. to characterise the composition of alloys.

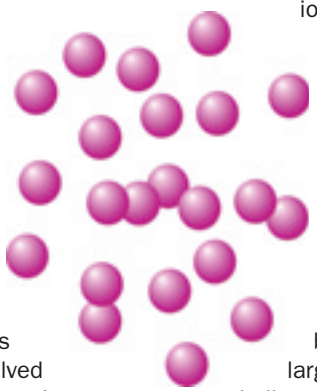

Fig. 1: Van der Waals clusters have no chemical bonds and are held together by weak interactions only. The energy and information transfer has to take place essentially through empty space.

It has been speculated, whether the process of energy loss by electron emission is always confined to a single atomic site. Recent progress in theory found that - contrary to intuition - the neighbouring atoms or molecules can as well be involved in the decay, if the transition energy is small, that is, if the emitted electron is very slow [1,2]. But from an experimental point of view slow electrons are difficult to study. Therefore such processes have never been conclusively seen. We now have found a system ideally suited for the study of electron emission processes, which are only viable due to simultaneous rearrangements at two atoms quite some distance apart.

This novel decay process, termed Interatomic Coulombic Decay (ICD), has been predicted to take place in a large number of weakly bonded systems containing first row elements of the periodic system, such as O, F and Ne [2,3]. In our experiment, we have studied van-der-Waals clusters of Ne (Fig. 1). When an excited ionic state in a Ne cluster is created by removing an inner valence (2s) electron at one of the Ne atoms, it cannot lose energy by conventional (one-site) Auger decay, since the energy of the excited state is not sufficient. It surely can decay by emitting radiation. But according to theory, the ICD process of electron emission by 2p→2s relaxation at the site of ionisation and simultaneous emission of a 2p electron at a neighbouring site will take place much more rapidly (Fig. 2).

The energy transfer necessary for the electron ejection, takes place on a time scale of 1-100 femtoseconds between the two atoms over a nearest neighbour distance, which is much larger than in typical molecules or bulk crystals. Similar processes are expected to occur in other weakly bonded clusters and hydrogen bridged systems such as aqueous solutions or biomolecules. This leads e.g. to a rapid equilibration of charge in cases of radiation damage and in planned experiments on single molecule X-ray diffraction with a Free Electron Laser.

References:

[1] J. A. D. Matthew and Y. Komninos, Surf. Sci. 53, 716 (1975).

[2] L. S. Cederbaum et al., Phys. Rev. Lett. 79, 4778 (1997).

[3] R. Santra and L. S. Cederbaum, Phys. Rep. 368, 1 (2002).

[4] S. Marburger et al., Phys. Rev. Lett. 90, 203401 (2003).

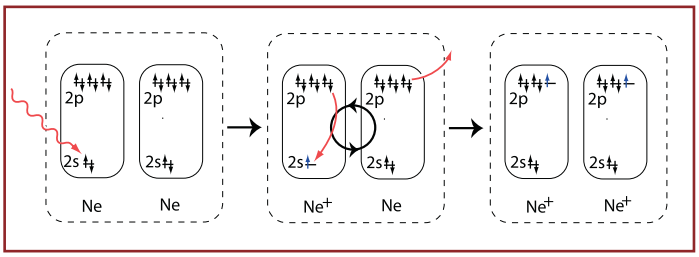

Fig. 2: The Interatomic Coulombic Decay (ICD) mechanism

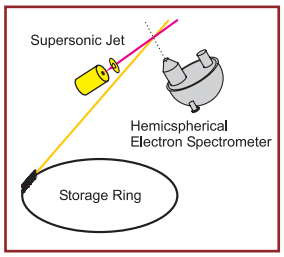

Fig: 3: Experimental Set-up

In our experiment, clusters were produced by expanding Ne gas through a liquid helium cooled nozzle into vacuum (Fig. 3) thus cooling the Ne gas to very low temperatures, so that single atoms freeze into the delicate clusters shown in Fig. 1. Clusters are then irradiated by the synchrotron radiation beam and the electrons emitted are detected in an energy resolving analyser. By tuning the photon energy it is possible to record electron spectra above and below the threshold for creation of Ne 2s electrons, allowing to turn the ICD process on or off on demand as sketched in Fig. 2.

Fig. 4 shows the kinetic energy distribution of electrons from Ne clusters exposed to synchrotron radiation of 37, 48 and 58 eV. 48 eV is the lowest excitation energy at which the ICD process can take place. Spectra recorded at this energy and above show a broad peak of electrons with energies between 1 and 2,5 eV, which is not present at lower photon energies, and disappears if the conditions for cluster formation are not met. The position of this feature does not change with photon energy indicating its ICD origin [4], since the kinetic energy of the emitted electrons is given by the spacing of the levels involved in the decay only. In contrast, the kinetic energy of primary electrons such as the 2s photoelectron depends on the initial radiation. Due to the broad distribution of cluster sizes, the energies of the ICD initial and final state levels get slightly modified, which leads to the appearance of a broad peak.

ICD is also feasible in mixed clusters consisting of Ne and Ar atoms (Fig. 5). We recorded spectra from Ne and Ne/Ar clusters at identical conditions at 62,1 eV. Under these conditions spectra of Ne clusters (Fig. 6a) show the features described above but with the ICD peak less pronounced due to a smaller cluster size and a lower degree of condensation. In spectra from mixed Ne/Ar clusters, however (Fig. 6b), all features have gained in intensity due to an increase in condensation by Ar serving as a seed for cluster formation. In addition, a broad peak appears between 6 eV and 8 eV kinetic energy. We attribute this peak to ICD involving a Ne and a neighbouring Ar atom.

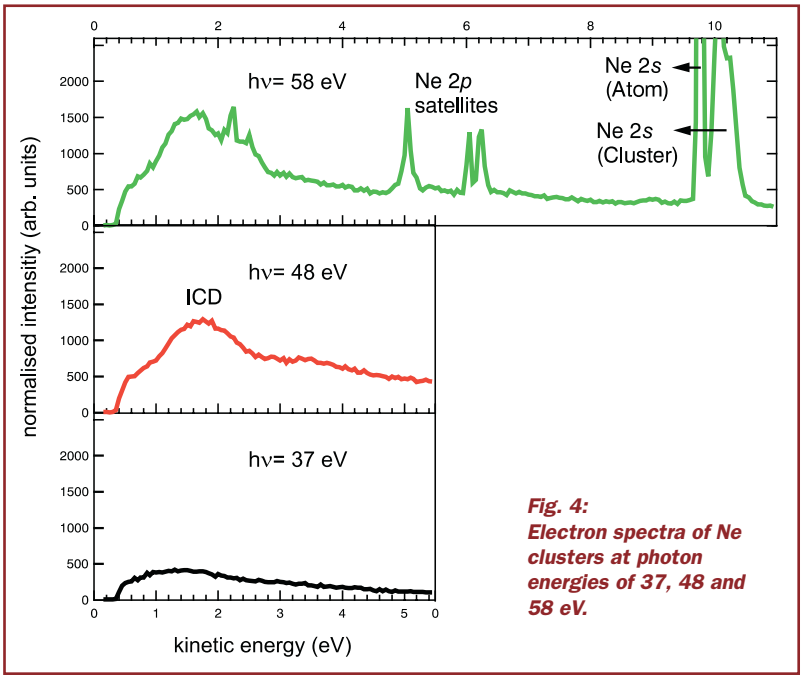

Fig. 4:
Electron spectra of Ne clusters at photon energies of 37, 48 and 58 eV.

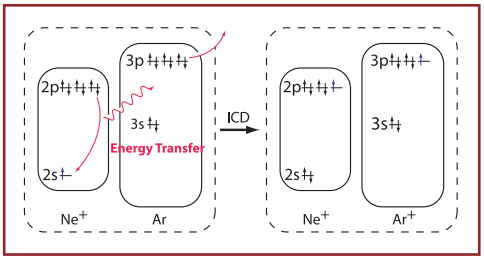

Fig. 5:
The ICD mechanism in mixed systems.

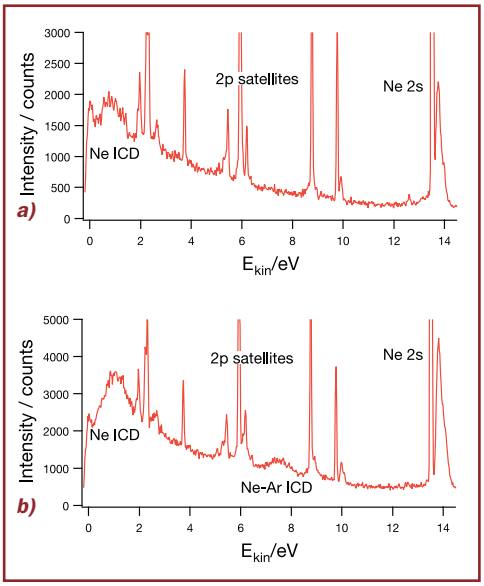

Fig. 6: Electron spectra of a) pure Ne clusters and b) mixed Ne/Ar clusters at 62,1 eV.

Contact
Uwe Hergenhahn
uwe.hergenhahn@ipp.mpg.de

Research Laboratories of Schering AG, Enabling Technologies, Berlin

Better brakes for cell cycles: Structural biology in the drug discovery process

U. Egner

Fig. 1:
The cell cycle.

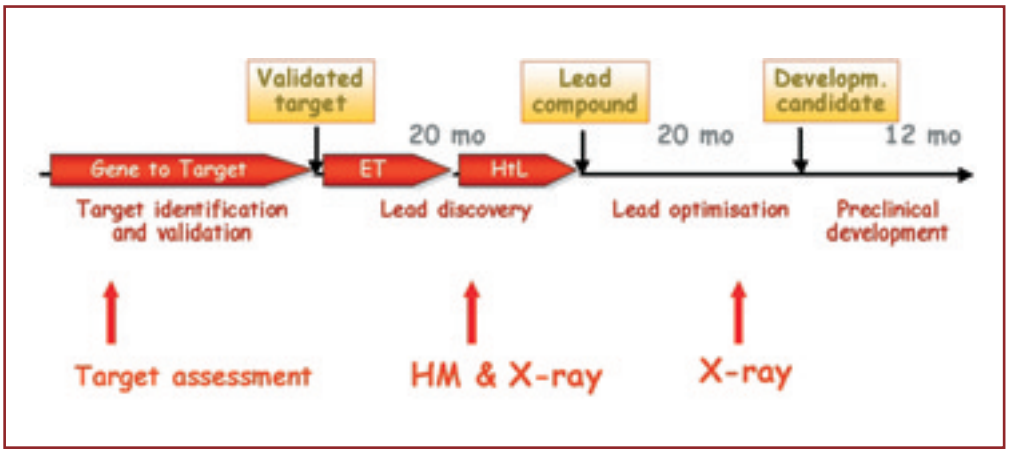

Fig. 2:
Integration of Structural Biology in the Drug Discovery process at Schering.
(HM = homology modelling,
ET = Enabling Technologies,
HtL = Hit-to-Lead).

In a growing tissue cells continuously multiply by 'cycling' through periodic phases in which the cells become larger (G1), double their genome (S) and eventually divide in two daughter cells in the M-phase (see Fig. 1). This 'cell cycle' is under very tight control, since uncontrolled growth of human tissue is characteristic for the development of cancer. Several proteins are involved in this regulation process with cyclins and cyclin-dependent kinases (cdk) being the key players. The binding of cdk to cyclin leads to phosphorylation of further regulatory proteins allowing the cell to proceed into the next phase of the cell cycle. Several cancer treatments are now focussing on inhibition of cdks in the cell resulting in cell cycle arrest (G_0) and in tumor selective apoptosis (programmed cell death).

The long process of identification and optimisation of potential inhibitors and their usability as drugs is now largely supported by the use of structural biology techniques [1,2], in particular by X-ray crystallography, which is used for protein structure determination at the atomic level (Fig. 2).
Using synchrotron radiation for protein crystallography has several advantages. At BESSY, the resolution of a data set is approx. 0.5-0.8 Å higher and the data collection time for a complex data set is reduced by a factor of 10-15 compared to our home source. The data quality from otherwise too small crystals is excellent with very accurate data (low R factors) in low resolution shells.

Knowing the three-dimensional structure, the interaction of the compound with the target protein can be studied. The binding mode of the inhibitor reveals regions which should be conserved or can be modified in the inhibitor in order to improve specificity and activity. Moreover, the size and the characteristics of the binding niche can be analysed in detail for additional features, e.g. water binding sites and hydrophilic/hydrophobic areas. Thus, crystal structures of protein-ligand complexes are starting points for further structure-guided approaches, and hence, speeding up the lead optimisation process.

Proteins of the cdk-family belong to the protein kinase class of enzymes which catalyse the transfer of the terminal phosphate from an adenosine triphosphate (ATP) molecule to the hydroxyl group of a tyrosine, serine, or threonine residue on an acceptor protein. Protein kinases have a highly conserved catalytic core of about 300 residues. The core structure consists of two lobes with the binding site of ATP located between these lobes (Fig. 3). This ATP binding site is the target for cdk-inhibitor molecules.

References:

[1] S.W. Muchmore et al., Curr Opin Drug Disc Dev, 6(4) 544-549 (2003)

[2] T.L. Blundell et al., Nat Rev Drug Disc, 1(1) 45-54 (2002)

[3] I.R. Hardcastle et al., Annu Rev Pharmacol Toxicol, 42 325-348 (2002)

[4] P. Furet, Curr Med Chem Anti Cancer Agents, 3 15-23 (2003)

[5] T.G. Davies et al., Structure, 9 389-397 (2001)

[6] R. Jautelat et al., in preparation

Acknowledgements:

The cdk2-ligand structures were all solved by Martina Schäfer, Structural Biology, Schering AG. The protein solution for crystallisation was provided by Uwe Eberspächer, Protein Chemistry, Schering AG.

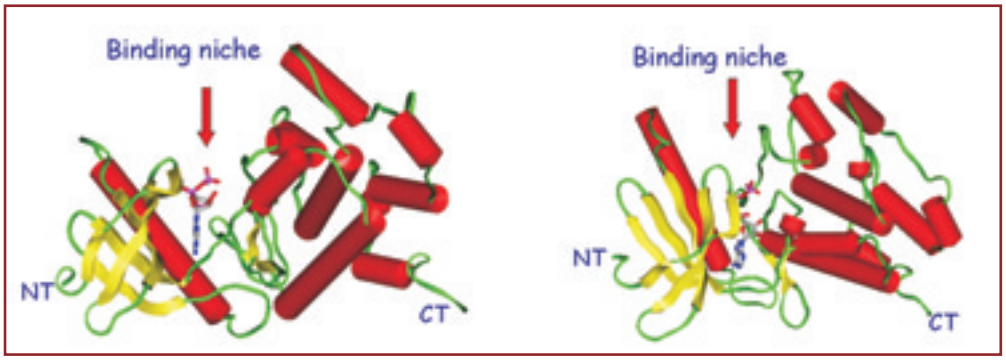

Fig. 3:
Structural cartoon of the catalytic core of a protein kinase showing the N- and C-terminal lobes and the binding niche of ATP and ATP-competitive inhibitors. Helices are depicted as red cylinders, β-strands as yellow bands. The cartoon on the right was tilted slightly along the x- and y-axes (NT = N-terminus, CT= C-terminus).

Extensive X-ray crystallographic studies have been carried out on cdk2 making this protein one of the best structurally characterised member of the protein kinase family [3,4,5]. More than 40 cdk2-ligand structures have been deposited in the Protein Data Base (http://www.rcsb.org/pdb) with ligands of various sizes and scaffolds.

However, this enormous amount of structures is not sufficient to explain the structure-activity relationships of all cdk2 inhibitors, since the orientation of the two lobes relative to each other and the flexibility of the nucleotide binding loop in the active site (which interacts with the phosphate moiety of ATP) often varies between different inhibitor scaffolds and thus renders the prediction of binding modes for compounds with new scaffolds difficult.

At Schering, a lead discovery programme was initiated on cdk2-inhibitors resulting in three classes of lead compounds: the aminopyrimidines, the pyrazoles and the indirubins. As expected, all the inhibitors bind in the deep groove between the N- and C-terminal lobe (Fig. 3). The three compound classes mimic the adenine ring of ATP (Fig. 4) and bind via two or three H-bonds to the hinge region of the protein between the two lobes (see Fig. 5 for the binding mode of the initial indirubin structure). The first hits within these compound classes were far from being optimal. Either the solubility of the compounds was very low (<0.1 mg/l) or the potency to bind to the enzyme was insufficient (>2 µM). Indirubins were modified to optimise their binding potency and to increase their solubility by introducing polar side chains in the structure. These modifications resulted in highly soluble compounds (>40 g/l) with a binding potency increased by a factor of thousand. X-ray structures of the optimised ligands for instance showed specific interactions of an introduced sulfonamide group with the backbone amide of Asp145 of cdk2 [6] thus increasing the binding contacts and hence the potency to bind to the enzyme (Fig. 5). Those compounds should become better 'brakes' for the unresting cell cycle in cancer cells.

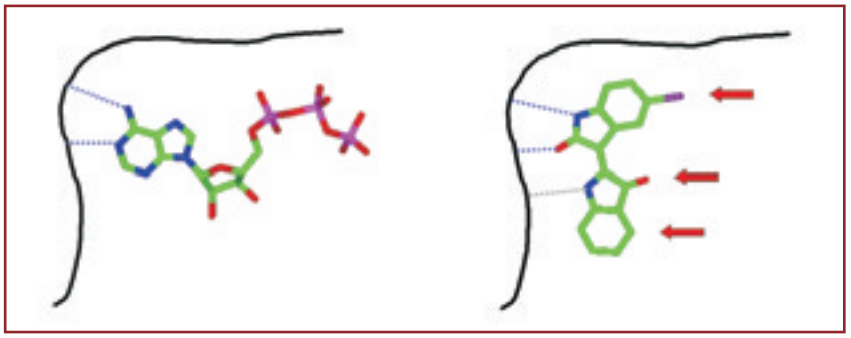

Fig. 4:
Mimicking ATP by Indirubin. Similar hydrogen bonds of ATP and indirubin to the protein are coloured in blue, an additional hydrogen bond of indirubin is highlighted in grey. Arrows indicate areas which are amenable to optimisation of the ligand.

However, the results are only the beginning of a long process to develop effective drugs to fight cancer. Many more crystal structures are needed to fulfil this ambitious goal. Accuracy and speed of data collection at synchrotrons facilitates to achieve the necessary throughput in X-ray structure analysis. In the past year for instance, Schering collected 25 data sets in 5 shifts (≈40 h) of beam time showing the very efficient data collection opportunities. In addition, the possibility to transport large amounts of crystals in liquid nitrogen and further automatisation at the beamlines will greatly enhance the efficiency of data and structure output.

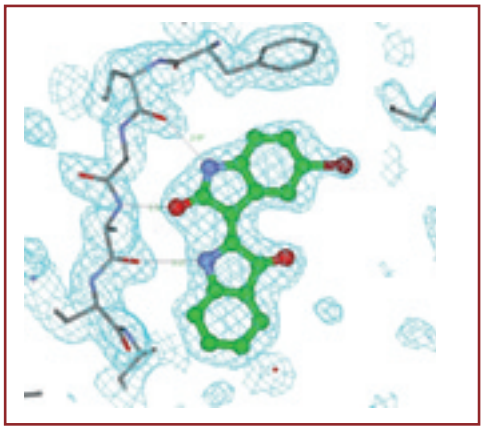

Fig. 5:
Electron density for the initial indirubin hit at the active site of cdk2. The purple sphere represents an area in the molecule where introduced changes in the molecular structure can improve binding and solubility of indirubin derivative.

Contact:
Ursula Egner
Ursula.Egner@Schering.de

X-rays shed light on the 'hidden' interfaces of solar cells

Ch.-H. Fischer[1], M. Bär[1], A. Grimm[1], I. Kötschau[1], I. Lauermann[1], J. Reichardt[1], S. Sokoll[1], M. Aggour[1], H.-J. Lewerenz[1], M.C. Lux-Steiner[1], L. Weinhardt[2], O. Fuchs[2], C. Heske[2], C. Jung[3], W. Gudat[3], T. P. Niesen[4], S. Visbeck[4], F. Karg[4]

1 Hahn-Meitner-Institut, Berlin

2 Experimentelle Physik II, Universität Würzburg

3 BESSY, Berlin

4 Shell Solar GmbH, München

The world-wide demand for energy is steadily increasing while the use of fossil fuels and nuclear energy is causing growing environmental problems. Furthermore, the world's resources of both fossil and nuclear fuels are limited and some will be depleted in the near future. The direct conversion of solar energy into electricity by photovoltaics is one way of meeting the energy demand in the future in a sustainable way. Solar cells are traditionally produced of crystalline silicon, achieving at best an efficiency of 24%. Alternative materials have also been tested or are in production. Among these, chalcopyrite thin film solar cells are very promising because of lower material consumption, cheaper deposition methods, shorter energy pay-back times, and, nevertheless, high conversion efficiencies (η > 19 % [1]).

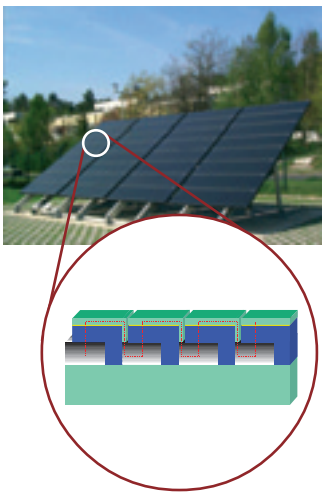

Fig. 1: Test array for CIGSSe solar modules at the Hahn-Meiter-Institut (for details see Fig. 5).

Fig. 2: CISSY endstation at BESSY.

Solar cells and modules (Fig.1) based on the chalcopyrites Cu(In,Ga)(S,Se)$_2$ ('CIGSSe') are complex layer systems. As an example, Fig. 3 shows a schematic drawing and a scanning electron micrograph of a solar cell cross-section. The industrial preparation of the layers involves thermal and chemical energy impact, which can lead to intermixing and reactions at the interfaces. This, in turn, strongly influences the performance of the solar cells. In the past, progress of the CIGSSe technology was widely based on empirical know-how and a trial and error approach. To push a knowledge-based development of solar modules of the next generation, the CISSY project was initiated. The CISSY endstation combines soft X-ray emission (XES) and photoelectron (PES) spectroscopy with in-system preparation in one single ultra-high vacuum apparatus, allowing the layer deposition to be interrupted for the analysis of (buried) interfaces, surfaces, and layers without exposure to ambient conditions (Fig. 2).

XES and PES have been shown to provide valuable complementary information about the chemical composition from different depth (XES ~100 nm, PES ~1 nm) as well as laterally resolved composition maps of the cells [2]. We used the CISSY endstation (at U41-PGM) to investigate different etching procedures in order to optimise efficiencies and to study aging and long-term stability of chalcopyrite modules.

One promising material for solar cells currently under investigation is $CuInS_2$ (CIS). In order to achieve high solar cell efficiencies, the CIS absorber layers have to be deposited with an excess of copper. A consequence of this preparation method is the formation of a copper sulphide segregation layer at the surface. This layer is typically removed by potassium cyanide (KCN) etching. Since KCN is a highly toxic compound, alternative etching techniques have been developed, i.e. an electrochemical etching method introduced by Lewerenz et al. [3]. However, the cell efficiencies were much reduced (η ~3%).

Using the CISSY endstation we employed sulphur $L_{2,3}$ XES spectra to establish the differences between several etching techniques in comparison to the pre-etching conditions (Fig. 4). A detailed analysis of the S 3s→2p peak positions (close to 148 eV) and the transitions from the upper valence band (Cu 3d, In 5s, Se 4s, Se 4p) at higher energies reveals a reduction of the copper sulphide contribution after electro-etching as compared to the non-etched sample (Fig. 4; right panel). However, the spectra still differ from those of the CIS reference crystal and the KCN-etched CIS, in particular, with respect to the S-In bonds (154-156 eV).

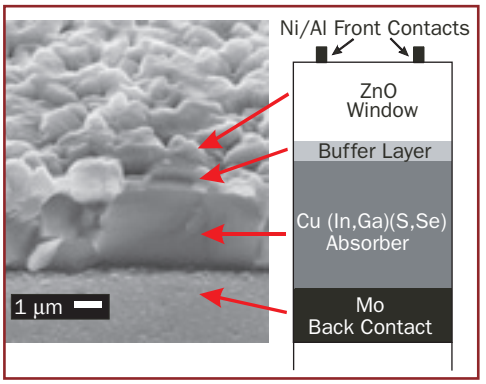

Fig. 3: Scanning electron micrograph of a chalcopyrite solar cell with its functional layers.

References:

[1] K. Ramanathan et al., Prog. Photovolt.: Res. Appl. 11, 225 (2003).

[2] C. Heske, Appl. Phys. A, in print.

[3] M. Aggour et al., Thin Solid Films 403-404, 57 (2002)

[4] Ch.-H. Fischer et al. to be published

Acknowledgements:

Funded by BMWi and BMBF

Based on these results we were able to improve the etching process to obtain chalcopyrite solar cells with up to 8% efficiency.

One particular advantage of chalcopyrite solar cells is that this technology offers cost-efficient preparation of monolithically integrated modules by single layer deposition on large area substrates. After deposition, the layers are sectioned by laser or mechanical 'scribing', leading to an array of solar cells, which are connected by an overlapping, conducting n-ZnO layer (see insert Fig. 1). To fulfil the requirements for long-term stability the modules have to be encapsulated, at present. In particular the scribe lines of the modules are a potential origin of device instabilities, e.g. due to oxidation. The identification of such local changes demands spatially resolved characterisation methods, which can be provided by CISSY [4].

To study alteration processes we examined a CIGSSe module test structure without encapsulation before and after accelerated ageing tests. For the XES line scans the modules were moved under the beam spot (50 x 800 µm^2) perpendicular to the scribe line while recording the integral sulphur $L_{2,3}$ XES signal (140-165 eV). The scribe lines P2 and P3 can be identified as maxima, since the surface of the Mo layer is sulphurised during absorber preparation (Fig. 5b). The S-XES signal in the P2 line is reduced as compared to the P3 line due to a thin n-ZnO cover layer.

After the accelerated ageing test (DH test), during which the sample is exposed for 100 h to damp-heat (DH), i.e. 85°C at 85% relative humidity, the fluorescence signal in the P2 scribe is strongly enhanced (Fig. 5b). While the S-XES spectrum before DH points to a contribution of MoS_2 and CIGSSe (due to particles remaining from the scribing process) the spectrum after DH reveals a pronounced contribution of sulfate (Fig. 5c). Complementary PES measurements show the extension of this alteration up to the surface (data not shown). If the formation of (insulating) sulfate in the interconnects between the individual cells of a module will also be observed with thicker n-ZnO layers, one source of efficiency loss under environmental conditions is found.

The development of highly efficient CIGSSe thin film solar cells requires exploration of various material systems and preparation approaches. With its unique combination of preparation and analysis equipment, the CISSY endstation provides a valuable tool to enhance the CIGSSe research efforts.

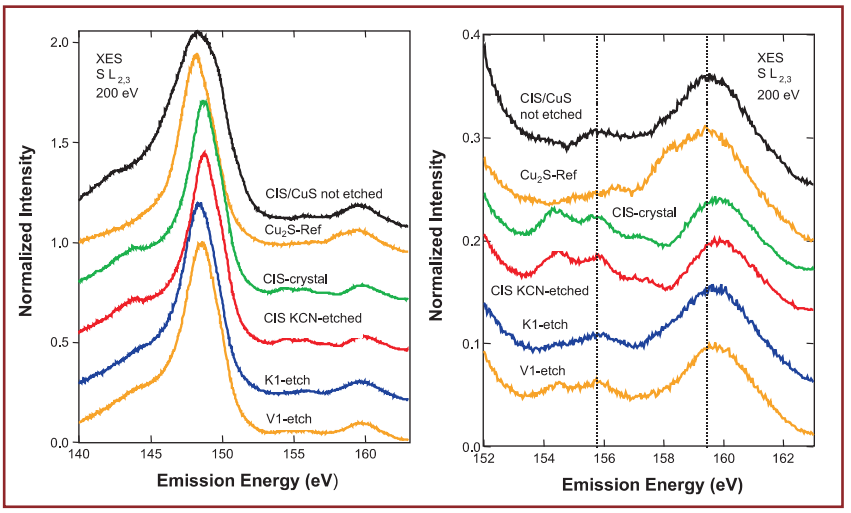

Fig. 4:
The range of the transitions from the upper valence band of the S $L_{2,3}$ XES spectra of CIS as deposited, KCN etched, and electrochemically etched with two different recipes (K1 and V1) together with CuS and $Cu2_s$ references. A detailed view of the spectra is shown in the right panel.

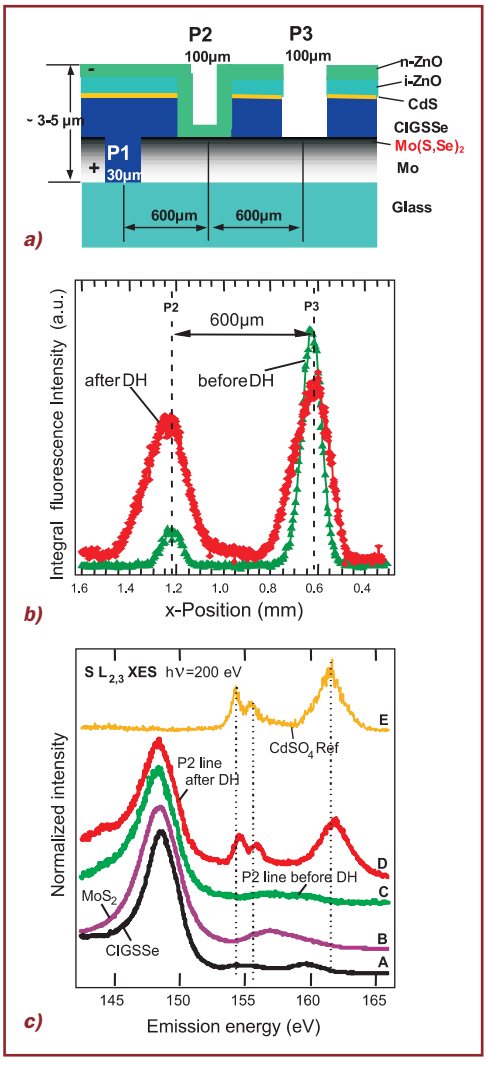

Fig. 5:

a: Schematic cross section of a CIGSSe test module.

b: S $L_{2,3}$ XES line scan over the test module perpendicular to the scribe lines before (green) and after (red) a damp-heat test. The spectrally integrated fluorescence signal (140-165 eV) is plotted via the local position.

c: S $L_{2,3}$ XES spectra from the P2 scribe line before and after damp-heat test. For comparison, the spectra of CIGSSe, MoS_2, and a metal sulfate are given.

Contact:
Christian-Herbert Fischer
Fischer@hmi.de

Watching electronic charge order in a crystal lattice

1
II. Physikalisches Institut, Universität zu Köln

2
Institut für Experimentalphysik, Freie Universität Berlin

Ch. Schüßler-Langeheine[1], J. Schlappa[1], Z. Hu[1], O. Friedt[1], E. Schierle[2], H. Ott[2], E. Weschke[2], G. Kaindl[2], M. Benomar[1], M. Braden[1], L. H. Tjeng[1]

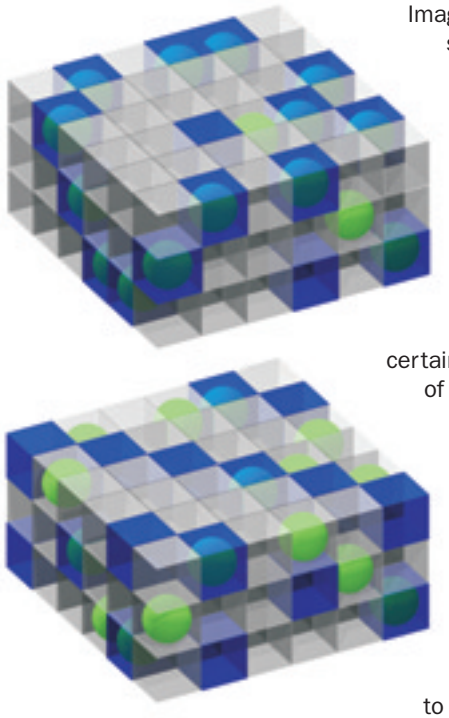

Fig. 1:
A doped crystal without (top) and with (bottom) charge order. The green spheres represent the dopant, the blue cubes are those with additional charge.

Imagine a block consisting of many small identical plastic cubes. Now add randomly some paint to the block, just enough to change the colour of a fraction of the small cubes. In the nanoworld, the block is a crystal of a transition-metal oxide; the small cubes are the lattice sites of the crystal. The colour indicates the number of electrons (or the valence) on a certain lattice site and the paint is made of doped atoms, 'impurities' in the crystal. Now, in the nanoworld something strange happens. Neighbouring cubes can exchange their colour (charge), even though the paint (the doped atom) stays in the same cube. In other words, the colour moves independenly from the paint. Theoreticians predict an even stranger thing to happen: When the block is cooled the coloured cubes start to arrange themselves in an ordered array or, in other words, the system develops charge order [1]. Charge order is believed to play an important role in some of the most spectacular effects in modern solid-state physics like high-temperature superconductivity [2], metal-insulator transitions and colossal magneto-resistance. This effect has been studied before by various techniques, but all experiments had in common that they were actually blind for different 'colours' (charge) and had to rely on indirect observations like the possibility of slightly different sized 'coloured' and 'uncoloured' cubes. We now apply a novel synchrotron-radiation based technique, which for the first time can see the 'colour' directly. Moreover, we can achieve a unique sensitivity to variations of the doping level in the sample allowing us to see that charge order is much better developed than it was believed to be.

First indications of charge order were found by neutron diffraction in La_2NiO_4, which can be doped by replacing La by Sr or by adding excess oxygen [3]. In this compound modulations in the bond length were observed, which are expected to be the consequence of charge order. However, since there is no contrast between lattice sites with different valence in neutron diffraction charge order can only be inferred indirectly. In order to study charge order directly, we use resonant soft X-ray diffraction, a newly developed synchrotron-radiation based technique, which combines electron spectroscopy with diffraction. In this technique, the photon energy for the scattering process corresponds to an electronic excitation in the sample (Fig. 2) and the excitation process is involved in resonant scattering as it is in X-ray absorption (XAS). For transition-metal oxides, such experiments are best performed at soft X-ray energies, where the intermediate state is either a transition-metal 3*d* or an oxygen 2*p* state, because these are the electronic states that determine the system properties. From XAS experiments it is known that the excitation energy and the shape of the excitation multiplet is extremely sensitive to the valence of the ion. The excitation process is also sensitive to the orientation of orbitals in the intermediate state as well as to the orientation of magnetic moments in the sample. The latter is used in soft X-ray magnetic scattering. Therefore, not only charge order but also orbital and magnetic order can be studied.

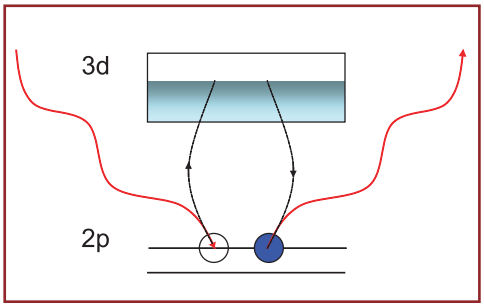

Fig. 2:
Resonant scattering process at a transition metals L_3 resonance (schematic).

References:

[1] J. B. Goodenough, Phys. Rev. 100, 564 (1955).

[2] J. Orenstein and A. J. Millis, Science 288, 468 (2000).

[3] J. M. Tranquada et al., Phys. Rev. Lett. 73, 1003 (1994).

[4] H. Yoshizawa et al., PRB 61, R854 (2000).

Acknowledgments:

Supported by the DFG through SFB 608 and by the BMBF.

The experimental challenge comes from the strong absorption of soft X-ray photons. Unlike for higher energy X-rays, which can propagate through air over meters and allow to build complicated diffractometer with many degrees of freedom, a soft X-ray diffraction experiment has to be built up completely inside vacuum. This leads to serious restrictions for sample movement and cooling, temperature measurement etc. For our experiment, we used the two-circle ultrahigh-vacuum diffractometer built at the Freie Universität Berlin, which provides an open axis to mount the sample directly to a cryostat for good cooling and reliable temperature measurement (Fig. 3). As our first sample we chose a single crystal of $La_{1.8}Sr_{0.2}NiO_{4.04}$ which was grown in our lab in Cologne. The proposed structure for this layered perovskite consists in stripes of Ni^{3+} going diagonally through the NiO_2 planes (Fig. 4). In the magnetically ordered phase, these Ni^{3+} stripes form antiphase domain walls for the antiferromagnetic order on the Ni^{2+} sites. Both, the charge order and the magnetic order lead to additional superstructure peaks in the diffraction pattern, whose positions in momentum space depend on the doping level.

Both superstructure peaks show pronounced energy dependence and a huge resonant enhancement at the Ni resonances. Fig. 5 shows the charge order superstructure peak at a photon energy corresponding to the Ni L_3 resonance in comparison to neutron scattering data from the same crystal. Interestingly, the charge order superstructure peak as observed by resonant soft X-ray scattering is about 10 times narrower than the one observed by all other scattering techniques before. From these old results it was concluded that the charge order is not well developed. This interpretation, however, is wrong, because the larger peak width observed with, e.g., neutrons is only caused by slight variations of the oxygen content across the sample, which appears to be inherent to all samples studied so far in the literature. The well focused X-ray beam available at the beamlines U49/2-PGM1 and UE52-SGM together with the relatively short penetration depth of soft X-rays allows us to choose a homogeneous part of our sample for the experiment, while other scattering techniques, which are integrating over larger sample volumes, see only a broad superposition of superstructure peaks from different compositions. Locally the charge order is much better developed than it was believed before. Apparently reliable information about the correlation length of charge order can only be obtained properly with well-focused soft X-ray beams.

A microscopic analysis of our results is presently being carried out based on an extension of the atomic multiplet configuration interaction model successfully used for XAS data. Very detailed information about order phenomena can be expected that no other technique can provide.

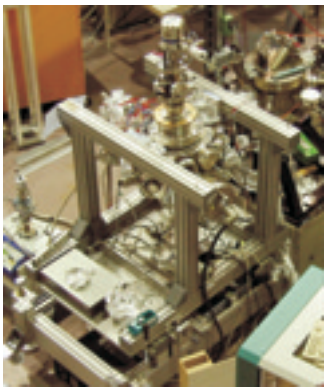

Fig. 3:
UHV soft X-ray diffractometer at UE52/SGM1.

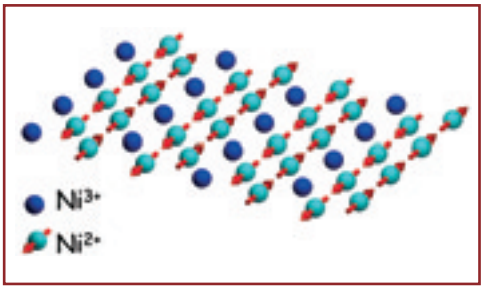

Fig. 4:
Model for the charge and magnetic order in the NiO_2 planes of 1/3 doped La_2NiO_4. The arrows show the orientation of the magnetic moments. Oxygen atoms are not shown (after Ref. 4).

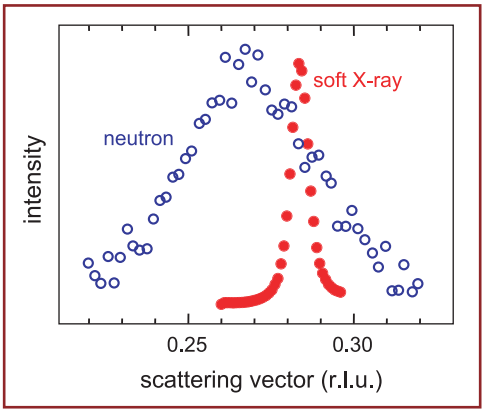

Fig. 5:
Soft X-ray diffraction data from the charge-order superstructure peak in $La_{1.8}Sr_{0.2}NiO_{4.04}$ (red). For comparison neutron data from the same single crystal are shown (blue).

Contact:
Christian Schüßler-Langeheine
schuessler@ph2.uni-koeln.de

Caution: Supramolecules under stress may become magnetic

Y. Bodenthin[1], U. Pietsch[1], D. Kurth[2], Th. Geue[1], J. Grenzer[1], H. Möhwald[2]

1 Institut für Physik, Universität Potsdam

2 Max-Planck-Institut für Kolloid- und Grenzflächenforschung, Golm

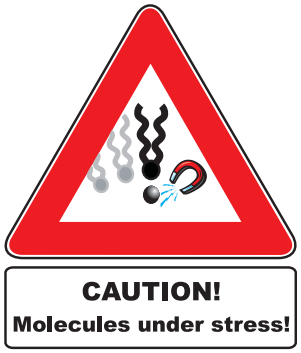

Using the big variety of structural elements of bigger (organic) molecular assemblies like a building brick kit allows to construct thin layers with the preferred properties at either sides. Thin films of supramolecular assemblies extracted from an aqueous solution show physical properties quite different of bulk samples or solid layers. Due to their higher flexibility they can be switched by structural changes.

For example, magnetism in the bulk is a subject of great technological potential and widely investigated in basic research. Here we choose a system with unusual magnetic behaviour. We observed a high temperature mechanism of molecular magnetism that differs from that of other magnetic materials, in which spin ordering competes with thermal disorder.

Combining various synchrotron radiation techniques we investigated thin films of metallo-supramolecular assemblies which show a transition from diamagnetism to paramagnetism above room temperature. A paramagnetic material has permanent magnetic moments which can be aligned in an external field, while those of a diamagnetic material have to be first created by the field and are oriented against it. We found that a change in the structure induces sufficient mechanical stress strong enough to induce a spin crossover from a non-magnetic state to a magnetic state.

The system is based on metallo-polyelectrolytes (MEPE) and is prepared in an aqueous solution by self-assembly of ditopic 1,4-bis(2,2':6',2''-terpyridin-4'-yl)benzene and Fe^{2+} ions [1] (Fig. 1). Subsequent self-assembly of metallo-polyelectrolytes and dihexadecyl phosphate amphiphiles (DHP) results in a completely non-covalent, hydrophobic polyelectrolyte-amphiphile-complex (PAC) [2]. Thin films of PAC were prepared by means of Langmuir Blodgett technique. Typically the films consist of 15 monolayers on solid support.

We determined the magnetic moment of the Fe^{2+} ions in X-ray magnetic circular dichroism (XMCD) experiments in reflection mode performed at the UE 56-1 PGM.

The upper part of Fig. 2 shows the reflectivity of the multilayer measured under grazing incidence (α_i=2°) using left and right circularly polarised light (I_+, I_- respectively). A magnetic field of about 3,000 Oe supplied by permanent magnets was applied in a longitudinal geometry. Due to the $1/E^2$ dependence of the reflectivity coefficient the overall reflectivity decreases as a function of energy. Additionally, there are two minima at about 706 eV and 718 eV corresponding to the L_3 and L_2 absorption edges of iron [3]. A resonant dichroic signal up to 3 % was found which is a clear evidence for molecular magnetism. Applying ab initio calculations [4] and sum rules to the absorption parts we obtained a magnetic moment of (0.5±0.3) μ_B per iron ion. This value is in a qualitative agreement with the results of spin-resolved neutron reflectivity and SQUID measurements [5].

In order to determine the origin of the diamagnetic-paramagnetic transition we have studied the coordination sphere of iron ions using Extended X-ray Absorption Fine Structure (EXAFS) measurements [6]. The experiments were performed at the KMC2 beamline exploiting the fluorescence signal of the iron ions.

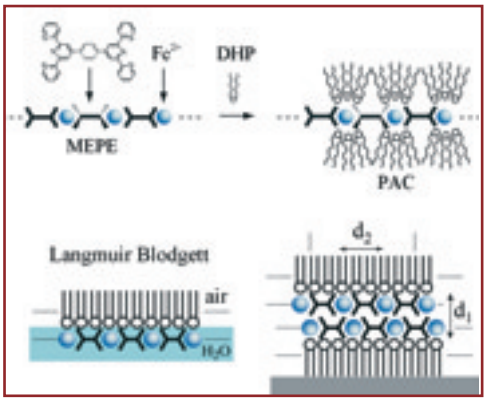

Fig. 1:
Self-assemblies of ditopic bis-terpyridine ligands, transition metal ions and amphiphiles results in metallo-supramolecular coordination polyelectrolytes (MEPEs) and the corresponding polyelectrolyte-amphiphile complexes (PACs). Thin films of PAC were prepared by means of Langmuir-Blodgett technique.

References:

[1] M. Schütte et al., Angew. Chem. Int. Ed. 37, 2891-2893 (1998)

[2] D. G. Kurth et al., Proc. Natl. Acad. Sci. 97 , 5704- 5707 (2000)

[3] C.T. Chen et al., Phys. Rev.Lett. 75, 152 (1995)

[4] J. Kuneš et al., Magn. Materials 240, 454-456 (2002)

[5] Y. Bodenthin, U. Pietsch, ILL Experimental report, 7-09-72, (2002)

[6] J. Als-Nielsen, D. McMorrow, Elements of Modern X-Ray Physics, John Wiley and Sons Ltd,

[7] Y. Bodenthin et al., Synchr. Rad. 9, 206-209, (2002)

Acknowledgements:

This work is supported by the DFG.

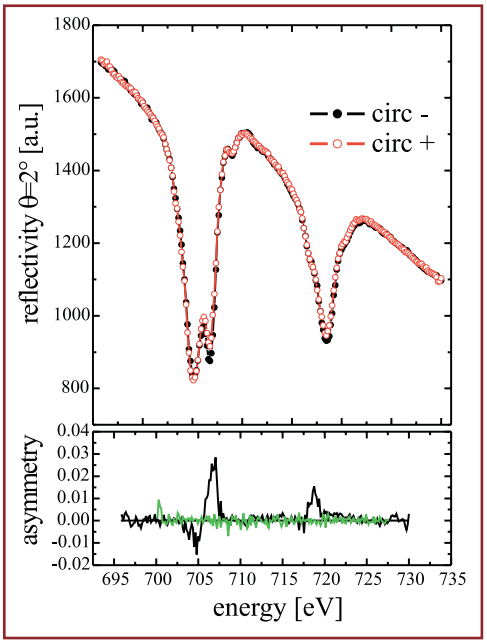

Fig. 2:
XMCD measurements at the $L_{3,2}$ edge of iron (top). Bottom: The asymmetry A(E) = $(I_+ - I_-)/(I_+ + I_-)$ between left and right circularly polarised light indicates the appearance of molecular magnetism. The green line indicates A(E) without an applied magnetic field.

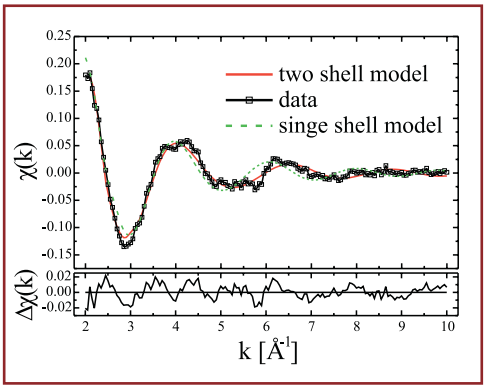

Fig. 3:
Typical EXAFS function of PAC films. The data can only fitted using a two shell model with iron-nitrogen distances r_1 = 0.176 nm and r_2 = 0.218 nm and occupation numbers 4 and 2, respectively.

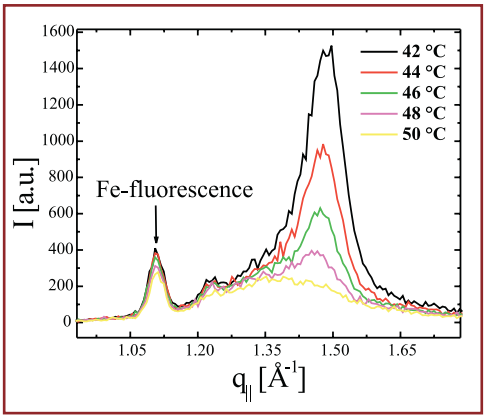

Fig. 4:
Temperature resolved grazing incidence diffraction measurements of a PAC Langmuir Blodgett film. The amphiphile phase transition is indicated by the loss of the in-plane diffraction peak (yellow curve).

The measured EXAFS can only be simulated by a two-shell model assuming two different Fe-N bond distances, r_1= (0.176±0.002) nm and r_2=(0.218±0.002) nm, and occupation numbers of 4 and 2, respectively.
Fig. 3 shows a typical EXAFS function of PAC measured at the iron K edge. These values correspond to a deformed octahedral ligand field with the long axis parallel to the sample surface. With increasing temperature (T > 45°C) the average distance increases from 0.197 to 0.201 nm, whereas the ratio r_2/r_1 remains unchanged at 1.24. The increasing size of the Fe-N octahedron might be accompanied with an additional shear deformation which would be in accordance with the strong rearrangement of the film structure observed in temperature resolved measurements of the energy-dispersive X-ray reflectivity (EDR) and in-plane diffraction (GID) [7]. These measurements were simultaneously performed at the EDR beamline. The EDR data reveals thickness oscillations as well as Bragg peaks, confirming the high ordering of the supramolecular units with an interlayer lattice spacing of d_1=(5.6±0.1) nm. This spacing corresponds to the head-to-head arrangement of two adjacent polyelectrolyte-amphiphile-complex layers. In addition, a distinct in-plane ordering was observed characterised by the appearance of a single in-plane Bragg peak with an in-plane lattice parameter of d_2=(0.42±0.01) nm. Therefore, the DHP alkyl chains are hexagonal packed.

Upon heating, both the in-plane and out-of-plane ordering change indicating a phase transition. Above 45°C, we observe a change of the interlayer spacing from d_1=(5.6 ± 0.1) nm to (5.2 ± 0.1) nm related to the disappearance of one MEPE layer (Fig. 5). Additionally, the in-plane Bragg peak reduces (Fig. 4). At this temperature, the alkyl chains of DHP undergo a phase transition from a laterally ordered into a free rotator phase inducing stress to the Fe-N octahedron. Upon cooling, the in-plane Bragg peak is recovered indicating the reversibility of this phase transition. The disorder of the amphiphilic molecules induces a deformation of the Fe-N octahedron, which reduces the effective energy gap between low and high spin states and opens the way for spin crossover. The system becomes paramagnetic.

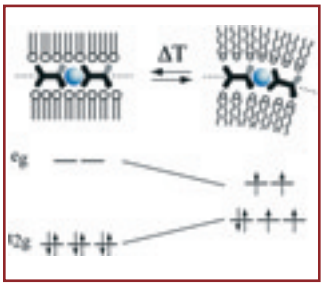

Fig. 5:
Key concept: The temperature induced phase transition in the amphiphilic mesophase is utilized to distort the coordination geometry of the metal centres. Consequently, the energetic separation of the subsets of the orbitals changes giving rise to spin crossover.

Contact:
Ullrich Pietsch
upietsch@rz.uni-potsdam.de
Yves Bodenthin
bodenth@rz.uni-potsdam.de

Bottom-up nano-technology: molecular engineering at surfaces

S. Stepanow[1], M. Lingenfelder[1], A. Dmitriev[1], N. Lin[1], Th. Strunskus[2], Ch. Wöll[2], J.V. Barth[3,4], K. Kern[1,3]

1 Max-Planck-Institut für Festkörperforschung, Stuttgart,
2 Lehrstuhl für Physikalische Chemie I, Ruhr-Universität Bochum,
3 Institut de Physique des Nanostructures, Ecole Polytechnique Fédérale de Lausanne, Schweiz
4 Advanced Materials and Process Engineering Laboratory, University of British Columbia, Vancouver, Canada

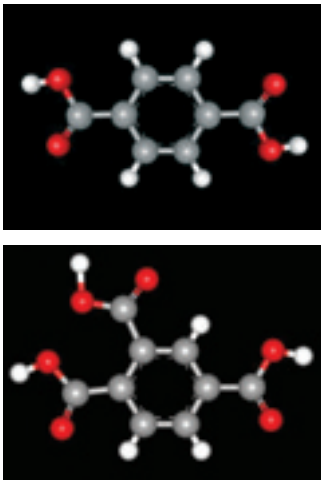

Fig. 1:
Terephthalic acid - tpa (top) and Trimellitic acid - tmla (bottom) comprise two respectively three functional carboxyl groups.

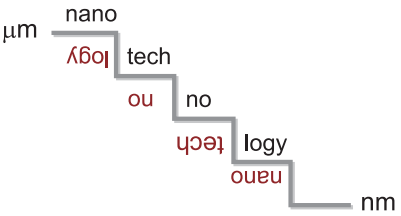

A key issue in nanotechnology is the development of conceptually simple construction techniques for the mass fabrication of identical nanoscale structures. Conventional top down fabrication techniques are both top down fabrication techniques are both energy intensive and wasteful, because many production steps involve depositing unstructured layers and then patterning them by removing most of the deposited films. Furthermore, increasingly expensive fabrication facilities are required as the feature size decreases. The natural alternative to the top-down construction is the bottom-up approach, in which nanoscale structures are obtained from their atomic and molecular constituents by self-organised growth. Self-organised growth can be driven by thermodynamic forces or be the result of kinetic processes. The archetype of a thermodynamically driven structure formation at the mesoscopic scale is molecular self-assembly. This refers to the spontaneous association of molecules under conditions close to equilibrium into stable, well defined nanostructures joined by noncovalent bonds; it is one of the key building principles of all living matter [1]. To make full use of this approach in nanotechnology we have to understand the noncovalent intermolecular interactions and to develop methods to manipulate them in a controlled way [2].

We have performed combined scanning tunnelling microscopy (STM) and synchrotron investigations addressing the bonding, ordering and surface chemistry of the related molecules 1,4-benzenedicarboxylic acid (terephthalic acid - *tpa*) and 1,2,4-benzenetricarboxylic acid (trimellitic acid - *tmla*) on the Cu(100) surface. Molecules of this type are frequently employed in 3-D crystal engineering [3] and have proven to be useful for the fabrication of nanoporous supramolecular layers [4-7]. The molecules *tpa* and *tmla* with their respective twofold and threefold exodentate functionality are shown in Fig. 1. While the formation of organic layers and nano-structures can be nicely monitored by STM, X-ray photoelectron spectroscopy (XPS) and near-edge X-ray absorption fine structure (NEXAFS) resolve conclusively the deprotonation of carboxylic acid group and molecular orientation.

Distinct hydrogen-bonded assemblies were obtained at low temperature (up to 275 K) with *tpa*. The STM image in Fig. 2 reveals that molecular ribbons evolve on the square substrate. The corresponding C 1s and O 1s XPS data confirm that the *tpa* carboxyl groups remain largely complete, i.e., the well-known splitting of the C 1s peak is observed reflecting the contribution from the atoms in carboxyl and phenyl moieties at an

Fig. 2:
Low-temperature supramolecular ordering of tpa on Cu(100): H-bonded molecular ribbons clearly resolved by STM are stable up to 275 K. In the corresponding O 1s XPS data a broadened peak appears due to overlaping hydroxyl and carbonyl intensities, i.e., tpa carboxylic groups remain complete. In conjunction with the NEXAFS analysis demonstrating flat adsorption, the modeling indicates a 2-D H-bond coupling scheme.

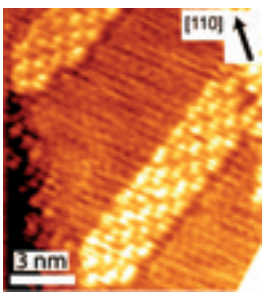

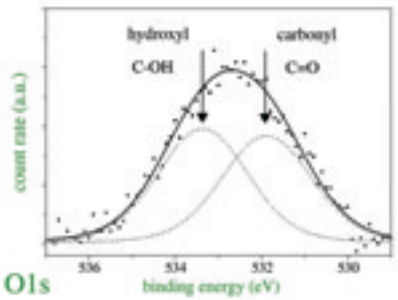

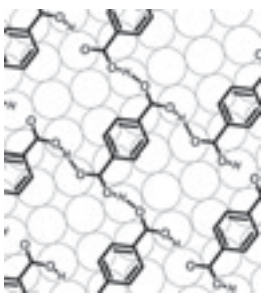

References:
[1] Lehn, J.-M. Supramolecular Chemistry, Concepts and Perspectives (VCH, Weinheim, 1995).
[2] J. V. Barth et al., Appl. Phys. A 76, 645 (2003).
[3] O.M. Yaghi et al., Nature 423, 705 (2003).
[4] A. Dmitriev et al., J. Phys. Chem. B 106, 6907 (2002).
[5] A. Dmitriev et al., Angew. Chem. Int. Ed. 41, 2670 (2003).
[6] M. A. Lingenfelder et al., Chem. Eur. J., in print (2004).
[7] S. Stepanow et al., Nature Mat., in print (2004).
[8] M. Wühn et al., Langmuir 17, 7605 (2001).
[9] C. Mainka et al., Surf. Sci. 341, L1055 (1995).
[10] D. S. Martin et al., Phys. Rev. B 66, 155427 (2002).

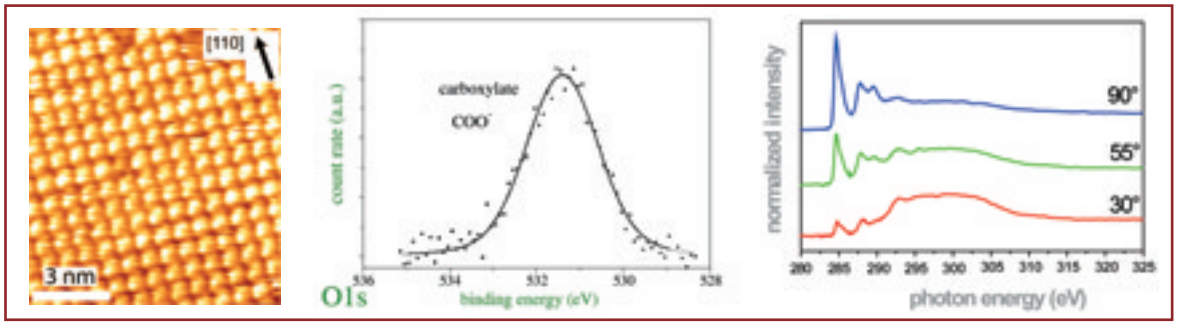

energy of 285.2 and 289.8 eV, respectively [8]. Accordingly, the O 1s peak appears broadened due to overlapping carbonyl and hydroxyl intensities (531.9 and 533.4 eV, Fig. 2). The NEXAFS analysis of this phase indicates that adsorption with the aromatic ring parallel to the substrate prevails. Interestingly, the modelling reveals that the H-bonds formed between the adsorbed molecules do not obey the R-COOH pairing motif typically observed for pure *tpa* or other carboxylic acids, rather the interplay between substrate corrugation and functional group interactions makes a lateral 2-D coupling scheme preferable. For the related case of low-temperature *tmla* adsorption (T < 200 K) synchrotron data similarly reveal flat adsorption of integral molecules. However, no supramolecular ordering could be observed by STM, which is associated with the reduced symmetry and mobility of the molecule.

At increased temperatures (T=300 - ~500 K) regular organic layers can be obtained with both molecules, already imaged by STM (Figs. 3,4). The photoemission data show that a (partial) deprotonation of the carboxylic acid groups occurs because of the catalytic activity of the Cu substrate. With tpa the formation of a biterephthalate is encountered, as deduced from the reduced separation of the splitted C 1s contributions (now at 285.1 and 288.2 eV, respectively) and the existence of a narrowed O1s peak centred at 531.4 eV (Fig. 3). Again the NEXAFS analysis reveals that the *tpa* phenyl ring is oriented parallel to the substrate lattice - the pronounced C 1s -> π* resonance exhibits a marked intensity variation with the angle of incidence. The fact that the intensity of the resonance does not vanish completely at an incidence angle of 90° as expected for a perfectly flat lying *tpa* molecule is attributed to adsorption induced intramolecular distortions, involving a bent of the CH-bonds out of the ring plane. Such distortions of aromatic compounds interacting with metal surfaces are observed frequently [9]. Surprisingly, the STM data show that the packing density with the negatively charged biterephthalate species is increased as compared to the integral molecule, which is associated with a lateral coupling scheme where the anionic *tpa* carboxylate groups are engaged in O···HC hydrogen bridges with phenyl rings of adjacent molecules. For comparison, on Cu(110) under similar conditions an upright standing monoterephthalate layer is formed [10]. This demonstrates that the geometry and symmetry of the substrate can be used to tune the orientation of functional organic layers. A somewhat different scenario is encountered with *tmla* layers evolving with the substrate held at elevated temperature (450 K), whose topography is shown in Fig. 4. Now the XPS data indicate merely a partial deprotonation of the carboxyl groups, which signals the formation of a monocarboxylate species. Moreover, the NEXAFS analysis of this phase clearly reveals a striking change in the bonding geometry (Fig. 4). The phenyl ring plane of the monotrimellate is, on average, oriented at an angle of approximately 65°±5° relative to the Cu(100) surface. This observation is consistent with the only partial deprotonation of the tmla molecule, where the carboxylate anchoring is dominated by just one of the three functional groups.

Fig. 3:
A molecular monolayer with a biterephthalate species is obtained upon room temperature deposition. STM data reveal an increased packing density of the overlayer lattice oriented along [110]. While the O 1s XPS data indicate a deprotonation of both tpa carboxyl groups, the NEXAFS analysis shows that the phenyl ring is oriented parallel to the substrate lattice.

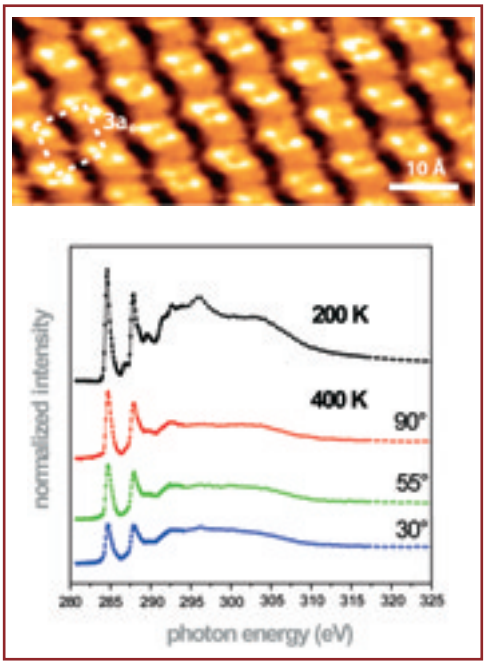

Fig. 4:
Regular organic layer upon deposition of tmla at 450 K, with a characteristic three-lobe inner structure of individual molecules in STM imaging. Corresponding NEXAFS data indicate a reorientation of the phenyl ring oriented approximately 65°±5° relative to the Cu(100) surface.

Contact
Johannes Barth
johannes.barth@epfl.ch
Thomas Strunskus
strunsku@pc.ruhr-uni-bochum.de

Queuing atoms: Self-Assembly of Silicide Nanowires

1 Institut für Festkörperphysik, Technische Universität Berlin

2 Institut für Festkörperphysik, Technische Universität Dresden,

C. Preinesberger[1], D.V. Vyalikh[2], S.L. Molodtsov[2], F. Schiller[2], G. Pruskil[1], S.K. Becker[1], C. Laubschat[2], M. Dähne[1]

Self-assembly, a spontaneous organisation of small building blocks to larger entities is inherent to many processes in nature. When passing an ice cream shop in a shopping mall, one can experience self-assembly of humans to a queue in front of the sales counter. Self-assembly also occurs on the atomic scale. It is a key to nanotechnology, allowing the growth of structures on solid surfaces. However, to be able to "manufacture" devices through this process, methods have to be explored to control the assembly procedure.

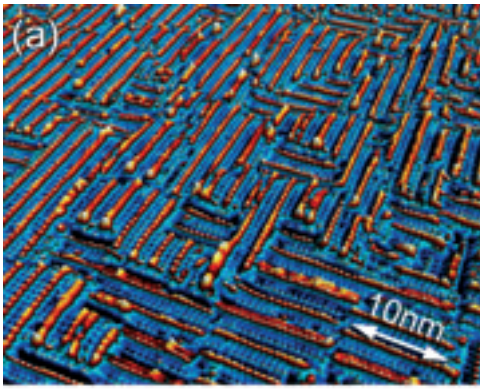

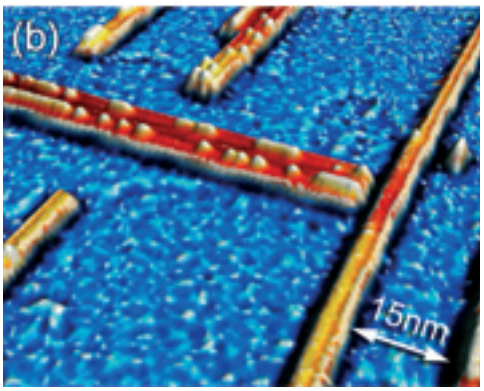

Fig. 1: Different nanowire types forming in a self-organised way on planar Si(001).

Self-assembly is of special interest to the manufactures of integrated circuits, especially microprocessors. Here the growth of one-dimensional silicide structures on silicon surfaces is a very promising candidate due to its compatibility with current device technology. With self-assembly nanostructures can be grown, which are easier to prepare, show lower defect density and obtain much smaller structure sizes than those formed on pre-patterned substrates using standard lithography. Such low-dimensional nanostructures show peculiar physical properties, which differ considerably from those of the respective bulk materials and are related to quantum effects on the nanometer scale.

One-dimensional rare-earth silicide structures can easily be produced by depositing about 1 Å of the rare earth onto clean Si(001) and subsequent heating at around 500°C [1-5]. A typical scanning tunnelling microscopy image of Dy silicide nanowires is shown in Fig. 1. Two structurally different nanowire types can be distinguished: dense arrays of thin nanowires and freestanding broad nanowires. The thin nanowires usually form a regular grating, which is characterised by a non-rectangular 7x2 unit cell [4,5]. The broad nanowires, in contrast, are much higher and have larger separation from their neighbours. They consist of hexagonal $DySi_2$, which grows under highly anisotropic strain on the Si(001) surface, causing the formation of long narrow nanowires:
In the strained direction, the nanowire width is limited to a few nm, similar to the case of strained quantum dots. In the unstrained direction, in contrast, unlimited growth is possible, and indeed nanowire lengths of more than 200 nm can be observed [3].

Because of the anisotropy of the Si(001) surface, the orientation of the nanowires rotates by 90° at every single surface step. For certain applications such as parallel data lines or X-ray gratings, a parallel alignment of the nanowires is required across the entire surface. Also for the investigation of the anisotropic electronic properties using angle-resolved photoelectron spectroscopy - as in the present study - a uniform alignment is desirable, so that the dispersion along and perpendicular to the wires can clearly be separated. Therefore strategies have to be developed to prevent the 90° turns at single surface steps.

Vicinal Si(001) surfaces with a misorientation of 3-4° in $[1\bar{1}0]$ direction are known to form double steps, so that the growth of

References:

[1] C. Preinesberger et al., J. Phys. D: Appl. Phys. 31, L43 (1998)

[2] M. Dähne et al., Adv. Solid State Phys 41, 227 (2001)

[3] C. Preinesberger et al., J. Appl. Phys. 91, 1695 (2002)

[4] C. Preinesberger et al., AIP Conf. Proc. 696, 837 (2003)

[5] S.K. Becker et al., Proc. 26th Int. Conf. Phys. Semicond.(2004)

Acknowledgements:

Supported by the DFG and the BMBF

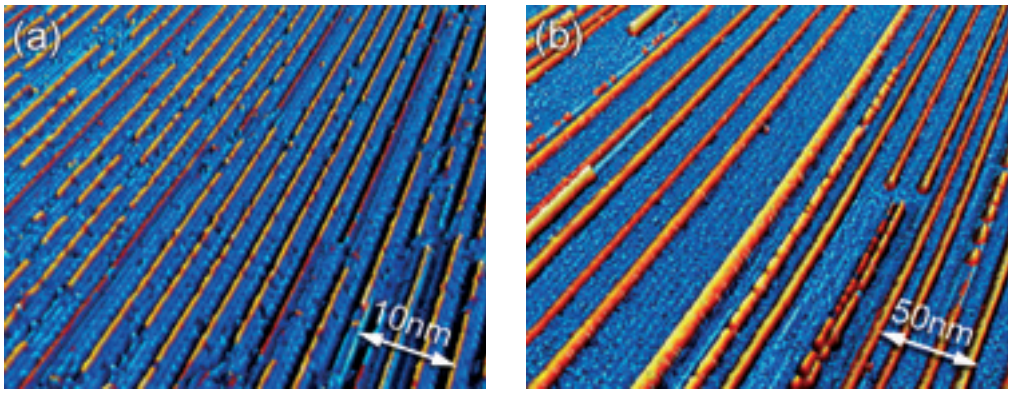

Fig. 2:
Parallel alignment of (a) thin as well as (b) broad nanowires on the vicinal Si(001) surface.

unidirectional nanowires along the direction can be expected. By deposition of 1 Å Dy on vicinal Si(001) and subsequent annealing, thin nanowires are formed at 500 °C and broad ones at 600°C, while both nanowire types show a nice parallel alignment across the entire sample surface (Fig. 2).

For these samples the electronic structure of both nanowire types were studied with angle-resolved photoelectron spectroscopy using a Vacuum Generators CLAM-4 spectrometer at the BUS beamline (U125/2-SGM). Representative spectra for the thin nanowires are shown in Fig. 3, and the corresponding colour images of the dispersion are presented in Fig. 4. Parallel to the nanowires, a strong dispersion of the electronic states is observed. In particular, two strongly dispersing states were found at the center and at the boundary of the surface Brillouin zone, which are crossing the Fermi energy. This behaviour clearly demonstrates a strong metallicity of the nanowires. In contrast, spectra taken perpendicular to the wires are not characterized by a significant dispersion, i.e. the nanowires are electronically well separated from each other. The data of the broad nanowires look very similar and are thus not shown here.

The observed strong one-dimensional metallic behaviour of the electronic states is an important property for future applications of these fascinating nanostructures.
The development of further techniques to control the formation of the nanowires is an important challenge for an incorporation of these nanowires into existing microprocessor technology.

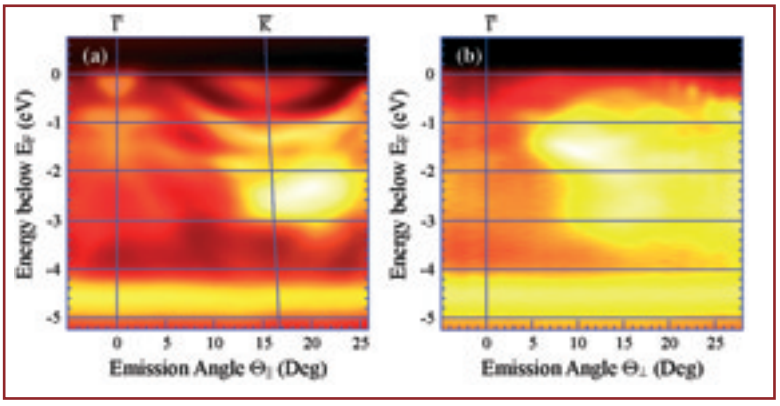

Fig. 4:
Colour image of the dispersion (a) parallel and (b) perpendicular to the thin nanowires.

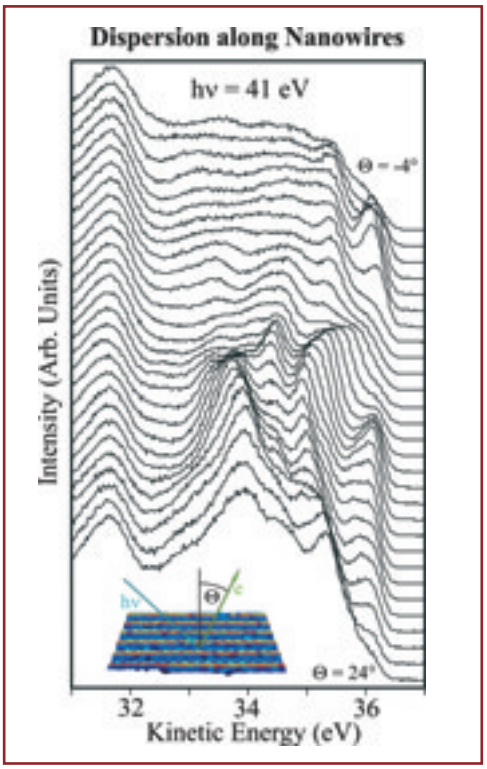

Fig. 3:
Angle-resolved photoelectron spectra showing the dispersion of the electronic states along the thin nanowires.

Contact:
Christian Preinesberger
preini@physik.tu-berlin.de
Mario Dähne
daehne@physik.tu-berlin.de

Lehrstuhl für Experimentalphysik/ Festkörperphysik Ruhr-Universität Bochum

Electrons journey across a magnetic sandwich

A. Nefedov, J. Grabis, A. Bergmann, F. Radu, H. Zabel

Imagine your favourite sandwich, i.e. two slices of toast in between a thick layer of for example salami. A stick holds the snack together. If you want a magnetic sandwich, you exchange the toast by two ferromagnetic layers, the salami by a non-magnetic metal. To learn more about your magnetic 'meal' you may use electrons as a 'stick'. While layers with the same magnetic orientation as the electron spin are easy to cross like soft bread those with opposite orientation are hardly permeable like thick slices of pumpernickel, bouncing back the electron. The giant magneto-resistance (GMR) effect, discovered only 15 years ago and applied today in hard disks, precision tools, and in ABS systems, requires exactly such a stack of at least three layers, as in the magnetic sandwich and is schematically shown in the left panel of Figure 1. For parallel alignment of the electron spins travelling in these layers, the resistance is low and for anti-parallel it is high. In zero magnetic field the GMR sensor has a high resistance due to the antiparallel orientation of the ferro-magnetic layers. With increasing field both layers rotate into the field direction thereby lowering their resistance. To enhance the effect a multilayer can be constructed with a periodic arrangement of the ferromagnetic layers and the non-magnetic metal spacer layers (see right panel of Fig. 1).

The prototype GMR multilayer consists of very thin Fe layers with a thickness of only a few nanometers separated by Cr spacer layers. The Cr layer thickness and the interface properties between Fe and Cr determine the sensitivity of the GMR device. Therefore, there is a great interest in the exploration and improvement of the interfacial magnetic properties. The structural properties can be analyzed via conventional X-ray scattering, which yields the layer thickness and the multilayer periodicity, as well as information on the interfacial disorder. However, with conventional X-ray scattering the magnetic properties of the multilayer remain hidden, since X-ray photons are not sensitive to the magnetic induction of the Fe layers. This is different for neutrons. As neutrons carry a magnetic moment, neutron reflectivity measurements reveal not only the structural but also the magnetic properties of the multilayer, including their magnetic periodicity. Recently, a method called X-ray resonant magnetic scattering (XRMS) [1] has been developed, making use of intense circularly polarised synchrotron light available at third generation synchrotron sources, such as BESSY. For a magnetic sample the X-ray absorption cross-sections for right and left circularly polarised light are different, leading to the magnetic signal referred to as the X-ray magnetic circular dichroism (XMCD) [2]. Using the element specificity additionally to the magnetic for diffraction purposes makes this method superior to neutron reflectivity. An overall higher sensitivity is achieved. This technique has been used in recent studies for the analysis of magnetic multilayers [3]. Still a quantitative fitting procedure is missing, which eventually will assist to exploit the full potential of this technique.

Fig. 2 reproduces magnetic X-ray reflectivity results, i.e. scattering at fixed angles, from an Fe/Cr multilayer [4]. The experiments were carried out at the bending magnet beamline PM3 and at the undulator beamline UE56/1 using the X-ray chamber ALICE of BESSY [5]. By tuning the incident energy to just below the Fe L_3 absorption edge, strong magnetic Bragg peaks are observed at the half-order and at the three-half peak position in units of the position of the first order structural Bragg peak associated with the chemical periodicity of the multilayer (black points in Fig. 2). Thus three orders of Bragg reflections are observed in addition to the interference fringes, originating from the finite thickness of the multilayer stack. These scattering features indicate a very high structural quality of the Fe/Cr multilayer with a roughness of not more than 0.3 nm at each interface.

References:

[1] G. an der Laan et al.,Synchro. Rad. News 12, 5 (1999)

[2] G. Schütz et al., Phys. Rev. Lett. 62, 2620 (1989)

[3] T.P.A. Hase et al., Physical Review B 61, 15331 (2000).

[4] A. Nefedov et al., submitted PRB

[5] J. Grabis et al., Review Scientific Instruments 74, 4048 (2003)

Acknowledgements:

This work was supported by BMBF.

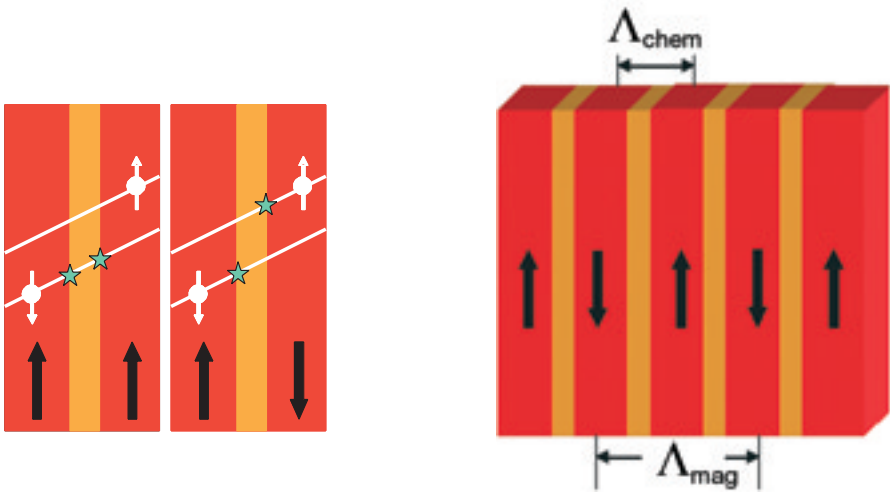

Fig. 1:
left: Transport of spin polarised electrons through a trilayer. right: A magnetic multilayer with antiparallel alignment of the ferromagnetic films, causes a doubling of the magnetic periodicity Λ_{mag} as compared to the chemical periodicity Λ_{chem}.

Furthermore, from the presence of a half-order peak in the reflectivity curve which is slightly detuned with respect to the specular condition (red points), two additional properties can be deduced: first, the individual ferromagnetic layers are decomposed into magnetic domains, and second, the ferromagnetic domains are strictly antiparallel correlated from left to right.

The magnetic field dependence of the first-order Bragg peak is sensitive to the total magnetization of the sample, while the half-order peak is sensitive to the degree of antiparallel alignment of the ferromagnetic layers. As expected, the hysteresis loop recorded at the half-order peak has a maximum in the remanent state (H = 0 Oe) and decreases with increasing magnetic field, just like the GMR effect itself (Fig. 3). Scans taken across the half-order peak in the transverse direction exhibit a sharp peak with a Lorentzian line profile superimposed on a flat shoulder of diffuse intensity. With increasing field the width of the central Lorentzian peak and the intensity of the diffuse intensity both drop by roughly a factor of two. From the Lorentzian line shape of the central half-order peak we infer a multidomain state in the remanent state of the sample, which diminishes with increasing field. At the same time the broad diffuse shoulder may reflect spin disorder at the Fe/Cr interface which also decreases with increasing field. Both components, the multidomain state and the interfacial spin disorder are instrumental for the performance and the sensitivity of the GMR device.

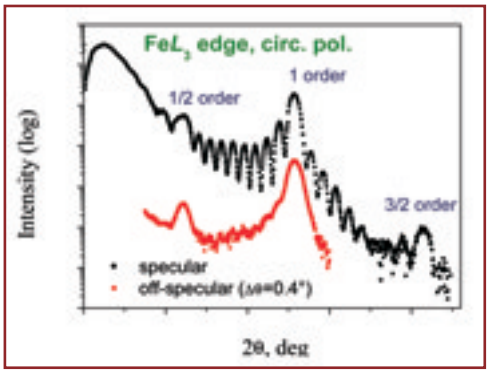

Fig. 2:
Magnetic X-ray reflectivity (black dots) from a Fe/Cr multilayer using circulary polarised X-rays tuned close to the L_3 absorption edge of Fe and slightly detuned from the specular condition (red points).

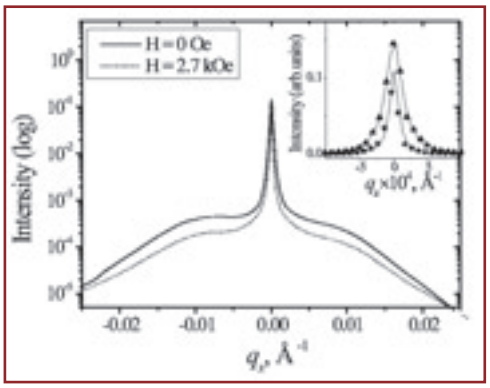

Fig. 3:
Transverse scans through the half-order peak measured with linearly polarised radiation in the remanent state (H = 0, solid line) and at the applied magnetic field H = + 2.7 kOe (dotted line). Inset: The sharp component of the transverse is shown on a linear scale. Symbols present the experimental data (triangles: H = 0 Oe, asterisks: H = 2.7 kOe), lines are corresponding fits with a Lorentzian line shape.

Contact:
Hartmut Zabel
Hartmut.Zabel@rub.de

The difference between manganese and manganese

1 BESSY, Berlin

2 Universität Würzburg

O. Rader[1], K. Fauth[2]

Who could tell the difference?

Switch on your computer, forget about booting, and start to work right away - this situation maybe soon realised with the help of spintronics. At the moment, two main parts of a computer make use of two different properties of electrons. In semiconducting microprocessors electrons are controlled via their charge while the ferromagnetic hard disks accomplish mass storage of data making use of the electron spin. An unit that would combine both electron properties could have capabilities significantly superior to present devices [1]. For the above mentioned convenience, a magnetic version of random access memories (MRAM) would be required which does not lose its information when switched off. Moreover, magnetic field effect transistors could switch currents of spin-polarised electrons by a magnetic instead of electric field. Programmable magnetic logic gates might revolutionise the way software is used in computing. And eventually, the ability to preserve coherent spin states in conventional semiconductors and quantum dots may enable quantum computing in the solid state.

Ferromagnetic semiconductors are the key materials to link the technologies of magnetic and electronic hardware devices. Europium sulfide is such a material but it is difficult to fabricate and has a low magnetic ordering temperature. A different approach, alloying a ferromagnetic metal with a nonmagnetic semiconductor does not necessarily lead to a ferromagnetic semiconductor as shown for manganese in II-VI semiconductors like $Cd_{1-x}Mn_xTe$. In 1996, however, $Ga_{1-x}Mn_xAs$, i. e., GaAs 'contaminated' with small amounts of Mn, was found to become ferromagnetic for concentrations x~0.05 at low temperature. Researchers were quickly raising the ferromagnetic ordering temperature T_c beyond 100 Kelvin [2], and recently T_c has been enhanced by a postgrowth annealing method up to 160 Kelvin, nurturing the hope that liquid nitrogen cooling still necessary to achieve the ferromagnetic phase might one day become obsolete. The origin of ferromagnetism in this system is still obscure although some basic principles are apparent: The Mn impurities in the GaAs host crystal fulfil two tasks at the same time: on the one hand they act as electron acceptors, this means they dope the semiconductor with holes as charge carriers. On the other hand they provide large magnetic moments their d-shell being just half filled (Mn d^5 configuration). To explain why these magnetic moments are ferromagnetically aligned, three very different models are under intense debate: the double-exchange model, the Zener model, and the polaron percolation model, but common basis is that the Mn magnetic moments are aligned even across large distances by the aid of polarised charge carriers. The polarization on the As holes is antiparallel to the Mn (Fig. 1). Magnetic circular X-ray dichroism (MCXD) experiments in absorption have shown that only a small portion of the Mn atoms takes part in the ferromagnetic order of $Ga_{1-x}Mn_xAs$ although they appear to have the same electron configuration as the ones that are not aligned [3].

We have used a special apparatus to generate magnetic fields as high as ~2.4 Tesla by a superconducting magnet at the PM3 bending magnet beamline for circularly polarised light. In our experiment, not only element specific magnetic informa-

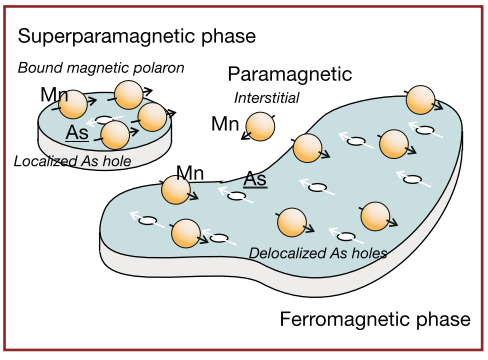

Fig. 1:
Mn impurities (orange) provide magnetic moments and charge carriers (holes on the As). The Mn electrons do not interact directly but via the As holes. The hole magnetic moments (white arrows) are coupled antiparallel to the ones of the Mn atoms (black arrows).

References:

[1] G. A. Prinz, Science, 282, 1660 (1998).

[2] H. Ohno, Science, 281, 951 (1998).

[3] H. Ohldag et al., Appl. Phys. Lett., 76, 2928 (2000);

[4] S. Ueda et al., Physica E, 10, 210 (2001).

[5] T. Dietl et al., Science, 287, 1019 (2000).

Acknowledgements:

Work supported by BMBF and performed as collaboration between BESSY and research groups Schütz (MPI Stuttgart) and Molenkamp (Univ. Würzburg).

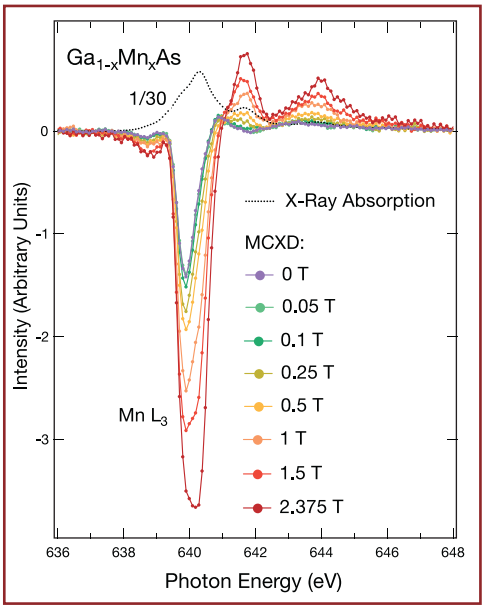

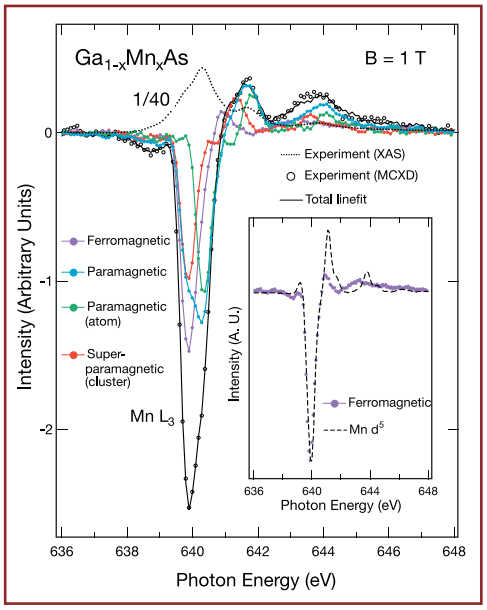

Fig. 3:
Decomposition of the spectrum for B=1 Tesla. Three components are identified, and the ferromagnetic one deviates most strongly from theory for a half-filled d-shell (inset).

Fig. 2:
The L_3 edge of Mn in X-ray absorption. The magnetic circular dichroism spectra (color) are defined as the difference of absorption spectra for opposite orientations of applied magnetic fields +B and -B. The larger the applied field B, the stronger the lineshape deviates from the ferromagnetic spectrum (B=0 Tesla). Temperature is 11 Kelvin.

tion is gained, i. e., telling Mn from As and Ga, but additionally chemical shifts are resolved. Fig. 2 shows the L_3 absorption edge of Mn for a sample with low Mn concentration of x=0.01 and various magnetic fields applied. Generally, it holds that the larger the negative amplitudes in Fig. 2, the higher the degree of alignment (paramagnetism). The spectra, however, change by shifting to higher energy and by developing a remarkable positive bump at 641.5 eV. Taking the ferromagnetic Mn, i. e., by definition the spectrum for zero applied field (violet), as reference, we see that the paramagnetic Mn is shifted by 0.5 eV to higher energy. A further observation is that also at the energy of the ferromagnetic Mn the signal apparently increases with applied field. In order to understand this, the spectra were decomposed by a fitting procedure, and Fig. 3 shows its result for the example of 1 Tesla. Then, the amplitude of each constituent was plotted versus magnetic field in Fig. 4. Ferromagnetic Mn (violet) and the chemically shifted and therefore extrinsic paramagnetic Mn (green) are easily distinguished by their respective field dependence. The energetically unshifted and therefore intrinsic Mn, however, seems to behave like a superparamagnet (red), and such behavior can indeed be explained by theory: The two-fluid model of diluted magnetic semiconductors [4] based on the Zener model places the ferromagnetism in such systems in the general framework of metal-to-insulator transitions with the concentration x as parameter. For lower x than the present x=0.01, $Ga_{1-x}Mn_xAs$ samples are nonmagnetic and insulating. So-called bound magnetic polarons are predicted to accompany the phase transition on both sides of the metal-to-insulator transition. We observe the effect of this phase separation and the bound magnetic polaron is, according to our Langevin fit, a unit of about four Mn atoms having a more localised electron configuration (half-filled) than the ferromagnetic Mn phase. On the basis of the decay length of the localised hole wave function, the radius of the polaron is expected to be 1 nm. This situation is depicted in Fig. 1. In the ferromagnetic phase, the As holes are no longer bound to the Mn atoms and the Mn configuration is more than half filled. With increasing concentration x, this phase extends at the expense of the polaron phase.

This confirmation of the two-fluid model is quite reassuring for spintronics applications. Based on this model, magnetic ordering temperatures for several hypothetical diluted magnetic semiconductors have been estimated. Magnetic ordering temperatures were found to scale with the gap size, and for $Ga_{1-x}Mn_xN$ a T_C well above room temperature was obtained [5].

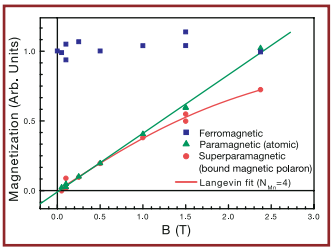

Fig. 4:
Magnetisation curves extracted from the spectral components. Superparamagnetic units are identified with bound magnetic polarons. The size is 20 Bohr magnetons or 4 Mn atoms, according to a Langevin fit.

Contact:
Oliver Rader
rader@bessy.de
Kai Fauth
fauth@physik.uni-wuerzburg.de

Magnetisation dynamics in spin-valves: how fast can a hard disk be read?

J. Vogel[1], W. Kuch[2], J. Camarero[3], K. Fukumoto[2], M. Bonfim[4], Y. Pennec[1], S. Pizzini[1], A. Fontaine[1], J. Kirschner[2]

1 Laboratoire Louis Néel, CNRS, Grenoble, France

2 Max-Planck-Institut für Mikrostrukturphysik, Halle

3 Departamento Física de la Materia Condensada, Universidad Autónoma de Madrid, Spain

4 Departamento de Engenharia Elètrica, Universidade do Paraná, Curitiba, Brazil

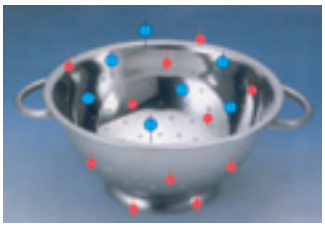

How long does it take to load this text from the hard disk of your computer? With the current technology this depends on the time needed to switch the magnetisation of a soft magnetic layer in the read head of the hard disk drive (Fig. 1). The essential part of this device is a spin-valve. This could be imaged as an electron sieve, which changes the size of its holes depending on whether it reads a 1 or a 0. The spin-valve consists of a trilayer system in which two ultrathin ferromagnetic layers are separated by a non-magnetic spacer. The magnetisation of one layer is always oriented in the same way, i.e. upwards, while the orientation of the other one is switched (up or down) by the bits over which the head passes. Electrons are transported more easily if the magnetisation directions of the two magnetic layers are pointing in the same direction. If the two ferromagnetic layers of the spin-valve are antiparallel aligned, it is more difficult for the electrons to pass, thus leading to a giant magneto resistance (GMR). Presently, read and write times approach one nanosecond, corresponding to 1 GHz frequency.

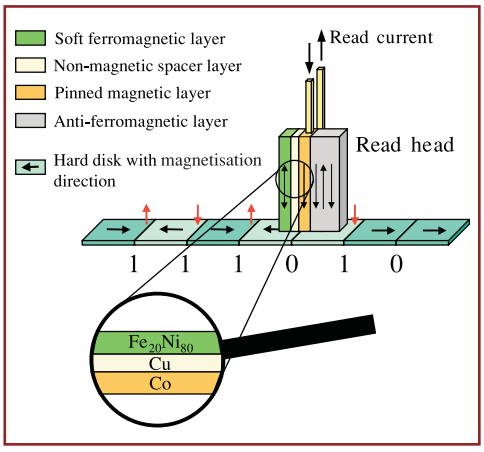

Fig. 1:
Working principle of a spin valve used in computer hard disks. The small stray field (red arrows) at the borders of the bits polarises the soft magnetic layer (green) of the read head. A small electrical current is applied parallel to the magnetic layer system. The read head has either a low resistance for parallel alignment or a high resistance for antiparallel alignment of the soft and the pinned magnetic layer (yellow).

Investigating the magnetisation dynamics in spin valves is thus very important from both a fundamental and an applied point of view.

We have carried out microscopic domain imaging measurements of the magnetisation reversal dynamics in a spin valve with time and layer resolution. Photoelectron emission microscopy (PEEM) in connection with X-ray magnetic circular dichroism (XMCD) is used to obtain magnetic domain images [1]. Because of the element selectivity of XMCD, different magnetic layers in a multilayered stack can be imaged separately [2]. Time resolution is obtained using a pump-probe approach (Fig. 2). Magnetic field pulses provided by a microcoil and a fast power supply (the pump) are synchronised with the X-ray photon pulses (the probe) in single bunch mode [3]. Images are then acquired for different constant delays between pump and probe, i.e., at different times before, during, or after the application of the magnetic field pulses. In this way the magnetisation dynamics of each magnetic layer can be visualised separately with a time resolution limited by the X-ray pulse width (about 60 ps).

A typical spin-valve sample was chosen which consisted of a 5 nm magnetically soft permalloy $Fe_{20}Ni_{80}$ layer and a 5 nm magnetically harder cobalt layer, separated by a 4 nm non-magnetic metallic Cu spacer layer, deposited on a SiO_2/Si(100) substrate. The $Fe_{20}Ni_{80}$ and Co layers are magnetically coupled across the copper spacer layer due to the presence of correlated roughness at the $Fe_{20}Ni_{80}$/Cu and Co/Cu interfaces (magnetostatic 'orange-peel' coupling [4]).

The aim of these measurements is to study the magnetisation reversal of the $Fe_{20}Ni_{80}$ layer upon application of nanosecond-long magnetic pulses, and to investigate how the interaction between the two layers influences this reversal. To obtain a good signal to noise ratio, images have to be averaged over a total acquisition time of several minutes, corresponding to several hundreds of millions of pulses [5]. This method therefore can only work for systems in which the magnetisation reversal is reproducible, i.e., it is the same for each of the applied

References:

[1] J. Stöhr et al., Science 259, 658 (1993).

[2] W. Kuch, Appl. Phys. A 76, 665 (2003).

[3] M. Bonfim et al., Phys. Rev. Lett. 86, 3646 (2001).

[4] L. Néel, C.R. Acad. Sci. Paris 255, 1676 (1962).

[5] J. Vogel et al., Appl. Phys. Lett. 82, 2299 (2003).

Acknowledgments:

We thank F. Petroff and A.Vaurès for sample preparation. Financial support by BMBF, EU and the Laboratoire Européen Associé "Mesomag" is gratefully acknowledged. We also thank the beamline staff of UE56/2-PGM2 (B. Zada and W. Mahler) and UE52-SGM (F. Senf) for their help.

magnetic pulses. The measurements were carried out at beamlines UE56/2-PGM2 and UE52-SGM, using circularly polarised soft X-rays. The magnetisation of the sample lies in the plane of the layers, and no preferential magnetisation axis exists within this plane.

In Fig. 3 we show time-resolved images of the $Fe_{20}Ni_{80}$ layer (domain contrast presented in blue and green) and of the Co layer (domain contrast red and yellow). The projection of the X-ray incidence direction on the sample surface is pointing up in the images, and is parallel to the direction of the field for positive fields. The magnetisation of the sample is first saturated in the negative direction (pointing down in Fig. 3), giving rise to completely green and yellow images for the FeNi and Co layer, respectively. Short bipolar magnetic pulses as shown at the left bottom of Fig. 3 were then applied to the sample. The repeated application of these pulses quickly leads to the zero field $Fe_{20}Ni_{80}$ and Co domain structures shown in panels a and d, respectively. Once this domain structure is stabilised, the magnetic pulse has no further influence on the Co magnetisation, which shows the same pattern as in panel d for all times, i.e. the magnetic pulse amplitude is adjusted so that the magnetisation of the cobalt layer is not affected by the magnetic field. In the $Fe_{20}Ni_{80}$ layer, the positive part of the magnetic field pulses favours the growth of the blue domains through propagation of domain walls (panel b). Negative fields favour the growth of green domains (panel c).

The shape of the domains is very irregular due to the absence of a preferential direction of magnetisation (or anisotropy) within the plane of the layers. The interaction through the Cu spacer layer favours a parallel alignment of the magnetisation direction of the two magnetic layers. One would therefore expect that for field values close to zero the domain structures in the two layers were the same. In Figs. 3b and c the red domains of the Co layer have been schematically outlined by black lines onto the $Fe_{20}Ni_{80}$ images. A certain correlation exists between the domain structures in the two layers, but this correlation is not perfect for any value of the field. The role played by the intrinsic properties of the permalloy layer, in particular the anisotropy and the pinning of the domain walls by small defects, is at least as important as the local coupling with the

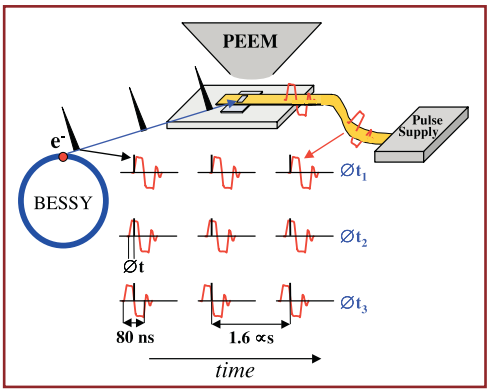

Fig. 2:
The principle of a pump-probe experiment with PEEM microscopy. A short magnetic field pulse is periodically applied to reverse the magnetisation of the soft layer. The magnetic pulses (red) are synchronised with the photon pulses (black) in single bunch mode. Images are taken for several time delays Δt between field pulses (pump) and synchrotron X-ray pulses (probe).

Co layer. Measurements on similar samples have shown that the competition between intrinsic properties and local coupling strongly depends on sample characteristics. The combination of temporal, spatial and chemical resolution makes this technique extremely powerful for studying magnetisation dynamics in heterogeneous magnetic systems.

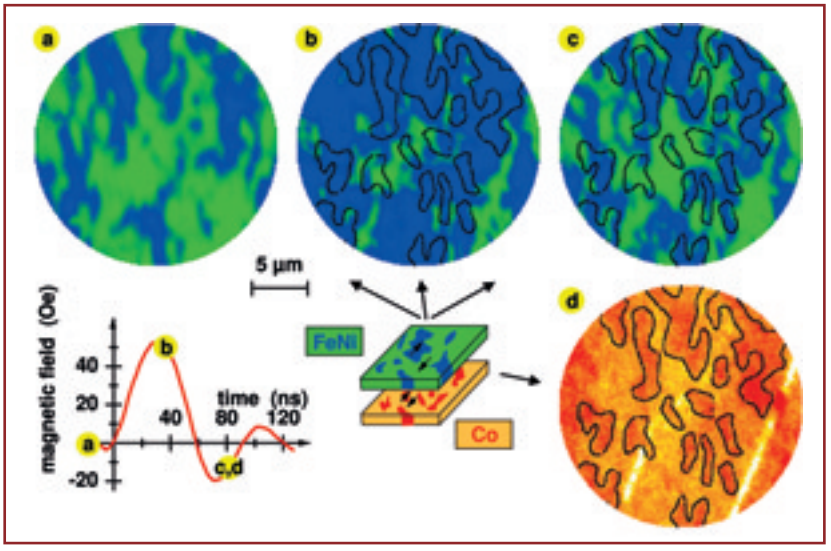

Fig. 3:
Time and layer-resolved XMCD-PEEM images (diameter 22 µm) for the magnetisation state of the $Fe_{20}Ni_{80}$ (a-c) and Co (d) layer in a $Fe_{20}Ni_{80}$/Cu/Co spin valve. The magnetisation direction points up for blue and red domains, while it points down for green and yellow domains. The different time delays with respect to the magnetic pulse are indicated on the graph at the bottom left, which shows the temporal shape of the magnetic field pulses. The most clearly visible red domains in the Co layer are denoted by black lines, and shown superimposed on the permalloy images b and c.

Contact:
Jan Vogel
vogel@grenoble.cnrs.fr
Wolfgang Kuch
kuch@mpi-halle.de

Exploring the world of microprocessors

M. A. Meyer[1], E. Zschech[1], P. Guttmann[2], G. Schneider[3]

1
AMD Saxony LLC & Co. KG, Materials Analysis Department, Dresden

2
Institut für Röntgenphysik c/o BESSY, Berlin

3
BESSY, Berlin

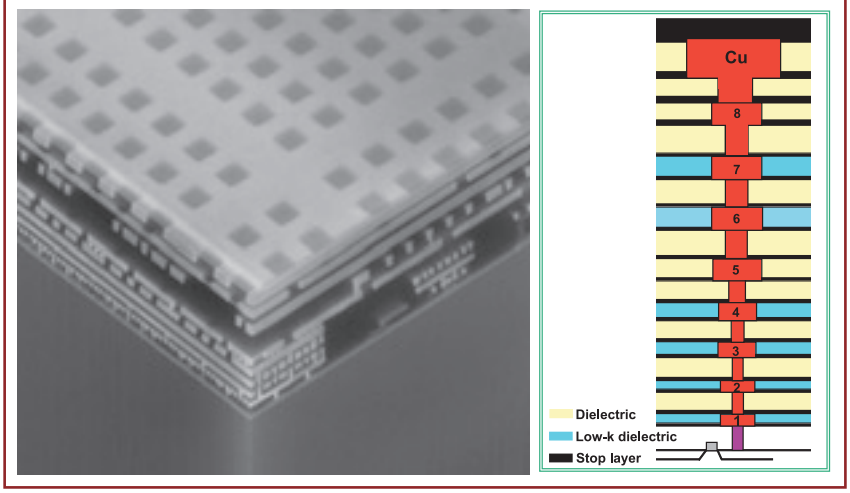

Fig. 1:
SEM micrograph of a cross-section of AMD Opteron™ and AMD Athlon™64 microprocessors showing the 9-metal interconnects hierarchy.

Currently, high-performance microprocessor chips contain more than 100 million transistors which are connected by on-chip metal wires (interconnects) (Fig. 1). The function of these interconnects is to distribute signals (e.g. clock signal) and to provide power/ground within the integrated circuit (IC). Both, performance and reliability of high-performance microprocessors are increasingly determined by design, technology and materials of interconnects and dielectric interlayers. These requirements have been described in the International Technology Roadmap for Semiconductors (ITRS) [1].

Further speeding-up of clock rates while continuing to down-scale feature sizes requires a new (smart) interconnect design in combination with new technologies and materials, in particular to minimise the so-called RC (Resistance x Capacitance) delay time. This task includes development and implementation of interconnect material with lower resistivity and of isolating interlayer material with low permittivity. The aluminium-based interconnects have been replaced by inlaid copper providing reduced electrical resistivity and improved electromigration behaviour [2]. The first microprocessors with inlaid copper interconnects in silicon dioxide (dielectric constant k = 4.0) were already introduced in 1998. Currently, technology development is focussing on insulator materials with lower dielectric constant (k < 3).

The required new process technologies and combinations of materials bring new reliability challenges, in particular, the mass transport due to the momentum exchange between conducting electrons and the diffusing metal atoms. Formation of voids in copper lines induced by electromigration during normal microprocessor operation will cause an interconnect open or high resistance resulting in malfunction or speed degradation [2]. Additionally, stress-induced degradation and mechanical weakness in case of low-k materials are reliability concerns for inlaid copper interconnects. Stress-induced degradation phenomena are not well understood so far. Particularly, fast diffusion paths have to be identified and failure mechanisms based on directed transport of atoms have to be understood. In passivated interconnects, the mass flow due to electromigration is constrained by the embedding dielectrics. This can lead to a high mechanical stress in the interconnect which significantly influences the material transport.

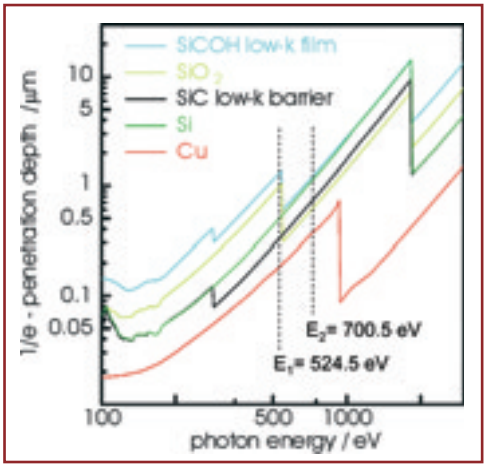

Fig. 2:
Attenuation length, the depth into the material measured along the surface normal where the intensity of X-rays drops to 1/e of its value at the surface for low-k, SiO_2, Si and Cu layers as a function of photon energy. Note that different dielectrics are distinguishable by their different absorption characteristics near the K-absorption edge of oxygen.

References:

[1] http://public.itrs.net

[2] R. Spolenak, E. Zschech: 'Interconnects for microelectronics', in 'Metal Based Thin Films for Electronics' (Eds. K. Wetzig, C. M. Schneider), Wiley-VCH Weinheim, 7, (2003)

[3] M. A. Meyer et al., Microelectronics Engineering 64, 375, (2002)

[4] G. Schneider et al., Appl. Phys. Lett. 81, 14 (2002) 2535

[5] G. Schneider et al., Characterization and Metrology for ULSI Technology: Eds. Seiler D G, Mc Donald R, Diebold A C, Khosla R, Schaffner T J, Zollner S, Secula E M, (2003) AIP Conf. Proc. 0-7354-0152-7/03

Acknowledgements:

Supported by BMBF

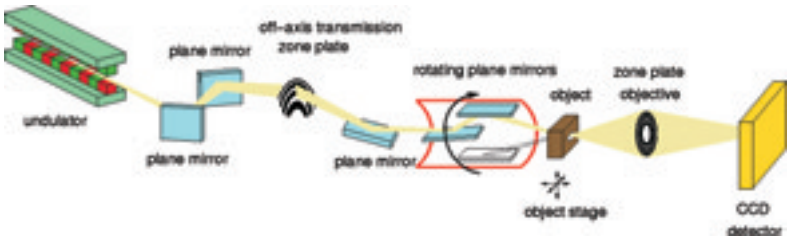

Fig. 3:
Schematic of the optical set-up of the full-field X-ray microscope operating at the undulator U41. A combination of an off-axis zone plate condenser and a rotating mirror system acts as a condenser for incoherent illumination of the sample. A zone plate objective forms a 2,000-fold magnified image onto the CCD camera.

Therefore, electromigration phenomena should be studied *in situ* at fully embedded interconnect structures using an intact layer system including barriers and passivation layers [3,4].

For physical failure analysis and reliability studies, electron microscopy is the dominating analytical technique in semiconductor industry. However, the structures of the new IC generation containing low-k materials shrink rapidly under observation in a scanning electron microscope (SEM) at usually applied acceleration voltages. In particular, the copper lines are bent during SEM observation. Compared to electrons, X-rays have the advantage that they penetrate IC layer stacks on top of the silicon substrate, which are several micrometers thick. Additionally, X-rays provide a natural image contrast between different elements which we exploit to image Cu interconnect lines embedded within dielectrics materials, consisting of low-Z elements. It is also possible to distinguish between different dielectric materials, e.g. Si compounds like SiCOH, SiC, and SiO_2, due to their different X-ray attenuation lengths (see Fig. 2).

In our studies we investigated a back-end-of-line stack of the high-performance microprocessors containing copper interconnects and low-k materials. We used the BESSY full-field Transmission X-ray Microscope (Fig. 3), which provides elemental contrast and chemical information with high spatial resolution. For elemental contrast, images before and after an X-ray absorption edge of a particular element have to be taken. At the low- and high-energy side of the K-absorption edge of oxygen at 524.5 and 700.5 eV, different low-k dielectric materials can be distinguished (Fig. 2). In the soft X-ray energy range, imaging compounds embedded in an IC stack requires cross-sections with a thickness in the micrometer range. For this purpose, a small sample was separated from the original wafer using a wire saw, and the focused ion beam (FIB) technique was applied to thin the lamella to about 1 - 2 µm. While the SEM provides very surface sensitive information the copper lines buried in the dielectric layers are not well resolved (Fig. 4, upper panel). Our study demonstrates that the X-ray microscope is a very useful tool which maintains high spatial resolution even for samples with several microns of dielectric material (Fig. 4, lower panels). Consequently, the passivation has not be removed for interconnect inspection.

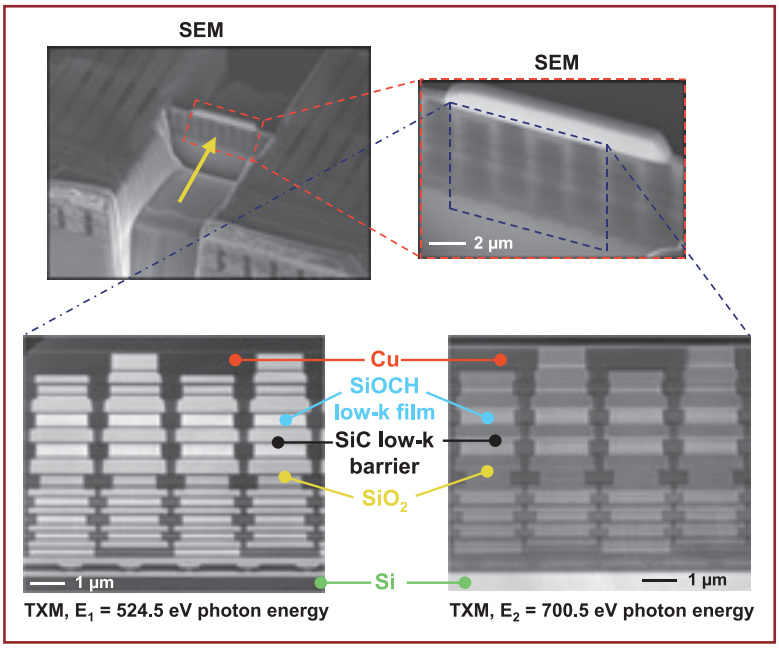

Fig. 4:
SEM micrograph (upper left) showing the FIB prepared fully passivated copper interconnect structures. Due to inelastic electron scattering in the passivation layer, the resolution in the magnified SEM micrograph (upper right) is limited. Passing photons through the prepared lamella in the X-ray microscope, images were taken at 524.5 eV and at 700.5 eV photon energy. Due to the different absorption properties of the used dielectric materials, these X-ray images reveal the different dielectric layers and the copper interconnects with a lateral resolution of about 20 nm.

As predicted by the model calculations shown in Fig. 2, the X-ray microscope even reveals different dielectric materials [5]. It is possible to take multiple images as required for real-time observations of electromigration degradation processes in buried copper interconnects without damaging the dielectric material. For SiO_2 as insulating material the electromigration has already been observed [4]. An electromigration study for a back-end-of-line structure with low-k dielectrics is planned for the near future. This experiment will provide important information about the influence of new processes and materials on interconnect reliability.
That means X-ray microscopy will help to understand better the physics behind electromigration.

Contact
Moritz Andreas Meyer
moritz-andreas.meyer@amd.com

Lensless Imaging of Magnetic Domain Structures

M. Lörgen[1], S. Eisebitt[1], W. Eberhardt[1], J. Lüning[2], W. F. Schlotter[3], J. Stöhr[2], O. Hellwig[1,4], C.T. Rettner[4]

1
BESSY, Berlin

2
SSRL, Stanford Linear Accelerator Center, Menlo Park, USA

3
Stanford University, Applied Physics, Stanford, USA

4
IBM, Almaden Research Center, San Jose, USA

How is an image of an object formed in a microscope? The object scatters the incident light and a lens recombines the scattered light to form an image. Mathematically speaking, the lens performs a Fourier transformation. However, under certain conditions it is possible to calculate this Fourier transformation with a computer and to image an object by measuring only the scattering pattern – thus eliminating the need for a lens and its associated aberrations. Unfortunately, there is a catch; the phase of the scattered light is not recorded in the scattering intensity and thus crucial information needed for the Fourier transformation is missing.

Under certain conditions, this phase problem can be solved in a coherent scattering experiment, making it possible to retrieve the phase of the scattered radiation field and thus to actually image the scattering object. Holography is a well known approach to determine the phase by coupling in a reference beam [1]. A sufficient coherent photon flux can be extracted from a high brilliance third generation synchrotron radiation source to move holography from the visible spectral range into the soft X-ray regime, where fully coherent radiation sources are not yet available. Shorter wavelengths enable higher spatial resolution. Even more importantly, soft X-rays make it possible to exploit special contrast mechanisms well known from spectroscopic experiments such as atomic, chemical or magnetic sensitivity.

We have carried out soft X-ray holography of magnetic domains on a CoPt multilayer on a Si_3N_4 membrane, utilising magnetic circular dichroism at the Co L_3 edge (λ=1.59 nm) in order to obtain magnetic contrast. The magnetic field exposure history of the sample determines whether magnetic domains are arranged mainly parallel or in a labyrinth pattern [2]. The experiment was performed in Fourier transform holography geometry where a reference source has to exist in the object plane [1]. We achieved this goal by placing a nanostructured gold mask containing a transparent sample area and a small reference hole directly on the multilayer sample (Fig. 1).

Coherent soft X-rays to illuminate the mask-sample sandwich structure are generated by passing monochromatised soft X-rays through an aperture of 20 µm diameter before they reach the mask. That way, we ensure that all optical path length differences in the experiment are shorter than the coherence lengths of our X-ray beam, which is a prerequisite to observe interference patterns with high contrast. Since the incident soft X-rays are also circularly polarised the magnetic domains give rise to small angle scattering because of X-ray magnetic circular dichroism [3].

The resulting intensity pattern at a CCD detector is shown in Fig. 2b. It can be understood by considering small angle scattering from the magnetic domains and diffraction from the apertures in the mask. The pattern is broken up into individual speckle due to interference. Intensity maxima to the left and right of the specular peak are due to the scattering from the magnetic domains, which appear to be oriented in a vertically periodic structure. The interference of the reference hole with the sample pattern can be observed as a high frequency horizontal stripe pattern across the scattering image.

Due to the holography set-up, an inverse Fourier transform of the scattering pattern, performed by a computer, directly shows an image of the object, revealing clearly a domain pattern (Fig. 2c). The resolution in

References:

[1] D. Gabor, Science, 177, 299, (1972)

[2] O. Hellwig et al., Physica B - Condensed Matter, 336, 136 (2003)

[3] S. Eisebitt et al., Physical Review B, 68, 104419 (2003)

[4] J. R. Fienup, Optics Letters, 3, 27 (1978)

[5] J.W. Miao et al., Nature, 400, 342, (1999)

[6] S. Eisebitt et al., Applied Physics Letters, in press (2004)

[7] H. He et al., Phys. Rev. B, 67, 174114, 2003

this type of holography is limited by the size of the reference hole and by the maximum momentum transfer. The reference hole has a protrusion to the lower right side. As a result, a weaker 'shadow image' is superimposed on the true image with a lateral offset. Nevertheless, the magnetic stripe domains are clearly visible. The number and orientation of the domains in the holographic image is the same as in the microscopy image, which has been taken from the same mask-sample sandwich structure in the XM-1 X-ray microscope at the Advanced Light Source (Fig. 2a), corroborating the validity of our holographic reconstruction. To our knowledge, this is the first 'magnetic hologram' recorded at X-ray wavelengths.

Even without a reference wave, it is possible to retrieve the scattering wave field phase and image a specimen. This type of lensless imaging requires a spatially oversampled measurement of the scattering pattern. In this approach, the sample must be localised within a certain region called 'support' (in our case the apertures in the mask) and the 'sample' structure outside this region must be known (in our case: no transmission outside the apertures). The phase lost in the intensity measurement can then be retrieved with an iterative algorithm [4, 5]. This approach has been successfully implemented in recent years, but magnetic objects have not been investigated so far.

The coherent scattering pattern shown in Fig. 1 is oversampled by a factor of 15 thus allowing iterative phase retrieval. A reconstruction of our magnetic object on the basis of the soft X-ray scattering pattern alone is presented in Fig. 2d. Again, the same stripe domains as in the X-ray microscopy image and in the holographic image are visible. The shadow image and the central beam artefact present in the holographic image are now absent. It is a particular advantage of our experimental set-up with the reference hole that the shape of the support can be directly seen in the inverse Fourier transform of the scattering pattern [6, 7]. In contrast, in most oversampling phase reconstructions so far, light microscopy images had to be used in addition to the X-ray scattering pattern in order to obtain this information.

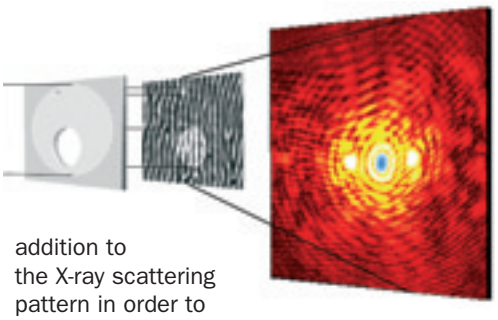

Fig. 1:
Concept of the coherent scattering experiment performed in transmission geometry. The illuminated area of the sample is defined by a pinhole of 1.2 μm in diameter.
The reference hole with a diameter of 200 nm is offset by 1.2 μm to the side. In reality, the pinhole mask is in direct contact with the sample membrane. The recorded intensity pattern is shown on the right image (logarithmic scale).

Both holographic and oversampling phase imaging will benefit tremendously from the current development of soft X-ray free electron lasers. Such sources will provide a coherent photon flux many orders of magnitude higher than available today, which will directly translate into increased sensitivity and higher resolution images.

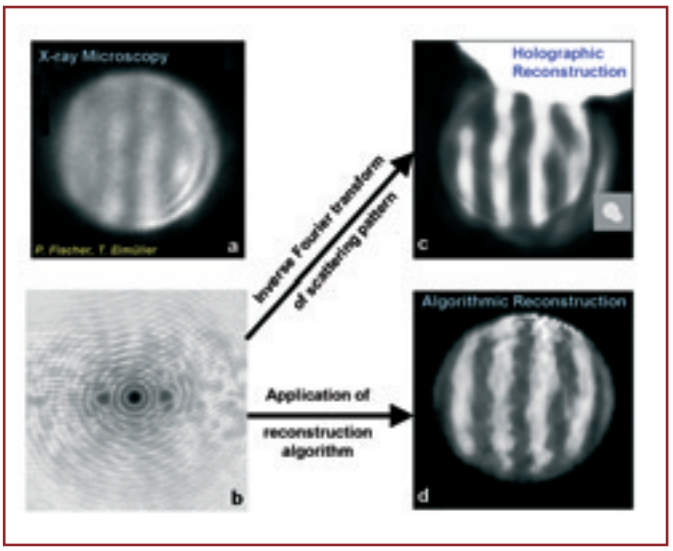

Fig. 2:
(a) X-ray transmission microscope image of the test object taken at the Advanced Light Source by P. Fischer and T. Eimüller. The image shows the parallel stripes of the magnetic pattern within the 1.2 μm diameter sample hole.
(b) Scattering intensity from the magnetic domains obtained in coherent scattering with circular polarised soft X-rays. The intensity map is a Fourier transform hologram. (c) Fourier transform obtained from the hologram, showing the image of the sample. (d) Iterative, non-holographic reconstruction of the magnetic domain pattern by 500 cycles of an error-reduction algorithm.

Contact:
Stefan Eisebitt,
eisebitt@bessy.de

3

News & Events

News

Hermann Dürr received the Röntgenpreis of the Justus-Liebig-Universität Gießen for 'extraordinary contributions to the microscopic characterisation of thin magnetic layers using circular polarised X-rays.' Since 1994, Dr. Hermann Dürr works with nanostructures and improved the techniques employed by him, the X-ray circular dichroism and resonant magnetic X-ray scattering.

Michael Grunze, chairman of the Scientific Advisory Committee was awarded a Max-Planck-Forschungspreis for the development of a new type of surfaces, i.e. covered with thin layers of highly polymerised molecules.

Joachim Treusch, chairman of the Supervisory Board was honoured the title 'Chevalier de la Legion d'Honneur' for his continuous effort on French-German research cooperations.

The 60th birthday of Wolfgang Gudat, the former scientific director of BESSY, was celebrated with a scientific colloquium. Prof. Franz Himpsel of University of Madison, Wisconsin gave a key note lecture on 'Spin Polarisation Spectroscopy and Magnetism', while Prof. Volker Saile, Forschungszentrum Karlsruhe, showed with his talk on 'Synchrotron Radiation at Work' how versatile this light is.

The user talks on work in progress called 'Science on the fly' have a vivid tradition by now. Additionally, several invited scientific lecturers gave insights into actual research topics. The talk of Prof. Ganten, then still Max-Delbrück-Centre, during the BESSY Forum found great response by the audience.

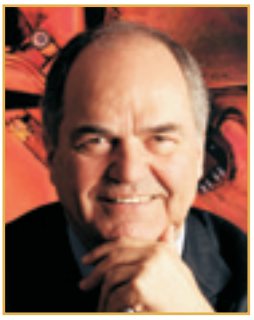

Hermann Dürr (top), Michael Grunze, Chairman of the Scientific Advisory committee (left), and Joachim Treusch, Chairman of the Supervisory Board (right).

Wolfgang Gudat's 60th birthday.

International visitors from Latvia, Australia, and African Embassies.

BESSY still attracts visitors from all over the world. In 2003 about 2,900 people were guided through BESSY, about one third are pupils and 640 students. Several high-ranking international delegations were welcomed at BESSY, among them a group of ambassadors from different nations, delegations of Brazil, Australia, the Basque region, and Latvia as well as from the Kosovarian parliament. During the Asia-Pacific weeks BESSY was visited by a group of interested participants attracted by BESSY and the Campus Adlershof.

Events

During 'Lange Nacht der Wissenschaften' at June 14th 2003, BESSY was again a magnet for visitors such as families with small kids, students and retired scientists. More than 5,500 people found their way to BESSY, making it the biggest attraction in Adlershof and also of the whole event. The Physics Show by Prof. Schmidt and his assistant enjoyed great popularity also by the children. This will be difficult to top in the future. A walk starting at the heart of BESSY following the way synchrotron radiation is produced and used, is opened during the night. A guided tour for children is always a highlight. Pupils of several schools prepared and explained together with BESSY staff members show experiments, transporting their fascination for sciences.

The German Sciences ministry (BMBF) announced 2003 as the 'Year of Chemistry', and BESSY contributed together with our on-site partner ACA (Institute of Applied Chemistry) two catalysis experiments to the exhibition boat 'MS Chemie' which cruised Rhine, Neckar, and Main. Also, BESSY participated in the exhibition 'Der Kuss', which marked the beginning of the 'Year of Chemistry' in Berlin.

During the summer holidays the 'Physik zum Frühstück' lectures took place again. The combination of a late Sunday breakfast and an experimental physics lecture under the motto 'There will be light ...' attracted more than 230 people at three dates. The increased number of participants encouraged us to continue in 2004.
The lecture was used to raise funds for school projects, e.g the donation of a prize for science and mathematics at the Herder Gymnasium, a high school in Berlin-Prenzlauer Berg. The idea is to encourage pupils who show besides good marks in their major subject great social engagement. The prize is another step of on-going partnerships between Berlin schools and BESSY.

In the last year the efforts to gain new and especially industrial users have been intensified. BESSY participated in two fairs, i.e. the Hannovermesse and MST.

Two presentations for members of the European and the German Parliaments have been organised by the Leibniz Association. BESSY contributed a display of the principle of the new femtosecond slicing, a test experiment for the Free Electron Laser.

BESSY was for one day a centre of archeology. During a press conference about the 'Sky Disc of Nebra' journalists were informed about the results received with synchrotron radiation dating the stars and the other objects on the disk. While the press conference was a look back in the past, a talk show during the 'Stadt der 1000 Fragen' project lead in the future. It gave a platform for questions, fears and critics of people concerning biotechnology. 'What do we want if everything is possible?' was one of the questions. Under the headline 'Zukunft hoch 4' a sociologist, a physicist and a physician draw their scenarios. The talk show was recorded for the German television.

An After-Work-Party was organised together with the finissage of the Light Object exhibition by Micha Koch. The party was not only for the BESSY staff but brought together the people of the Adlershof campus. The success encouraged to go for another one in 2004.

School children at the BESSY display on board of the MS Chemie.

Wolfgang Eberhardt explains the difference between salami-slicing and femtosecond-slicing to H.-O. Henkel (Chaiman of the Leibniz Association) and representative of the European Commission in Brussels.

Children and adults explore the 'nature of light' in the sunday morning lecture.

Users' Meeting 2003

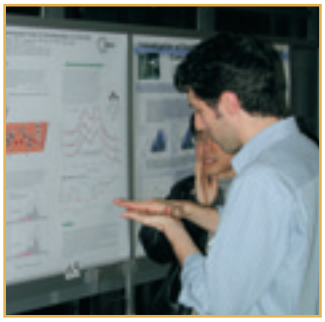

The BESSY users' meeting was held at December 4/5th, 2003 with more than 300 participants. The meeting was accompanied by a vendor exhibition.
35 companies showed their products and new technological developments and kindly sponsored the evening buffett. On about 130 posters scientific results obtained at BESSY were presented in the experimental hall. The poster prize was awarded to Joachim Bansmann (Universität Rostock) for magnetic circular dichroism studies on small magnetic clusters.

This years key note lecture by Liu Hao Tjeng, Universität zu Köln, addressed a 'New Look at Charges, Spin and Orbitals in Correlated Oxides'. The subjects of the following talks reflected the diverse fields of work carried out at BESSY, i.e magnetism, nanoparticles, time-resolved measurements, atomic physics, solar cell research and archeometry. An a industrial user, Ursula Egner from SCHERING reported on the successful use of the protein crystallography beamlines at BESSY. The status of the BESSY-FEL was summarised by Dieter Krämer, while Peter Kuske and William Peatman reported on the recent developments of the machine and beamlines, respectively. A new set-up for science with femtosecond X-rays was highlighted by Hermann Dürr.

At the second day of the meeting a user committee was elected. Its intention is to improve the contact between users, scientific director and beamtime coordinator. Eberhard Umbach moderated the plenum discussions where users expressed wishes for further improvements, open questions, and complains.

The remarks of Helmut Dosch, (Komitee für Forschung mit Synchrotronstrahlung) on the funding situation, also in regard to the planned FEL projects at DESY and at BESSY, gave a lot impulse for consideration. The community was reminded to learn from the failure of the European Spallation Source project.
It is essential to built-up a lobby including industrial partners with an inherent interest in the use of SR. Additionally, Centres of Excellence should grow around the light sources with high profile in e.g. magnetism, life sciences, micro engineering, etc. In this context on European level the GENNESYS (Great European Initiative on Nanoscience and Nanotechnology using Neutron and Synchrotron Radiation Sources) was started.

Innovation Award on Synchrotron Radiation

Several high-ranking candidates for the innovation award performed a neck-and-neck race in the decision of the bestowal committee of the Society of Friends and Sponsors of BESSY. Finally, the prize was awarded to the THz-Team.

After three years of work the physicist where able to produce very intense, broadband Infrared radiation (THz radiation) in a stable permanent operation, making BESSY at the moment the only synchrotron radiation source in the world capable of this mode. For details see Highlights 2002.

The THz-Team: Karsten Holldack, Michael Abo-Bakr (BESSY), Heinz-Wilhelm Hübers (DLR) and Godehard Wüstefeld (BESSY). The fifth team member Jörg Feikes is not on the picture.

Workshops 2003

Course on Experimenting with Synchrotron Radiation	February, 10- 21
Joined Workshop SLS, Uni Lausanne: 'Ultrafast Science with X-Rays and Electrons'	April, 9-12
Supramolecular Biostructures	April, 27-28
Inauguration PSF Beamlines	September, 15
SPP 1133 BESSY-Workshop “Magnetisation Dynamics”	September, 29-30
BESSY Forum	October, 21
Industrieforum 'In situ characterisation of catalytic processes'	November, 19
BESSY users meeting	December,4-5
X-Ray Spectroscopies of Magnetic Solids (XRMS)	December, 6-7

Participants of the XRMS workshop.

Opening of one of BESSY's regular art exhibitions - artwork by Stephanie Raetsch (Berlin-Dakar).

4

Future Facilities

Technical Design for 'The BESSY Soft X-Ray Free Electron Laser'

The FEL Project Group has worked out the Technical Design for an optimised 2nd generation Free Electron Laser User Facility in the VUV to soft X-ray spectral range as complement to the existing BESSY II light source. The project group proposes to build a FEL-Multi-User facility based on the High Gain Harmonic Generation (HGHG) principle [1,2] in the photon energy range 24 eV to 1,000 eV. The HGHG-principle has several advantages as compared to the previously considered Self Amplified Spontaneous Emission (SASE)-FEL. HGHG offers today's only possibility to generate ultra short high power pulses in a controlled way, as the FEL output is a map of the first external seed pulse. Also the pulse form and consequently the spectrum are smooth and 'clean' compared to a SASE-FEL (Fig 1).

The 'BESSY Soft X-Ray FEL' will utilise a superconducting CW-linac to produce flexible pulse patterns of mono-energetic variable polarization soft X-ray pulses of 20 femto-second duration at extremely high peak brightness and full transverse and longitudinal coherence. The use of an external seed in this cascaded HGHG-FEL provides full control on the output photon pulse in terms of pulse duration and pulse shape. Moreover, as a strong seed field is driving the electron beam spatial modulation the coherent emission is without statistical (shot noise) properties as for SASE-FELs, e.g. there are significant advantages in output power stability and a shot to shot reproducible non-spiky spectral power distribution. The BESSY Soft X-Ray FEL will operate with 3 independent FEL-lines in parallel. Later on, up to 5 FEL-lines are envisaged for user experiments.

Detailed analysis of the FEL process shows peak brilliance in the 10^{30} ph/(s mm^2 mrad^2 0.1% bw) range, which is nine orders of magnitude higher than at BESSY II, and a peak power in the 1.5 - 14 GW range. The BESSY-FEL User facility will operate a two stage cascade to cover the FEL wavelength 24 eV - 120 eV, a three stage cascade for 100 eV to 600 eV and a 4 stage HGHG-FEL for the 500 eV to 1,000 eV photon pulses.

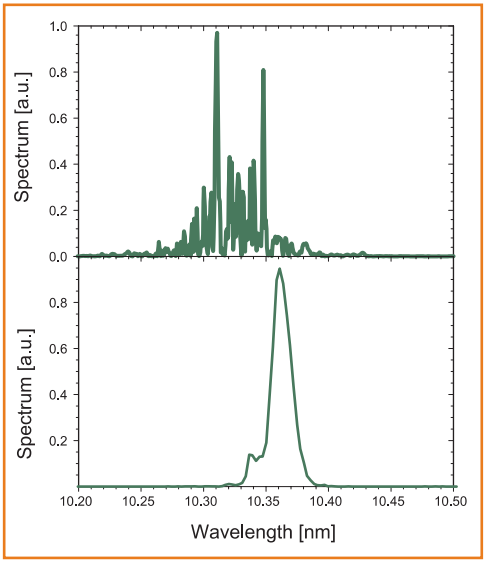

Fig. 1:
Calculated spectral distribution of a SASE-FEL (upper panel) and an HGHG-FEL (lower panel) at 10.3 nm.

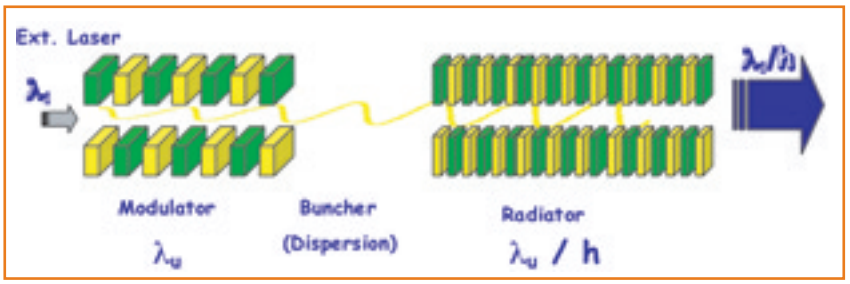

Fig. 2:
Schematics of a High Gain High Harmonic (HGHG)-FEL.

The HGHG-principle (Fig. 2) has been developed and experimentally proven at Brookhaven National Laboratory [1, 2]. In a short (2 m) long period undulator, called the modulator, the 1 ps electron bunch interacts with a 20 fs short pulse laser of wavelength λ_l (typically a Titanium-Saphire laser with 230 nm < λ_l < 460 nm), resulting in energy modulation of the electrons in this beamlet. In the following dispersive section the energy modulation is transferred into a density modulation of a period length equal to the laser wavelength. Then, when passing an undulator tuned in resonance to a higher harmonic of this wavelength, the modulated electrons will radiate coherently, e.g. proportional to their number squared (N^2), rather than linear as is the case for spontaneous emission.

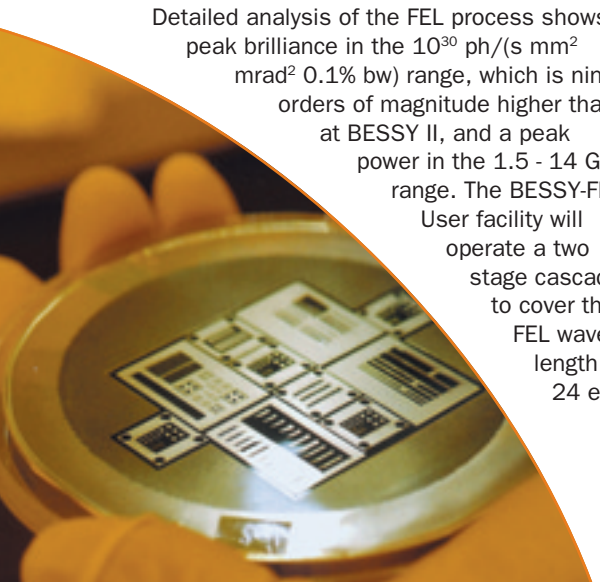

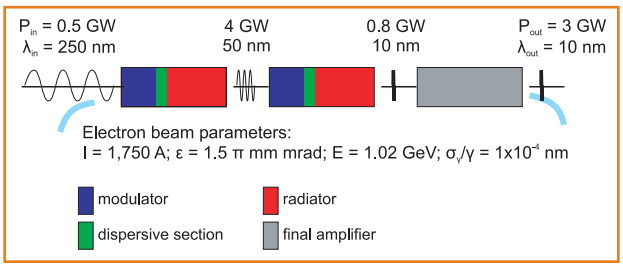

Fig. 3:
Schematics of a 2 stage cascaded HGHG-FEL as used for the BESSY Low-Energy FEL line covering the wavelength range 24 - 120 eV.

As N is in the order of some 10^5 electrons per beamlet with some thousand beamlets in the 20 fs long pulse, a high power photon beam of up to GW peak intensity is emitted from the radiator at the harmonic wavelength of λ_i/h, e.g. h = 3 or h = 5. This photon beam serves as the seed for the next HGHG-FEL. With a cascade of four FELs a 280 nm seed is converted to 1.24 nm serving as the seed to a last long undulator - called the final amplifier - in which, as set in resonance to its fundamental, the seed pulse drives the FEL-process into saturation (Fig. 3).

The electron bunch trains, generated in a room temperature RF photoinjector (3 or 6 bunches, 45 ps long , near-rectangular bunch shape, 65 A peak current, repetition frequency 1,000 Hz) are compressed in two bunch compressors to 0.75 ps long flat-top distribution accelerated up to 2.3 GeV in the superconducting CW linac. 144 cavities, grouped into 18 modules of a modified TESLA-type are required for the linac. With an even more flexible superconducting injector the bunch repetition rate can be further increased and is only limited by the beam dump capabilities.

The bunch pattern of the day-one photoinjector is depicted in Fig. 4. Bunch trains of 1 or 3 bunches are generated with a repetition rate of up to 1 kHz. A future superconducting photoinjector will produce single bunches at arbitrary bunch spacing just limited by the total beam power.

Detailed work has been performed in a BESSY-Cornell-DESY collaboration to qualify the TESLA type superconducting (s.c.) cavity modules for operation in CW mode as required for the BESSY-FEL. In a test stand (Fig. 5) at the BESSY site s.c. cavities as well as tuners and couplers will be tested in CW operation during the year 2004. Thus it will be possible to ensure proper functionality and risk minimization of the linac components.

Beamlines and monochromators to cope with the high brilliance photon beam for time resolved and high resolution experiments have been specified and a detailed design has been worked out (Fig. 6).

A detailed report on the building concept for the BESSY Soft-X-Ray Multi-User Facility based on the spatial and technical requirements for the FEL has been worked out by the Max-Planck Gesellschaft Bauabteilung, demonstrating the feasibility of the project on the BESSY site and deriving a sound cost basis. The central is a 20,000 m^2 hall following industrial standards giving space to the folded accelerator and the experimental areas (Fig. 7). Linac and undulator sections are located in the radiation tunnel. All sensitive equipment will be housed locally in thermally controlled properly shielded hutches.

More detailed descriptions will be available in the 'Technical Design Report' in April 2004.

Fig. 4:
Bunch pattern from a room temperature RF-photoinjector and (left) a future superconducting photoinjector (right).

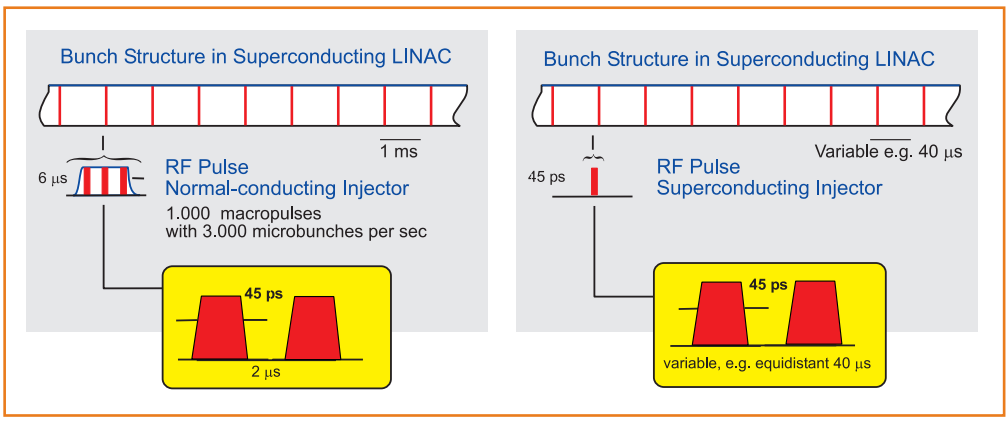

References:

[1] L.H. Yu, Phys. Rev. A 44, 5178 (1991).

[2] T. Shaftan et al., Proc. of the Part. Acc. Conf. Chicago, 246. (2001).

Fig. 5:
Horizontal Bi-Cavity Test facility (HoBiCaT) in its radiation vault in the 'Schwerlasthalle'.

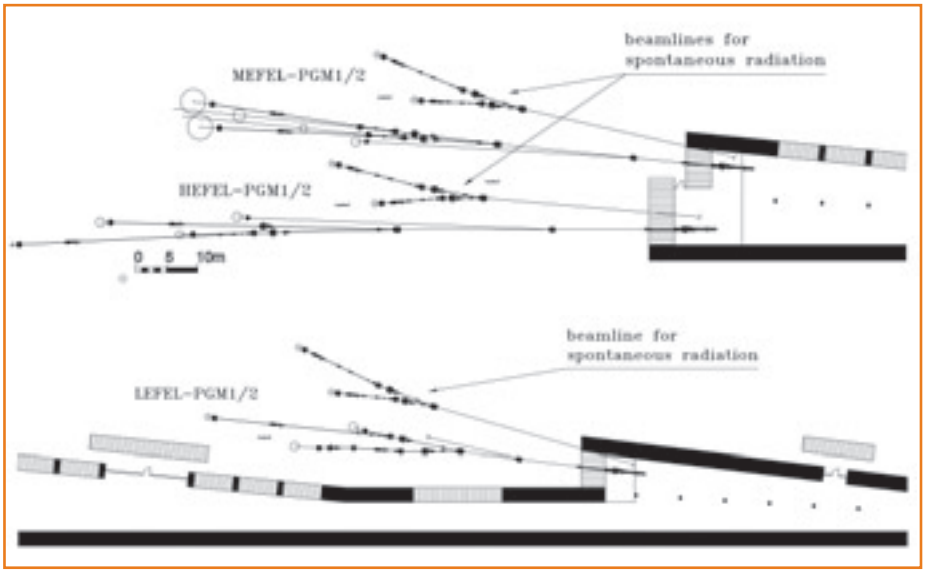

Fig. 6:
Beamlines for the Low Energy-FEL (lower panel), the Middle Energy- and High Energy-FEL (upper panel). The beamlines at the 3 FEL-lines have been designed for high resolution experiments and short pulse physics at the direct photon beam. Possible beamlines for spontaneous radiation are indicated.

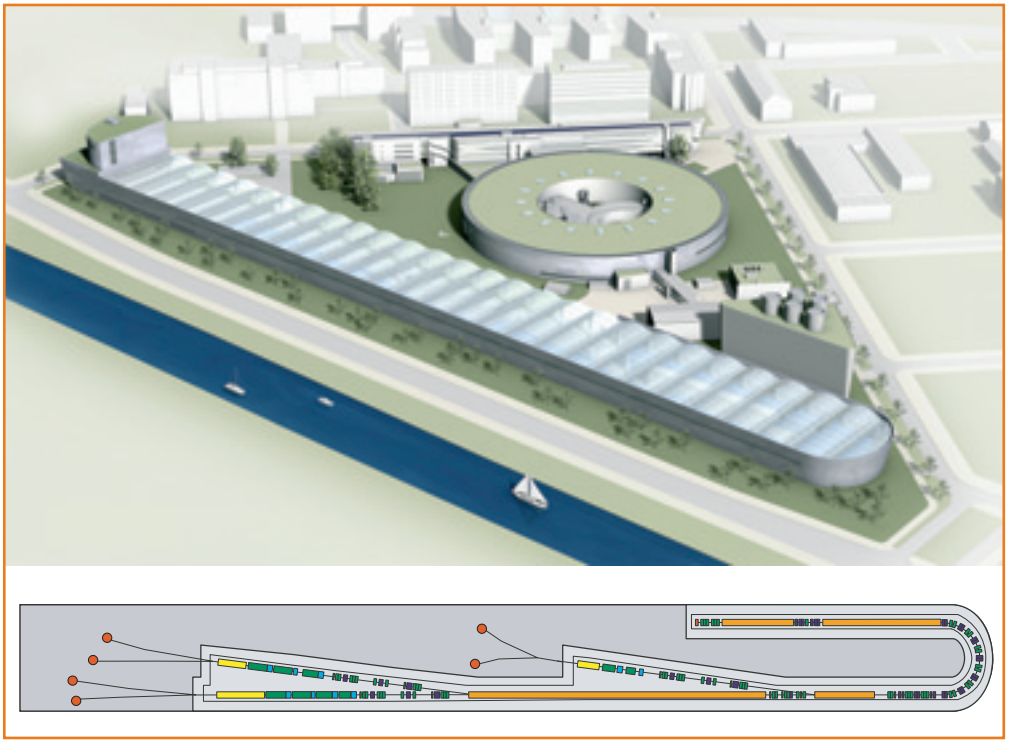

Fig. 7:
3D-impression of the BESSY-FEL site parallel to the Teltow Kanal with a sketch of the Low energy, Medium, and High energy FEL lines.

The FEL Project Group

M. Abo-Bakr, W. Anders, J. Bahrdt, R. Bakker*, K. Bürkmann, G. Bisoffi©, O. Dreßler, H. Dürr, V. Dürr, W. Eberhardt, S. Eisebitt, J. Feikes, R. Follath, A. Gaupp, K. Goldammer, M. v. Hartrott, S. Heßler, K. Holldack, E. Jaeschke, Th. Kamps, S. Khan, J. Knobloch, B. Kuske, P. Kuske, D. Krämer, F. Marhauser, A. Meseck, G. Mishra°, R. Mitzner, R. Müller, A. Neumann, M. Neeb, K. Ott, W. Peatman, D. Pflückhahn, H. Prange, T. Quast, M. Scheer, Th. Schroeter, F. Senf, G. Wüstefeld, Y. Xiang+ (BESSY), F. Noack, W. Sandner, M. Schnürer, P. Tzanko, I. Will (Max-Born-Institut), D. Janssen, J. Teichert, P. Michel (Forschungszentrum Rossendorf), and H. Quack, Ch. Haberstroh, G. Bartlock, A. Kutzschbach (TU-Dresden).

* now Sincrotrone Trieste,
° DAVV Indore, India,
\+ on leave from DESY,
© INFN Laboratori Nazionali di Legnaro

Contact
Dieter Krämer
dieter.kraemer@bessy.de
fel@bessy.de

The Metrology Light Source - a new dedicated electron storage ring of the PTB

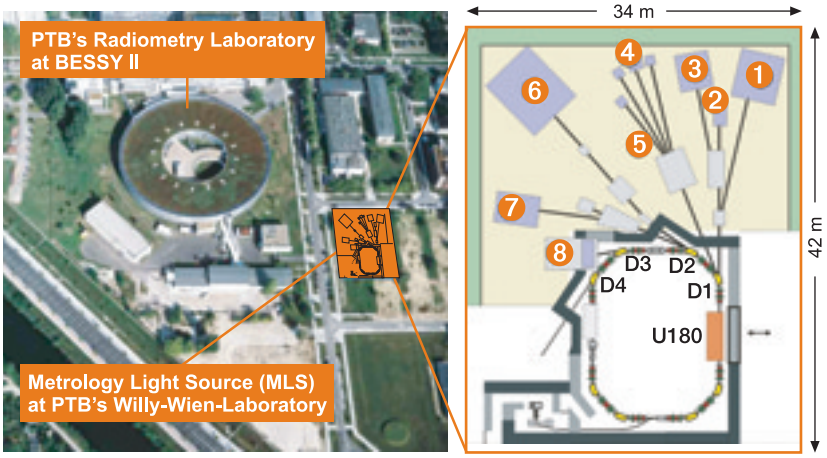

1. high flux experiments with deflected undulator radiation
2. high flux experiments with direct undulator radiation / Compton backscattering
3. high flux experiments with dispersed undulator radiation from 3 eV to 300 eV
4. calibration of energy-dispersive systems with calculable SR
5. spectral calibration of radiation sources with calculable SR from 3 eV to 300 eV
6. EUV detector radiometry and reflectometry from 30 eV to 400 eV
7. UV and VUV detector radiometry and reflectometry from 3 eV to 30 eV
8. IR radiometry and photon metrology

Fig. 1:
The Metrology Light Source (MLS) at PTB's Willy Wien Laboratory in the close vicinity of BESSY II. The blow-up shows the experimental area only.

In 2003, the Physikalisch-Technische-Bundesanstalt (PTB) obtained the authorisation to construct its *Willy Wien Laboratory* - in the close vicinity of BESSY II - to accommodate a low-energy electron storage ring, the *Metrology Light Source* (MLS). Starting operation in 2008, this MLS will be used by PTB for radiometry and photon metrology at five beam lines with eight experimental stations (Fig. 1). The design, construction, and operation of the MLS are realised in close co-operation between PTB and BESSY.

For more than 20 years, PTB has used synchrotron radiation at the storage rings BESSY I and II for photon metrology in the spectral range from UV radiation to X-rays [1-3]. Measurement capabilities which are unique world wide have been developed within the scope of source-based radiometry operating a storage ring as a primary standard for calculable synchrotron radiation according to Schwinger's equation [4]. This is applied to calibrate energy-dispersive X-ray detectors by direct measurement of the undispersed synchrotron radiation and radiation sources by comparison with the storage ring using a movable spectrometer [5]. Outstanding applications of this method were the calibration of the SUMER and CDS telescopes of the SOHO mission and detector calibrations for the astrophysical missions Chandra (NASA) and XMM - Newton (ESA). PTB's key role in European UV source calibration is demonstrated by EUROMET contracts with the British and the French national metrology institutes. Similar co-operations with the metrology institutes of China and the USA have been recently started.

However, for source-based radiometry, the spectral distribution and intensity of synchrotron radiation must be adjusted to the measurement requirements, i.e. the storage ring has to be operated at reduced electron energy and current. In this context, PTB has vigorously pursued the construction of a storage ring dedicated to metrology after BESSY I was shut down in 1999, also encouraged by the large demand of industry for metrology in the EUV at 13 nm. The MLS fills the current gap from 4 nm to 40 nm for source calibration and will be, in line with the sharing of responsibilities among European metrology laboratories, the European primary source standard for UV and VUV radiation - in addition to BESSY II which is the primary standard for X-rays (Fig. 2). The MLS has a circumference of 48 m. Using a microtron as pre-accelerator, the electron injection energy

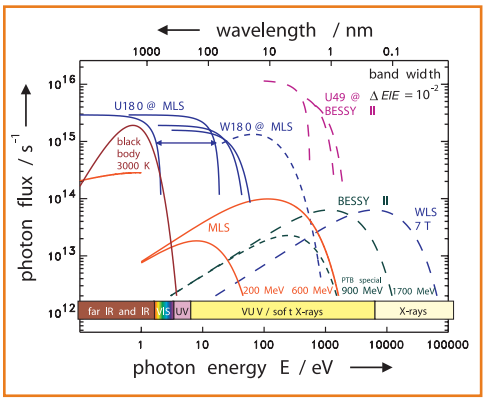

Fig. 2:
Photon flux available at the MLS for 200 MeV and 600 MeV electron energy and emitted from an undulator with a periodic length of 180 mm compared with BESSY II (- - -) and a high temperature black body radiator.

References:

[1] M. Richter and G. Ulm, J. Electr. Spectrosc. Relat. Phenom. 101-103, 1013 (1999)

[2] R. Klein et al., Synchrotron Radiation News 15, no. 1, 23 (2002)

[3] G. Ulm, Metrologia 40, S 101 (2003)

[4] R. Thornagel et al., Metrologia 38, 385 (2001)

[5] M. Richter et al., Metrologia 40, S 107 (2003)

[6] M. Richter et al., Appl. Phys. Lett. 83, 2970 (2003)

[7] M. Richter et al., Appl. Opt. 41, 7167 (2002)

[8] F. Scholze at al., SPIE 4344, 402 (2001)

[9] J. Tümmler et al., SPIE 5037, 265 (2003)

[10] M. Letz et al., Phys. Rev. B 67, 233101 (2003)

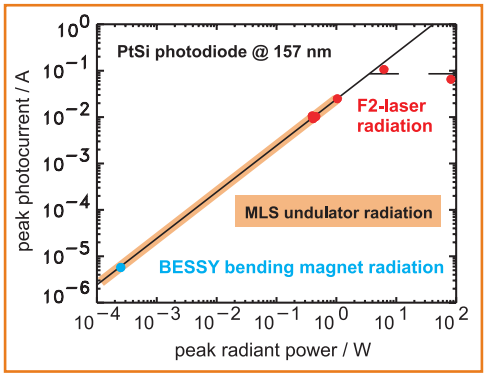

Fig. 3:
Peak photocurrent of a PtSi-nSi Schottky type photodiode at 157 nm as a function of peak radiant power [7]. The dynamic range covered by low-energy undulator radiation at the MLS is also shown.

is to 100 MeV. For operation, the electron energy of the MLS will be variable between 200 MeV and 600 MeV which corresponds to characteristic wavelengths in the VUV from 107 nm to 4 nm. The electron beam current may be varied from 1 pA (1 electron) to 200 mA. Moreover, a special operation mode for the storage ring to produce a largely increased coherent flux in the far IR and THz region will be prepared.

Besides its role as a primary standard, the MLS also provides undulator radiation from the IR to the VUV for photon metrology at high intensities within the framework of detector-based radiometry using a cryogenic radiometer as the primary detector standard (Fig. 2). In the VUV, highly intense and strongly pulsed radiation sources such as F_2 lasers, EUV lithography plasma sources, or Free Electron Lasers (FEL) are currently under development for the next generations of semiconductor nanostructuring and new fields of fundamental research. At the VUV-FEL of the Tesla Test Facility in Hamburg, e.g., radiation pulses with a peak radiant power of more than 100 MW were measured recently using a new type of gas-ionisation detector [6]. Semiconductor photodetectors widely used as transfer detector standards in the UV and VUV would be destroyed, degraded, or, at least, saturated when exposed to such an intense radiation field. Fig. 3 shows a saturation curve for a photodiode measured at 157 nm with dispersed bending magnet radiation at low peak radiant power and F_2-laser radiation at high power [7]. Undulator radiation from the MLS will perfectly fill the dynamic gap. For average radiant power, PTB's measurement capabilities at the MLS within the framework of detector-based UV and VUV radiometry will be extended to cover a dynamic range from fW to mW. This also provides the basis for developing and applying advanced (micro-) spectroscopy and metrology techniques for quantitative but standard-free analysis of gases and surfaces.

Extensive co-operation between PTB and partners from industry and research institutes at BESSY have been concentrated for many years on metrology for EUV lithography at 13 nm [8]. PTB's leading position in this field is underscored by a new reflectometer which enables highly accurate investigations of precision EUV multilayer mirrors of up to 50 kg in weight and 50 cm in size (Fig. 4) [9]. At the MLS, PTB will install optimised facilities to serve the increasing demand of industry for metrology with EUV radiation of extreme spectral purity. For 157 nm lithography, precision transmission optics built from CaF_2 is the key component. Fig. 5 shows the recently measured normal-incidence reflectance of two oriented CaF_2 crystals around the Γ exciton. The small but significant shift of the exciton resonance by about 0.2 nm between (100) and (111) surface orientation is due to the breaking of the cubic symmetry by the incident radiation [10].

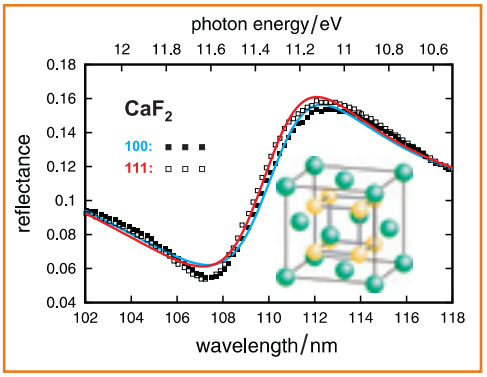

The effect qualitatively explains the birefringence of CaF_2 recently observed at 157 nm. However, application for quantitative materials testing for optical anisotropy requires polarisation dependent measurements such as ellipsometry on single samples which will be feasible with undulator radiation at the MLS.

Together with the high-energy storage ring BESSY II, the scheduled VUV Free Electron Laser, and numerous local activities in the field of optical technology, the MLS will add another jewel to the European Centre of Excellence in Berlin-Adlershof which may be used also by external groups.

Fig. 4:
PTB's new reflectometer for the characterisation of large EUV optics [9].

Fig. 5:
Experimental data (symbols) and fit (lines) of the normal-incidence reflectance around the Γ exciton of CaF_2 for a 100 and 111 surface [10].

The MLS Project Group:

A. Gottwald, R. Klein, R. Müller,
M. Richter F. Scholze,
R. Thornagel, G. Ulm (PTB, Berlin),
M. Abo Bakr, P. Budz,
K. Bürkmann-Gehrlein, D. Krämer,
J. Rahn, G. Wüstefeld (BESSY)

Contact:

Gerhard Ulm, PTB
Gerhard.Ulm@ptb.de

Klaus Bürkmann-Gehrlein, BESSY
klaus.buerkmann@bessy.de

5

Facility Report

Machine Status

The BESSY light source delivered 5,512 hours of beamtime during 40 weeks of user operation in 2003. Additional eight weeks were dedicated to machine development and beamline commissioning to further improve the performance of BESSY II. Among other machine tests, a fast local orbit feedback was successfully assessed in one of the straight sections. The reduction of the vertical and horizontal beam motion improved the signal-to-noise ratio for the UE52-undulator appreciably. Also, the experimental conditions at the infrared beam line were enhanced by decreasing noise at the mains frequency and multiples of the mains frequency originating from the corrector power supplies and from the RF system.

Single-bunch, Short bunch

Optimisation procedures for the injection into the microtron led to higher intensities in the injector allowing the storage of 20 mA in single bunch mode during user operation. Due to the improved lifetime only 5 injections per day were required. With the new injection timing system freely pre-selectable few bunch filling pattern can be created in addition to the already existing multi bunch, single bunch, and hybrid mode of operation. Machine shifts have been also used for fine tuning of the machine parameters in order to operate the storage ring with shorter bunches (e.g. low-alpha mode) with a reliability suitable for user experiments. According to our measurements, bunches which are up to 4 times shorter as compared to the usual operation mode can be offered with beam currents of 50 mA and the 8 h lifetime (see Table). In the meantime, further dedicated studies showed that sub-ps long Gaussian bunches can be produced at usable intensities. These short pulses cannot be measured with the streak camera and can only be analysed by spectroscopy of the emitted coherent radiation.

Low Alpha Optics

optics parameter		normal optics	low-alpha optics
Nat. emittance		6 nmrad	30 nmrad
Betas x/y at D-ID		18.0 m/3.5 m	16.0 m/2.5 m
Betas x/y at T-ID		1.3 m/1.3 m	16.0 m/2.5 m
Dispersion at ID		0.0 m	-0.35 m
bunch fill pattern		**buckets filled**	**buckets empty**
Multi bunch (MB)		200	200
Single bunch (SB)		1	399
current		**rms bunch length**	**lifetime**
SB	**MB**		
0.250 mA	50 mA	7.5 ps	8 h
0.100 mA	20 mA	5.5 ps	20 h
0.025 mA	5 mA	3.5 ps	40 h

Frequency maps

Frequency maps are collections of measurements in a tune diagram obtained by kicking the beam in the transverse planes with systematically increasing amplitudes and analysing the resulting beam oscillations in terms of their fundamental or dominant frequencies, for example with a Fourier transformation. Recently, the measurements and the analysis have been improved considerably and systematic studies are now possible.

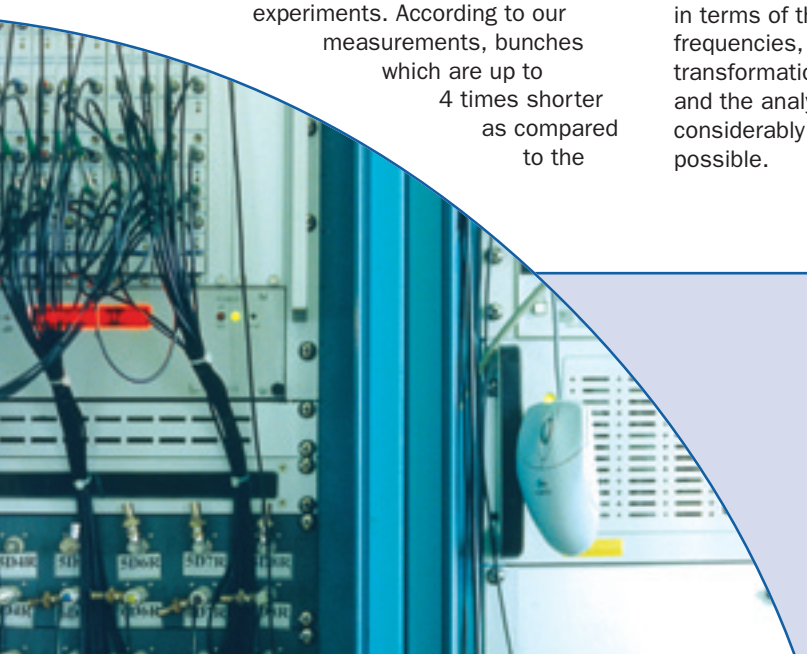

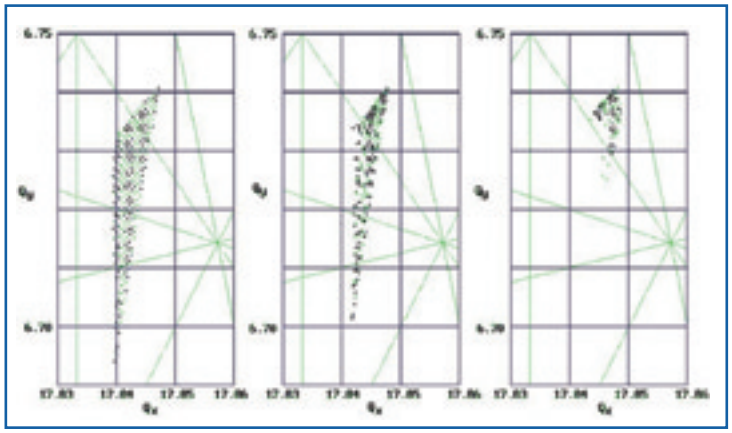

Fig. 1:
Measured frequency maps on the nominal working point of Q_x=17.848 and Q_y=6.741: left - plain storage ring without any insertion device, middle - with four superconducting wavelength shifters in operation, and right - with the upstream part of the UE56ID3R set to its smallest gap in addition.

Typical experimental results with resonances up to the sixth order are shown in Fig. 1. The reduced size of the maps in tune space reflects the smaller dynamical aperture and the shorter lifetime due to the increasing number of insertion devices being operated. Obviously the $[3Q_x+2Q_y]$-resonance plays a key role and we are confident that these maps will be a guide on how to improve the lifetime of the stored beam in the future.

Insertion devices

By moving the tools for beam diagnostic to other places in the storage ring, the last available straight section has now been cleared and undulator UE49 will be inserted during the spring shutdown. Also the 7 T Multipole Wiggler has been re-inserted with an improved version of the vacuum chamber (Fig. 2) followed by studies of the impact of this insertion device on the storage ring operation. The wiggler could be excited to 5.2 Tesla during normal user operation with beam currents up to 300 mA. The resulting lifetime reduction of the stored beam (up to 40%) could be attributed to the increase of the vacuum pressure accompanied by the excitation of the wiggler. In machine development shifts an optimised compensation scheme for the focusing effects of the insertion devices was developed. With the quadrupole corrections spread around the ring the phase jump and the beta beat can be made more localised. This leads to a significant improvement of the lifetime.

Fig. 2:
Installation of the improved water cooled version of the vacuum chamber in the beamline of the multipole wiggler.

Fig. 3:
Assembly of the central cryogenic plant.

During the summer, the central cryogenic plant and the gas distribution system was installed and went into operation shortly after (Fig. 3). Now all four superconducting wavelength shifters are supplied with liquid helium routinely once or twice a week by this system. Some modifications are still required in order to allow a continuing refill of helium, a prerequisite to switch off the local re-condensers which are the cause of the 1.6 Hz orbit motion.

Contact:
Peter Kuske
peter.kuske@bessy.de

Beamline Developments

Fig. 4:
The 3rd harmonic cavity at BESSY.

In contrast to the previous five years during which a total of 46 beamlines have been made available for the users, tantamount to commissioning a new beamline every 5 weeks, one can see only the 'tip of the iceberg' from our efforts in 2003. Nevertheless, extensive and exciting projects which will make significant qualitative changes in the nature of the experiments that can be performed at BESSY are in the works. The key to these developments is summarised in the prefix 'micro': microbunching for femtosecond pulses of SR and micrometer focus for very small spot experiments from 90 eV well into the hard X-ray range.

Future Developments

The superconducting 3rd harmonic-(Landau)-cavity for lifetime improvement to replace the four normal conducting ones has been delivered (Fig. 4). As further cold tests at BESSY and preparations of the RF electronics are still coming up, we expect installation into the storage ring in the winter shutdown 2004/5.

The prototype of the superconducting dipole magnet ('superbend') to possibly replace superconducting insertion devices of the BESSY storage ring in a later phase has been assembled by the Budker Institute Novosibirsk (BINP). The magnet is still subject of ongoing tests and will be delivered in 2004.

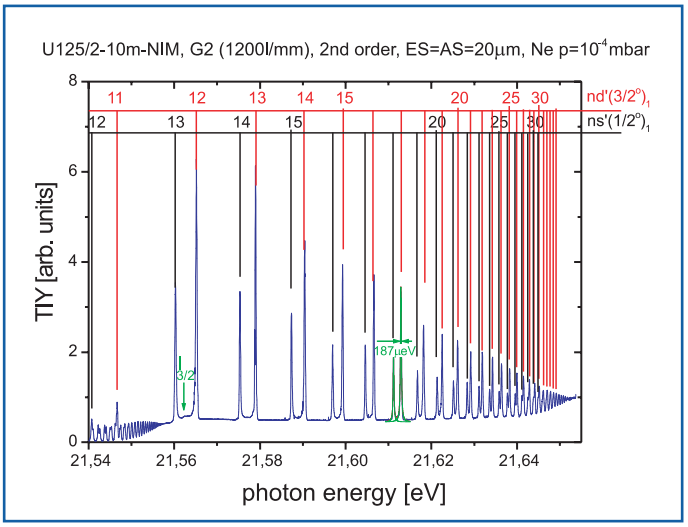

Fig. 5:
Comparison of the Ne ion yield data at 10m-NIM at U125/2 with spectroscopic data.

Several prominent developments have come to fruition since the last Annual Report was published. High resolution experiments at energies down to 5 eV are now possible on the newly commissioned 10m NIM on the U125/2 undulator. With its high linear dispersion and a completely new concept in grating drive, a resolution, $E/\Delta E > 200{,}000$ has been achieved (20 µm slits) (Fig. 5). With 100 µm slits ($E/\Delta E = 50{,}000$) a photon flux of 1,010 photon/sec·100 mA is delivered. In addition, the absolute wavelength scale is accurate to within a factor of 10^{-5} of spectroscopic data.

After nearly 20 years of operation, the BESSY I KMC-1 double crystal monochromator was replaced with the latest version of the Oxford Instruments DCM and the optical arrangement optimised. The result is a resolution of 0.2 eV at 3,820 eV, E/ΔE = 20,000 (Fig. 6). This monochromator together with the new PHOENEXS experimental station including a PHOIBOS 150 electron spectrometer makes possible high energy resolution photoelectron spectroscopy at photon energies up to 12 keV on buried interfaces etc.

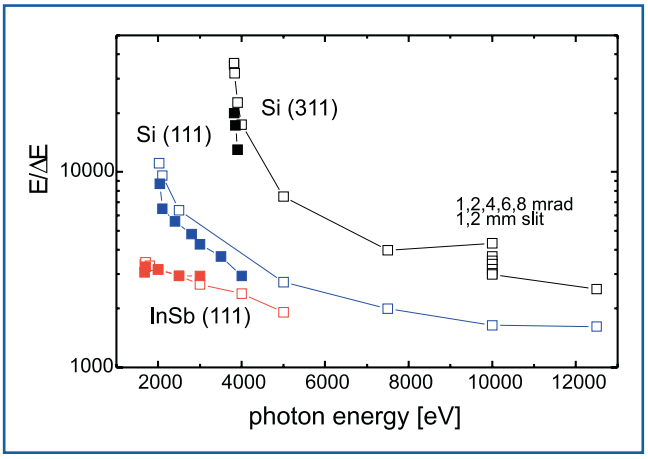

Fig. 6:
The resolution of the new KMC1 beamline from 2 to 10 keV.

Further development of the low alpha mode (short electron bunches leading to coherent synchrotron radiation) culminated in a full week of user beamtime for spectroscopy down to 2 cm^{-1} i.e. well into the terahertz region. Both, a single bunch mode and a multibunch mode have been cultivated with a minimum rms pulse length of 3.5 ps with 5 mA current (multibunch mode). Stable operation and a beam lifetime of 8 to 40 hours, depending upon the bunch length selected, made for successful user shifts during this week. Several non-IR users came especially to profit from the short pulses. Because of the import of this development, a week of low alpha operation has been again scheduled in 2004.

Last year we reported on the breakthrough made at BESSY in the metrology of optical elements: the sub-nanometer profiler, NOM. With measurements from the NOM, it was possible for a partner in the consortium to make very fine corrections to the geometry of an aspheric mirror. The result is a plane elliptical mirror of 190 mm length with a meridional tangent error of 0.14 arc sec rms. This mirror is now installed on the UE52/SGM where it demagnifies the source by a factor of 38 and focuses it horizontally on the sample to less than 8 µm rms. The vertical focus is a 1:1 image of the exit slit, produced by a second mirror. With the previous mirrors on this beamline the horizontal focus was 2-3 times larger (Fig. 7). This achievement will become increasingly important with regard to the several small spot systems being built at BESSY at the present time.

Several ongoing projects are nearing completion and can be mentioned here. A new high resolution monochromator on U125/1 will provide users with undulator radiation at energies from 5 to 300 eV. At the other end of the spectrum, the HMI-7T-MPW with 4 - 60 keV photons is presently being commissioned. A high energy micro-focus beamline on the BAM 7T-WLS is being built for 1.9 - 30 keV with a primary focal spot of 200 x 200 μm^2. With capillary optics this focus can be reduced to ca. 5 x 7 μm^2.

Two major long term projects have been keeping a large number of colleagues in both the machine and the experimental group busy for some time now: a new ID and beamline for SR of variable polarisation with a particularly small focus size, and the realisation of a system for generating femtosecond (fs) pulses of circularly polarized SR in the BESSY storage ring. The former project, in which the machine diagnostics in the last available straight section, L08, will be replaced with a new undulator, UE49, will take advantage of the low horizontal beta function there to yield a vertically and horizontally (very) small spot at the experiment: 15 μm^2. This PGM beamline will have two outlet arms so that two large experimental stations for photoelectron microscopy can alternatively receive light from the UE49. A second complete beamline for high flux experiments is planned with an

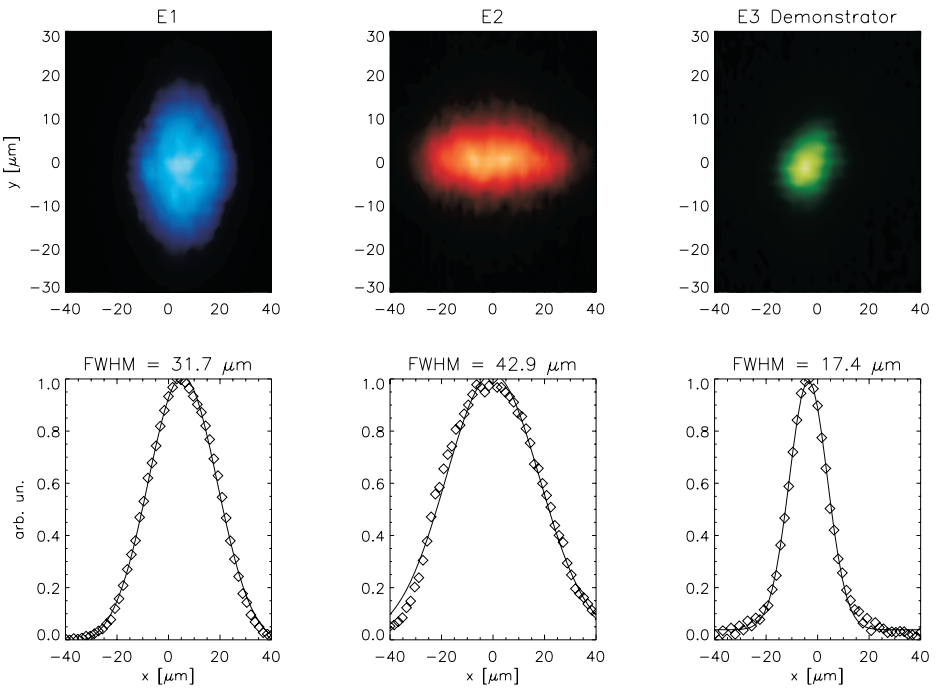

Fig. 7:
Horizontal focus at the experiment on the UE52/SGM with three different refocussing mirrors. Left to right, Tangent error 1.08 arcsec rms, 1.49 arcsec rms, 0.14 arcsec rms. The profiles are horizontal scans of the focus. The vertical size reflects a 1:1 image of the exit slit opening which was different for the three images.

exceptionally high transmission and small spot, in this case ~1 μm². However, because of financial and manpower limitations this latter beamline will be built after completion of the first.

For the second major project, fs-slicing, the UE56/1 double undulator will be replaced by a combination of its downstream half (radiator) and a new undulator (modulator), U139, on the upstream side and three new dipole chicane magnets (Fig. 8). Together with a high power fs laser, pulses of radiation in the UE56 photon energy range will be generated with a length (rms) of the order of 50 fs. Because of the changes in the source parameters, both beamlines on UE56/1 had to be redesigned and relocated. Special care had to be taken in the design to minimise dispersive pulse lengthening. The in-tunnel components for both of these projects are ready for installation in the five week long shutdown in March-April 2004. The realisation of these and the other ongoing projects will make 2004 a particularly exciting year.

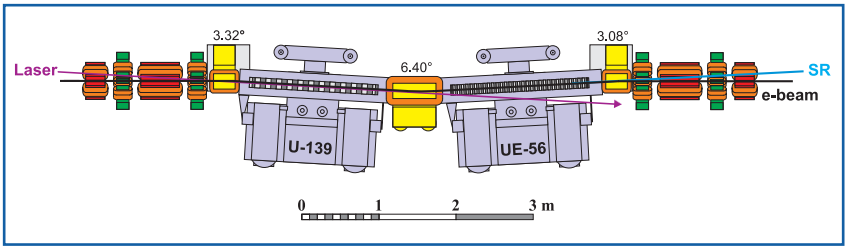

Fig. 8:
Sketch of the fs-slicing setup with modulator (U-139), radiator (UE-56) and three new dipole chicane magnets.

Contact:
William B. Peatman
peatman@bessy.de

6

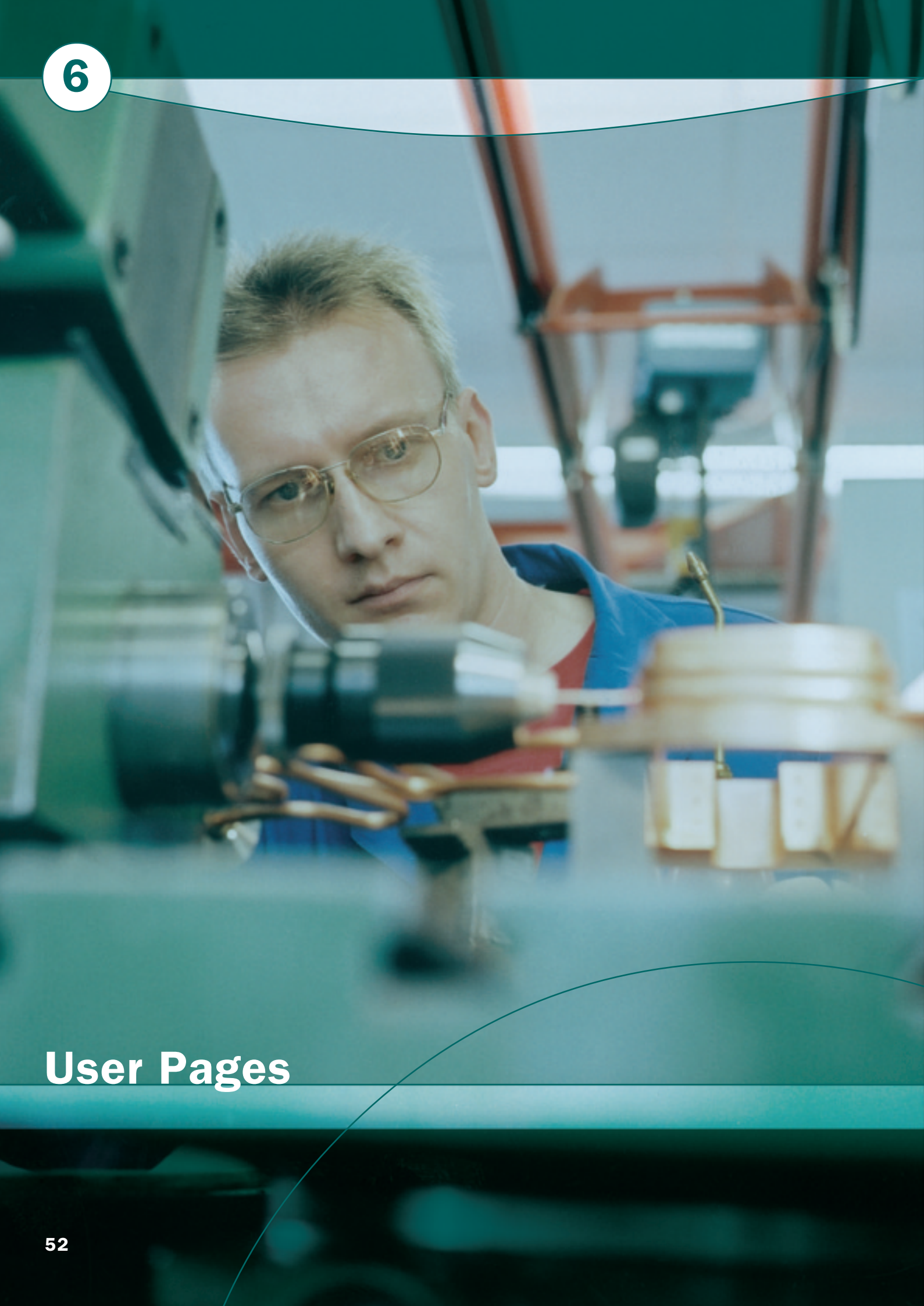

User Pages

Operation statistics

Currently, the facility provides over 40 weeks of dedicated beamtime per year. Operation is based on a schedule of 7 days a week, 24 hours per day (three 8 hour shifts) which after subtracting the service shifts, amounted to 5,200 user-dedicated hours in 2003. In fact, 5,512 hours were delivered. In addition, some 800 hours were used for studies to optimise the light source and user instrumentation and to advance accelerator technologies and physics. The storage ring was operated for users 35 weeks in multi-bunch, 4 weeks in single bunch and 1 in low-α mode. Due to this years' demand a low-α mode is scheduled again for week 47 in 2004.

Today, only five years after the start of user operation, 26 insertion device (ID) beamlines and 20 bending magnet (BM) beamlines are available for the users. This unparalleled rapid growth of the facility was accomplished by establishing a well organised mix of facility-built and operated beamlines and of beamlines constructed and run by cooperating research groups (CRGs). At present, more than 1,000 external scientists carry out almost 400 independent projects per year in basic research at BESSY. The available time on the high performance ID beamlines is oversubscribed by a factor of two.

About 20 experimental endstations for research in basic sciences are operated by BESSY and CRGs. Users benefit from the new set-ups, which allow for challenging experiments even for those without their own equipment. The BESSY based activities (beamlines and endstations) concentrate on microfocus, high flux, and high energy resolution. Several new high performance beamlines, being developed and built in 2003, will be operational in the second half of 2004.

During the year three CRGs have been evaluated by external boards of referees appointed by the Scientific Advisory Committee of BESSY. The CRGs lead by the Max-Planck-Gesellschaft (UE 46/2), Max-Born-Institute (U 125/1-SGM) and Universität Cottbus (U49/2-PGM2) have all been recommended to continue with their successful scientific and instrumental programmes.

Beamtime at BESSY

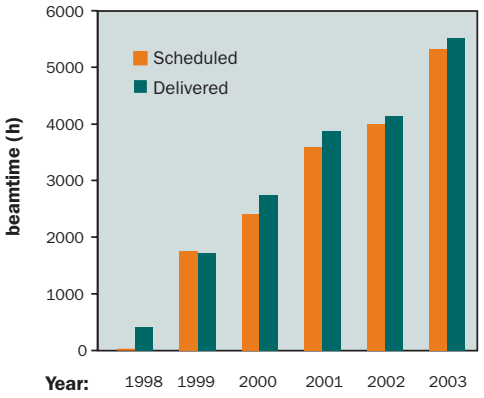

Beamtime allocation in 2002

Insertion Device Beamlines

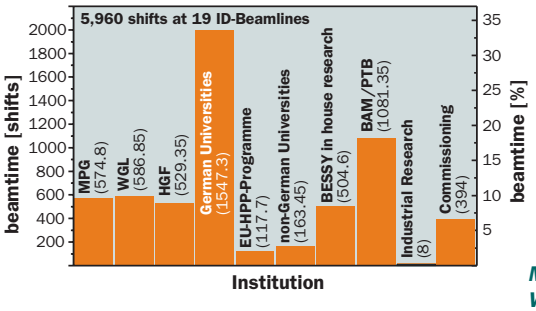

Bending Magnet Beamlines

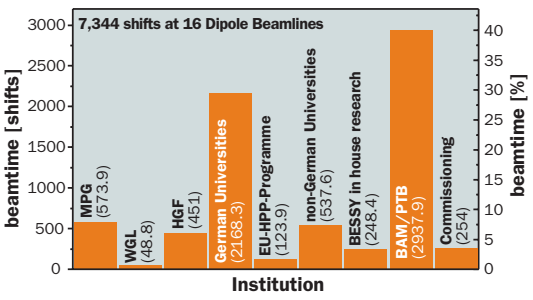

Main Research

Allocated beamtime

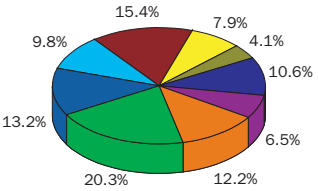

Number of projects

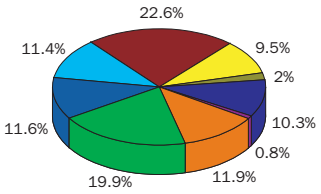

atoms, molecules, clusters
electronic and magnetic structure of solids
surface science
material sciences
life sciences
catalysis, chemistry and chemical dynamics
new methods and instrumentation
radiometry
LIGA and micromechanics

MPG = Max-Planck-Gesellschaft
WGL = Leibniz-Gemeinschaft
HGF = Helmholtz-Gemeinschaft
BAM, PTB = Bundesanstalten

Improvements for users

Impressions of the new IBZ guest house.

The increasing number of users has led to a housing shortage on site. Since January 2004, this has been relieved somewhat by the inauguration of the third building of the IBZ, now offering space for 139 people. The infrastructure in Adlershof has further improved benefiting strongly from the move of the scientific departments of the Humboldt Universität on site. The cafeteria in the Erwin-Schrödinger-Zentrum offers meals weekdays until 19 h. A shopping centre with supermarket, department store and cafes has opened.

For the first time, a User Committee (UC) was elected by the registered participants at the BESSY Annual Users' Meeting. The UC is the link between users and management. It advises individual users, user groups and the scientific director on operational matters concerning the conduction of experiments at BESSY. The panel consists of the beamtime coordinator, the machine operations coordinator and the following four external members:

Dr. U. Hergenhahn (chairman)
Max-Planck-Institut für Plasmaphysik, München

Dr. W. Braun
Paul-Drude-Institut, Berlin

Dr. Ch.-H. Fischer
Hahn-Meitner-Institut, Berlin

Dr. W. Kuch
Max-Planck-Institut für Mikrostrukturphysik, Halle

The individual tenure is for two years.

BESSY works on improving user services and is grateful for the critical remarks at the Users' Meeting. The following issues were brought up there.

- The pros and cons of changing the present system on having user blocks starting on weekends have been set down on paper and the User Committee brought into the discussion. A decision will be announced during the year.
- We are attempting to alleviate the problems resulting from the limited number of beamline scientists by seeing to it that at the beginning of every shift the beamline scientist or his deputy will be available until the beamline works to the satisfaction of the users.
- It was pointed out that a request can be addressed to the management asking for permission to let an experiment run unattended, should there be good reason for this. In no case, however, will a remote controlled opening of the beamshutter be allowed. Thus, after an injection before which the beamshutters are automatically closed, a scientist must restart his experiment directly at the beamline.
- Top-up injections, as requested by some users, have been shown to produce radiation damage on insertion devices at other synchrotron radiation facilities leading to a degradation in their performance. Aside from that, there are some questions regarding personal radiation safety that must still be clarified.

Users may benefit of the ongoing improvements of the software. The new EMP 4 program allows one to scan different regions with high resolution and jump to the next one without measuring in between. The software group is very aware of the problems that can arise when scanning both monochromator and undulator, in the worst case, a computer crash. Improvements in the software are presently being made to alleviate this problem.

Some may already have noticed that the electronic noise on the electron beam has been greatly reduced. Replacing the power supplies of the pumps significantly decreased the 50 Hz noise. The remaining 1.6 Hz oscillation due to the switching of the WLS re-condensers is expected to be largely reduced as soon as the new cryogenic plant works to our full satisfaction.

Industrial users

BESSY offers services for industrial users in the broad spectral range from Terahertz to X-rays. Cooperation partners work on the fields of micro-engineering, chip technology, optical metrology, protein structures, surface analysis and magnetic materials. BESSY is open to the requests of industrial users. It will provide the opportunity for a test experiment on the shortest possible time scale. Depending on the scientific area, contact to cooperation partners, support of the individual experiments, including evaluation of the data, can be offered.

In addition, the three major German synchrotron radiation facilities ANKA, HASYLAB and BESSY have started a series of workshops called 'Industrieforum'. In 2003 the subject of the workshop was 'In situ characterisation of catalytic processes'. The series will continue on the topic 'micro-engineering' taking place at BESSY in the autumn of 2004.

Contact for industrial activities:
Dr. Walter Braun (braun@bessy.de)

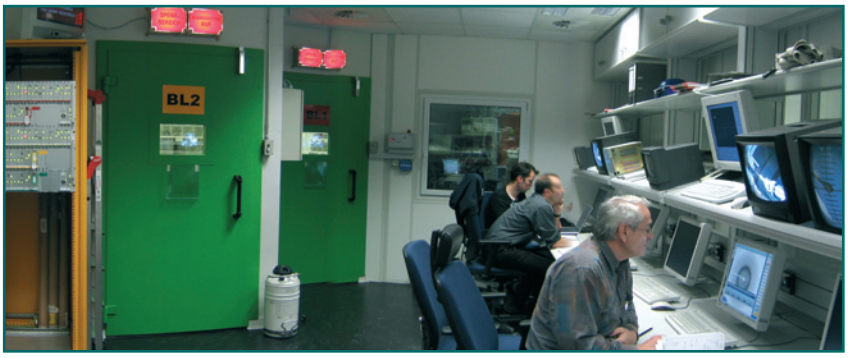

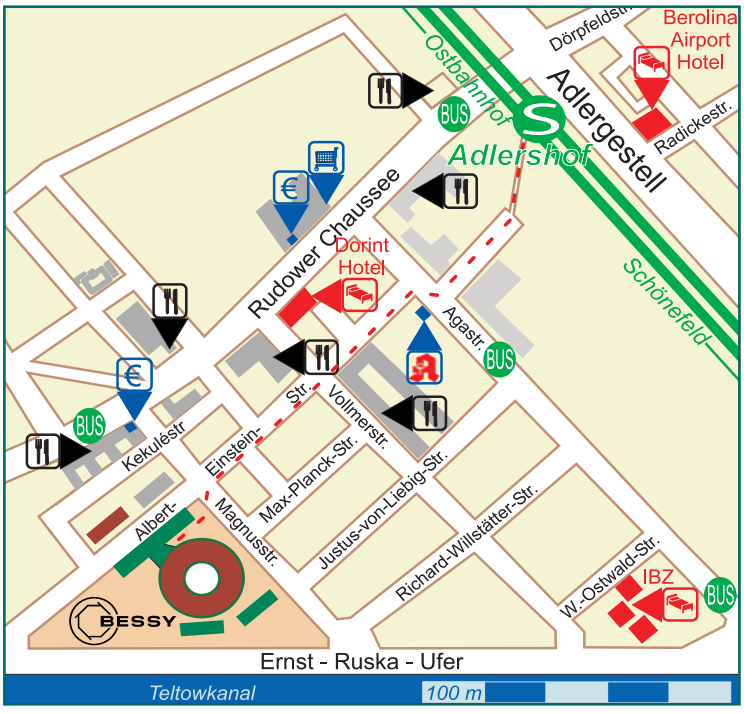

ID Beamlines at BESSY

(January 2004)

BAM Bundesanstalt für Materialforschung und -prüfung

BTUC Brandburgische Technische Universität Cottbus

FUB Freie Universität Berlin

FZJ Forschungszentrum Jülich

HMI Hahn-Meitner-Institut

MBI Max-Born-Institut, Berlin

MPG Max-Planck-Gesellschaft

PSF Proteinstruktur-fabrik

PTB Physikalisch-Technische Bundesanstalt

U Bi Universität Bielefeld

TUD Technische Universität Dresden

U Gö Universität Göttingen

U Po Universität Potsdam

U Wü Universität Würzburg

Insertion Device	Monochromator	Energy Range (eV)	Contact Persons	
7 T WLS/1	KMC-1	6 k – 50 k	H. Riesemeier (BAM) B. Müller (BAM)	A. Erko
U 125-2	SGM	20 – 500	R. Püttner (FUB)	G. Reichardt
U 125-2	KMC	6 k – 12 k	W. Braun (PDI) B. Jenichen (PDI)	A. Erko
U 125-2	10m-NIM	< 10 – 35	G. Reichardt	I. Packe P. Rotter
UE 56-2	PGM 1	60 – 1,300	W. Mahler (MPG)	B. Zada (MPG)
UE 56-2	PGM 2	60 – 1,300	W. Mahler (MPG)	B. Zada (MPG)
6 T WLS	LITHO	> 2,000	B. Löchel H. Köhrich	H.-U. Scheunemann M. Bednarzik
0.4 T	LITHO	> 2,000	B. Löchel H. Köhrich	H.-U. Scheunemann M. Bednarzik
U 180 / (U 49-1)	13°		R. Klein (PTB)	A. Gottwald (PTB)
U 180 / (U 49-1)	PGM	20 – 1,900	B. Beckhoff (PTB)	
U 180 / (U 49-1)	-	direct beam	R. Klein (PTB)	
UE 52	SGM	85 – 1,600	K. Godehusen F. Senf	T. Zeschke
UE 52	PGM	85 – 1,600	T. Schmidt (U Wü)	C. Jung
UE46	PGM	120 – 1,700	H. Rossner (HMI) D. Schmitz (HMI)	F. Senf
UE 56-1**	PGM	60 – 1,300	T. Kachel J. Schmidt	T. Zeschke
UE 56-1**	SGM	60 – 1,300	S. Cramm (FZJ)	
U 41	STXM	~ 250 – ~600	P. Guttmann (U Gö)	G. Schneider
U 41	TXM	~ 250 – ~600	P. Guttmann (U Gö)	G. Schneider
U 41	PGM	170 – 1,800	C. Jung	M. Mast
U 125-1	SGM	15 – 180	B. Winter (MBI) T. Gießel (MBI)	R. Follath
U 125-1	Multilayer	80 – 700	M. Pohl (U Bi)	
U 125-1	PGM	20 – 700	P. Bressler	F. Eggenstein
7T WLS/2	KMC-1	4.5 k – 17.5 k	U. Müller (PSF)	M. Fieber-Erdmann (PSF)
7T WLS/2	KMC-2	4.5 k - 17.5 k	U. Müller (PSF)	M. Fieber-Erdmann (PSF)
7T WLS/2*	KMC-3	13.7 k	U. Müller (PSF)	M. Fieber-Erdmann (PSF)
U 49-2	PGM-1	85 – 1,600	O. Schwarzkopf R. Follath	J.-S. Schmidt
U 49-2	PGM-2	85 – 1,600	P. Hoffmann (BTUC)	

** under construction*
*** reconstruction for fs-slicing*

For general information on beamlines see BESSY website under www.bessy.de.

ID02-2 7TWLS/1-KMC1	BAM/PTB
ID03-1 U125/2-SGM	BUS
ID03-2 U125/2-KMC	PDI/HUB
ID03-3 U125/2-NIM	UKL/BESSY
ID05-1 UE56/2-PGM1	MPG
ID05-2 UE56/2-PGM2	MPG
ID06-1a 6T-LITHO	BESSY
ID06-1b 0.4T-LITHO	BESSY
ID07-1 U49/U180 13°	PTB
ID07-2 U49/U180-PGM	PTB
ID07-3 U49/U180 direct beam	PTB
ID09-1 UE52-SGM	BESSY
ID09-2 UE52-PGM	UFF-CRG
ID10-1 UE46-PGM	HMI
ID11-1 UE56/1-PGM	BESSY**
ID11-2 UE56/1-SGM	FZ Jülich**
ID12-1a U41-STXM	U Gö/BESSY
ID12-1b U41-TXM	U Gö/BESSY
ID12-2 U41-PGM	BESSY
ID13-1 U125/1-SGM	MBI/BESSY
ID13-2 U125/1-ML	U Bielefeld
ID13-3 U125/1-PGM	BESSY
ID14-1 7TWLS/2-KMC1	Protein
ID14-2 7TWLS/2-KMC2	Protein
ID14-2 7TWLS/2-KMC3	Protein*
ID15-1 U49/2-PGM1	BESSY
ID15-2 U49/2-PGM2	BTUC

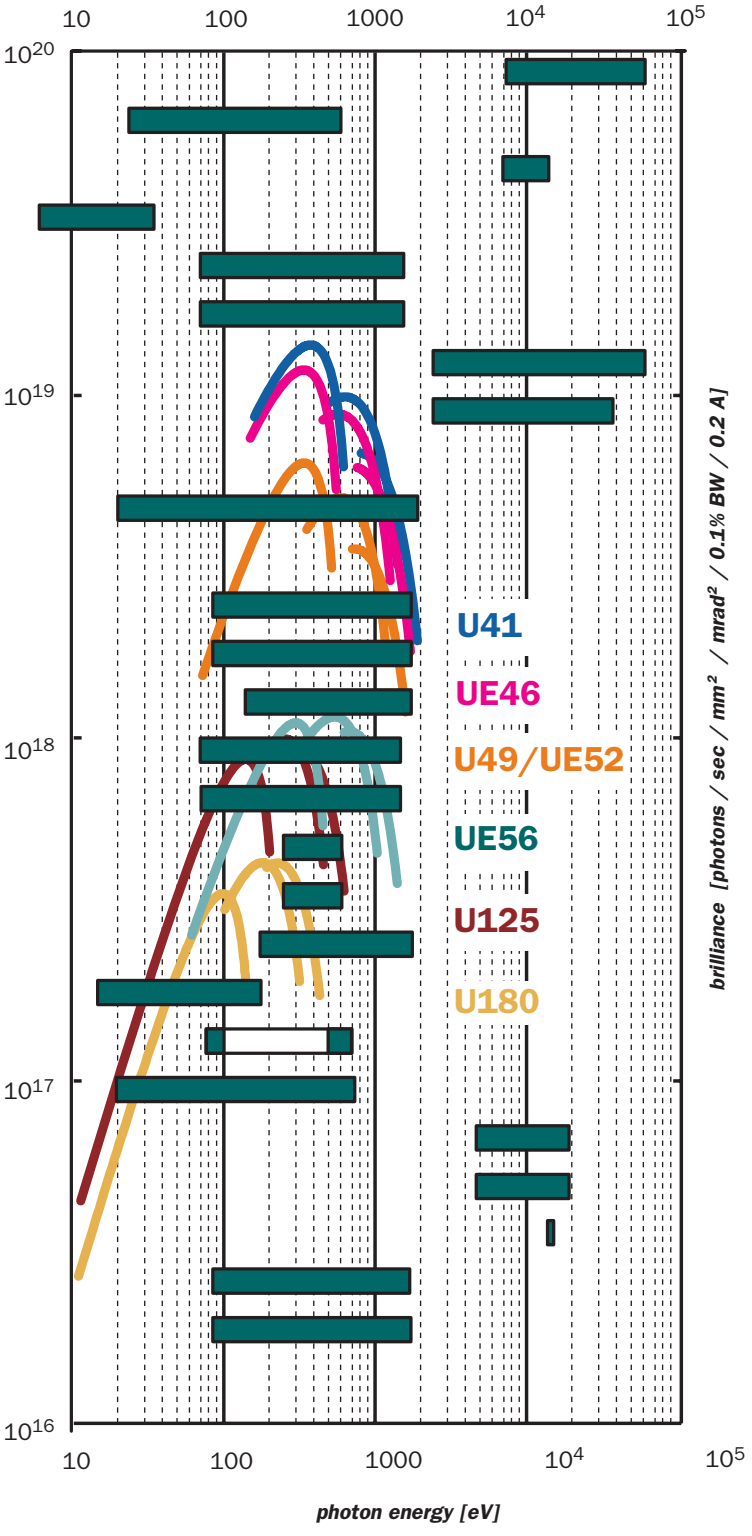

BESSY II,
1.7 GeV, 200 mA coupling 1%

Dipole Beamlines at BESSY

(January 2004)

BAM
Bundesanstalt für Materialforschung und -prüfung

BTUC
Brandburgische Technische Universität Cottbus

FUB
Freie Universität Berlin

FZJ
Forschungszentrum Jülich

HMI
Hahn-Meitner-Institut

MBI
Max-Born-Institut, Berlin

MPG
Max-Planck-Gesellschaft

PSF
Proteinstrukturfabrik

PTB
Physikalisch-Technische Bundesanstalt

U Bi
Universität Bielefeld

TUD
Technische Universität Dresden

U Gö
Universität Göttingen

U Po
Universität Potsdam

U Wü
Universität Würzburg

Monochromator	Energy Range (eV)	Contact Persons	
Litho EUV	95	H.-U. Scheunemann H. Köhrich	
KMC-1	1.7 k – 10 k	F. Schäfers	M. Mertin
FT-IR	IR	U. Schade	
3m-NIM-2	4 – 35	I. Packe	G. Reichardt
LITHO	direct beam	B. Löchel H.-U. Scheunemann	H. Köhrich M. Bednarzik
1m-NIM-1	3 – 35	M. Richter (PTB)	
1m-NIM-2	3 – 35	M. Richter (PTB)	
	white beam	R. Thornagel (PTB)	
KMC	1.7 k – 10 k	M. Krumrey (PTB)	
PGM	30 – 1,800	F. Scholze (PTB)	
HE-SGM	200 – 700	A. Lippitz (BAM)	O. Schwarzkopf
Optics-BL	20 – 2,000	F. Senf	
KMC-2	4.5 k – 15 k	A. Erko	I. Packe
PM-3	20 – 1,900	T. Kachel	F. Eggenstein
3m-NIM-1	4 – 35	I. Packe	G. Reichardt
EDR	2 k – 12 k	W. Leitenberger (U Po) Y. Bodenthin (U Po)	A. Erko
TGM-4	8 – 120	K. Godehusen	M. Mast
TGM-7	8 – 120	C. Pettenkofer (HMI) W. Bremsteller (HMI)	
PGM-RG-BL	30 – 1,500	D. Vyalikh (FUB) S. Molodtsov (TUD)	
CP-NIM	4 – 35	F. Schäfers	M. Mertin

For general information on beamlines see BESSY website under www.bessy.de.

D01-1A ML-LITHO	BESSY
D01-1B KMC1	BESSY
D02-1A FT-IR	IRIS/BESSY
D03-1B 3m NIM2	BESSY
D06-1A LITHO	BESSY
D06-1B 1m NIM1	PTB
D07-1A1 1m NIM2	PTB
D07-1A2 white beam	PTB
D07-1B KMC	PTB
D07-2 PGM	PTB
D08-1B1 HE-SGM	CRG
D08-1B2 Optics-BL	BESSY
D09-2 KMC2	BESSY
D11-1A PM3	BESSY
D12-1B 3m NIM1	BESSY
D13-2 EDR	U Potsdam
D15-1A TGM4	BESSY
D15-1B TGM7	HMI
D16-1A RG-BL-PGM	U Petersburg
D16-1B CP-NIM	BESSY

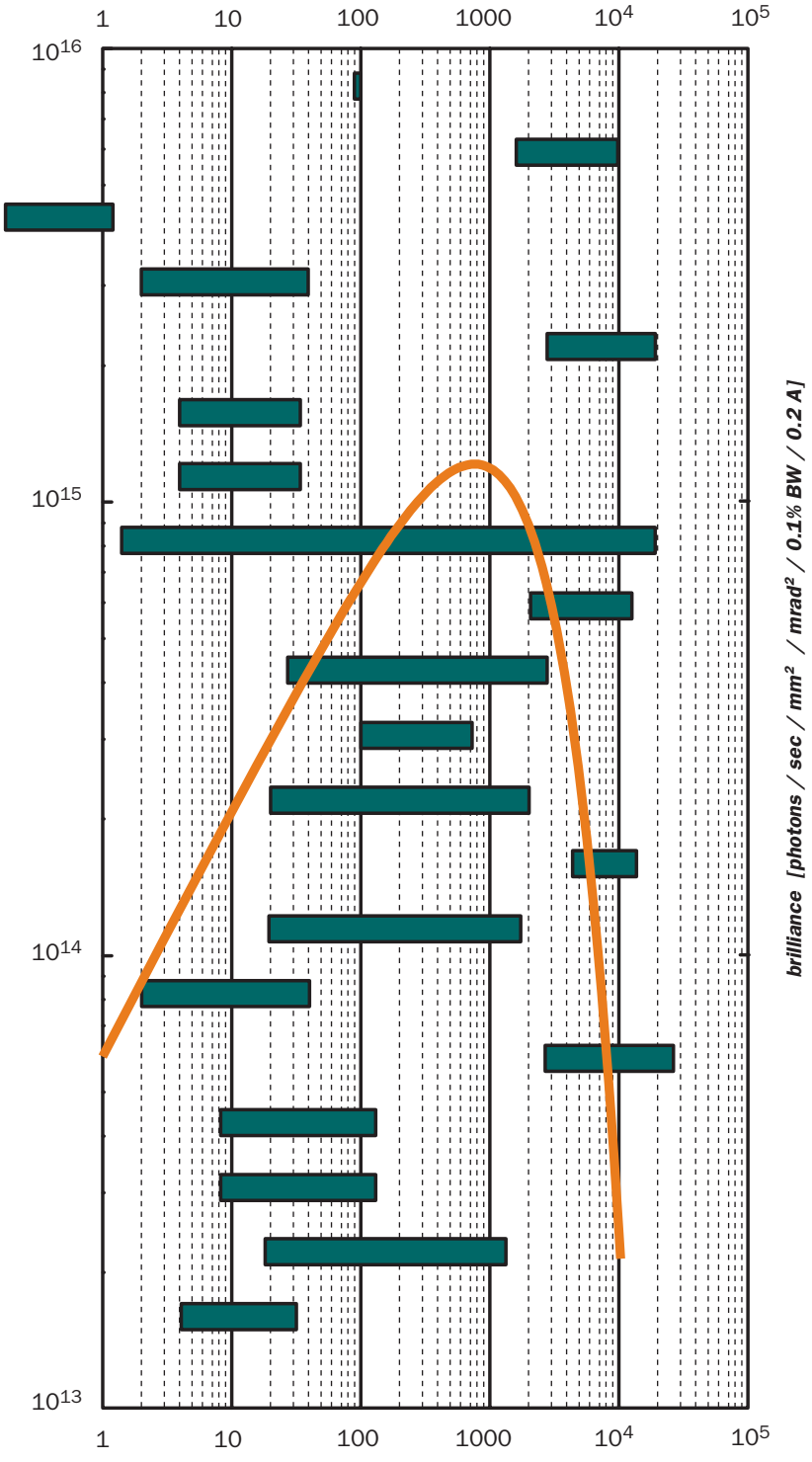

BESSY II
1.7 GeV, 200 mA coupling 1%

Experimental stations

For more information please look on the BESSY website (www.bessy.de)

or contact W. Braun (braun@bessy.de) or Ch. Jung (jung@bessy.de).

Experiment	*Contact*	*Location*
THz spectroscopy[BioSR, Ind]	holldack@bessy.de	IR
IR-spectroscopy -microscopy[BioSR, Ind]	schade@bessy.de	IR
IR ellipsometry[Ind]	hinrichs@isas-berlin.de	IR
HIRES - high resolution electron spectrometer	rader@bessy.de	variable
PHOENEXS - photoemission and near edge X-ray spectroscopy	bressler@bessy.de	variable
MUSTANG - multi-user stage for angular resolved photoemission	sperling@bessy.de	variable
SAMIC - spectroscopy and microscopy integrating chamber[Ind]	patrick.hoffmann@tu-cottbus.de	U49/2-PGM/2
Two-Photon-Photoemission Experiment	bwinter@mbi-berlin.de	variable
XPEEM - Photemission microscopy	pohl@physik.uni-bielefeld.de	U125/1-Multilayer
HIRE-PES - energy resolution photoemission	christoph.jannowitz@physik.hu-berlin.de	variable
Stored Nano Particels	ruehl@phys-chemie.uni-wuerzburg.de	variable
Photoemission microscope for time resolved spectroscopy in the ps-regime[Ind]	schoenhe@mail.uni-mainz.de	variable
High resolution spinpolarisation photoelectron spectroscopy	c.m.schneider@fz-juelich.de	variable
So-Li-AS - solid-liquid-analysis system	mayerth@surface.tu-darmstadt.de	TGM 7
VUV/XUV ellipsometry[Ind]	esser@isas-berlin.de	variable
UVIS - protein circular dichroism spectroscopy[BioSR]	baumgaer@rz.uni-potsdam.de	3m-NIM-1
Scattering experiments in the VUV/XUV-range	eugen.weschke@physik.fu-berlin.de	variable
MPG Catalysis Beamline[planned]	knop@fhi-berlin.mpg.de	variable
EUV-lithography[Ind]	scheunemann@bessy.de	variable
X-ray lithography[Ind]	loechel@bessy.de	variable
Fluorescence spectroscopy[Ind]	ruediger.mitdank@physik.hu-berlin.de	variable
Soft X-ray emission spectrometer	eisebitt@bessy.de	variable
CISSY - CIS- diagnostic using Synchrotron radiation	cissy@hmi.de	variable
ROSA - rotateable spectrometer apparatus	szargan@rz.uni-leipzig.de	variable
SMART - spectro-microscope with highest spatial resolution	thomas.schmidt@physik.uni-wuerzburg.de	UE52-PGM
XM - X-ray Microscopy[BioSR, Ind]	guttmann@bessy.de	U41-XM
Reflectometry[Ind]	schaefers@bessy.de	PM 4
Polarimetry	schaefers@bessy.de	variable
Diffraction	erko@ bessy.de	KMC-2
micro-XANES, -EXAFS, -fluorescence[BioSR]	erko@bessy.de	7T-WLS-1
X-ray diffraction during MBE	braun@pdi-berlin.de	U125/2-KMC
PSF - protein crystallography[BioSR, Ind]	umue@bessy.de	7T-WLS-2
BAMline - nondestructive testing in analytical chemistry[Ind]	heinrich.riesemeier@bam.de	7T-WLS-1
EDDI - energy dispersive diffraction	genzel@hmi.de	7T-MPW
MagS - resonant magnetic scattering	feyerherm@hmi.de	7T-MPW

planned under construction *BioSR suitable for biological samples* *Ind suitable for industrial users*

Status of BESSY

in operation

under construction

planned

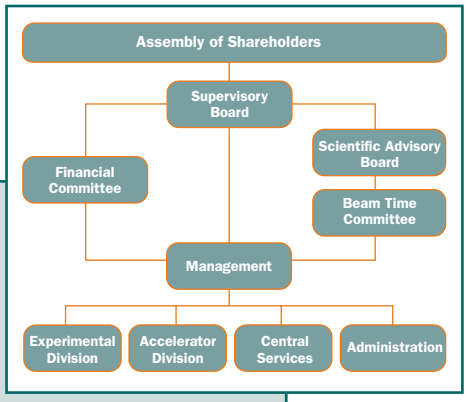

Supervisory Board:

Prof. Dr. J. Treusch (Chairman)	Forschungszentrum Jülich
Prof. Dr. E. Umbach (Vice Chairman)	Universität Würzburg
Min.Dir. Dr. H.F. Wagner	Bundesministerium für Bildung und Forschung
Prof. Dr. E. O. Göbel	PTB, Braunschweig
Prof. Dr. R. Maschuw	Forschungszentrum Karlsruhe
Dr. H. Braun	Max-Planck-Gesellschaft München
Frau Prof. Dr.-Ing. L. Blessing	Technische Universität Berlin
Prof. Dr. J. Schneider	DESY Hamburg
Dr.-Ing. P. Szent-Ivanyi	Bundesministerium für Wirtschaft und Arbeit, Berlin
Prof. Dr. M. Steiner	Hahn-Meitner-Institut, Berlin
Senatsdirig. W. Eckey	Senatsverwaltung für Wissenschaft, Forschung und Kultur Berlin

Scientific Advisory Committee:

Prof. Dr. M. Grunze (Chairman)	Universität Heidelberg
Dr. A. Wrulich (Vice Chairman)	Paul-Scherrer-Institut, Villigen
Prof. D.S. Chemla	ALS Berkeley
Prof. M. Eriksson	MAX-Lab
Prof. Dr. K.C. Holmes	Max-Planck-Institut für Medizinische Forschung Heidelberg
Prof. E.J. Nordgren	Universität Uppsala
Prof. Dr. V. Saile	Forschungszentrum Karlsruhe
Prof. Dr. W. Sandner	Max-Born-Institut, Berlin
Prof. Dr. R. Schlögl	Fritz-Haber-Institut, Berlin
Prof. Dr. G. Schütz	Max-Planck-Institut für Metallforschung, Stuttgart
Prof. Dr. J. Stöhr	SSRL Stanford

Permanent Guests

Prof. Dr. J. Richter	Bundesministerium für Bildung und Forschung
Prof. Dr. R. Gerhardt-Multhaupt	Universität Potsdam
Prof. Dr. J. Kirschner	Max-Planck-Institut für Mikrostrukturphysik, Halle
Dr. T. Möller	HASYLAB/DESY, Hamburg
Dr. R. Schuchhardt	Senatsverwaltung für Wissenschaft, Forschung und Kultur Berlin

Members of the Beam Time Committee (January 2004)

Prof. Dr. E. Rühl (Chairman)	Universität Würzburg
Prof. Dr. W. Wurth (Vice Chairman)	Universität Hamburg
Prof. Dr. D. Arvanitis	Universität Uppsala
Prof. Dr. S. Blügel	Forschungszentrum Jülich
Prof. Dr. J. Fink	IFW Dresden
Prof. Dr. K. Horn	Fritz-Haber-Institut, Berlin
Prof. Dr. K.-H. Schartner	Universität Gießen
Prof. Dr. G. Schütz	Max-Planck-Institut für Metallforschung, Stuttgart
Prof. Dr. L. Singheiser	Forschungszentrum Jülich

Subcommittee Proteincrystallography

Prof. Dr. R. Ficner	Universität Göttingen
Prof. Dr. P. Lindley	Universität Lissabon
Dr. M. Wilmanns	EMBL Hamburg

Members of the Financial Committee (January 2004)

S. Lettow (Chairman)	Forschungszentrum Karlsruhe
R. Kellermann (Vice Chairman)	Forschungszentrum Jülich
Dr. W. Buck	PTB, Berlin
M. Schleier	Max-Planck-Gesellschaft, München
Dr. R. Schuchardt	Senatsverwaltung für Wissenschaft, Forschung und Kultur Berlin
N.N.	Bundesministerium für Bildung und Forschung

Contact

Scientific Director

Prof. Dr. Dr. h.c. Wolfgang Eberhardt
Secretary: Ines Maupetit
phone +49 (0)30 / 6392 4633
fax +49 (0)30 / 6392 2989
wolfgang.eberhardt@bessy.de,
ines.maupetit@bessy.de

Technical Director

Prof. Dr. Eberhard Jaeschke
Secretary: Dr. Nikoline Hansen
phone +49 (0)30 / 6392 4651
fax +49 (0)30 / 6392 4632
eberhard.jaeschke@bessy.de,
nikoline.hansen@bessy.de

Administration

Thomas Frederking
Secretary: Katrin Rosenblatt
phone +49 (0)30 / 6392 2901
fax +49 (0)30 / 6392 2920
thomas.frederking@bessy.de,
katrin.rosenblatt@bessy.de

Beamtime Coordination

Dr. Walter Braun, Dr. Gerd Reichardt
Secretary: Stine Mallwitz
phone +49 (0)30 / 6392 2904
fax +49 (0)30 / 6392 4673
beamtime@bessy.de

User Office

Daniela Baum, Maha Dürr
phone +49 (0)30 / 6392 4734
fax +49 (0)30 / 6392 4746
useroffice@bessy.de

Public Relations

Dr. Heike Henneken, Dr. Markus Sauerborn
phone +49 (0)30 / 6392 4921
fax +49 (0)30 / 6392 4972
pr@bessy.de

Photos Credits

For providing photographs and drawings we would like to thank:

3dworks visual computing, Berlin
AMD, Dresden
Annette Weber, Berlin
Bernhard Schurian, Berlin
Bodo Nies, Wolfsburg
California Nutrition Network; CA, USA
Forschungszentrum Jülich
Jan Röhl, Berlin
Kraftwares Pvt. Ltd., India
Landesamt für Archäologie, Halle
Luftbildfoto R. Grahn, Berlin
Proteinstrukturfabrik, FU Berlin
Sean Doorly, CA, USA
Universität Heidelberg
University of Connecticut Libraries